NASA
Technical
Paper
1956

December 1981

Application of a Gaussian Multilayer Diffusion Model To Characterize Dispersion of Vertical HCl Column Density in Rocket Exhaust Clouds

G. L. Pellett
and W. L. Staton

NASA

NASA
Technical
Paper
1956

1981

Application of a Gaussian Multilayer Diffusion Model To Characterize Dispersion of Vertical HCl Column Density in Rocket Exhaust Clouds

G. L. Pellett
and W. L. Staton
Langley Research Center
Hampton, Virginia

NASA
National Aeronautics
and Space Administration

Scientific and Technical
Information Branch

CONTENTS

SUMMARY

A Gaussian multilayer diffusion model is used to calculate nine independent solid rocket motor (SRM) exhaust cloud dispersion cases in order to characterize potential environmental impact. These cases are based on seven standard meteorological regimes for the Cape Canaveral, Florida, area representing characteristic overland advection cases. The dispersion cases include the following: A modified "spring fair weather" Space Shuttle case, with about 60 metric tons HCl exhausted below 2.5-km altitude (a conservatively large HCl source strength); all seven meteorological cases for the chemically similar but smaller Titan III vehicle, with resultant HCl source strengths up to 15 metric tons for stabilized clouds bounded at 2.0 km; and an abnormal (pad abort) Titan III case. Downwind vertical HCl concentration profiles are analyzed, and vertical HCl column density σ is found to be well characterized by the decay expression $\sigma = \alpha X^{-\beta}$ when the downwind distance from launch site X is defined as the sum of the downwind distance from the cloud stabilization point X_{cs} and an effective virtual source distance upwind from the cloud stabilization point X_o. (α and β are empirical constants.) The dispersive σ decays are illustrated, and sets of α, β, X_o, and resultant HCl source strength are tabulated for use with either X or elapsed time t. Equivalent decays of vertically averaged HCl concentration C(HCl) are also presented.

The calculated decays of σ and C(HCl) differ greatly among the seven meteorological regimes. A range of more than two orders of magnitude in σ and C(HCl) is spanned at $X \geq 100$ km and $t \geq 2.0$ hr. At shorter distances, the total span in σ and C(HCl) still exceeds an order of magnitude for all $X > 10$ km and $t > 0.2$ hr. These results suggest that various meteorological conditions at Cape Canaveral lead to widely different exhaust cloud dispersion rates. Also, values of $\sigma \geq 6000$ ppmv-m and C(HCl) ≥ 5 ppmv are calculated for $X \leq 50$ km and $t \leq 5.0$ hr for the two least dispersive Titan III cases. This could result in acidic rainwater of pH ≤ 1.5, which can cause significant damage to some plants.

The set of calculated C(HCl) decays is compared with published analyses of in-cloud peak HCl concentration data from eight Titan III launches. Four major features are noted. First, straight-line fits of the log C(HCl) versus log t data are in agreement with the calculated power-law characteristics. Second, the data exhibit a similar spread (range) of two orders of magnitude for $t > 1.0$ hr, depending on launch meteorology. Third, an inclusive envelope that bounds the calculated decays of C(HCl) also bounds nearly all the in-cloud HCl concentration data for $t \geq 0.2$ hr. Finally, the measured decays of in-cloud HCl tend to be less dispersive than the calculated ones. This apparent difference is consistent with the use of model variances based on relatively small-scale (compared with SRM cloud size) turbulence measurements. Despite this last difference, we conclude that the calculated data agree well with the experimental data. In effect, this provides a partial validation of the model as an assessment tool, since individual model-prediction versus experimental-measurement comparisons are not made.

Several factors affect the validity of the calculated σ and C(HCl) values, especially at large X and t. First, the model assumes stable stratification conditions in the lower troposphere and, hence, lack of vertical convective motion. This oversimplification invalidates use of the model under many conditions. Second, neglect of convective loss of HCl from the SRM exhaust cloud's upper boundary, HCl

sorption at ground level, and variable advection for the respective MDM layers tends to result in unrealistically large values of σ and C(HCl) at large X. Neglect of these factors, however, is a convenient means of allowing the model to predict somewhat high at large X, so as to err on the safe side. Finally, the above-mentioned use of small-scale variances tends to result in underestimation of σ and C(HCl) at large X. Evaluation of this effect is beyond the scope of this paper.

Since the basic formulation of the modified Gaussian dispersion models is statistical-analytical in nature and does not treat the essential physics of cloud-scale and mesoscale dynamics, a need is apparent for resuming development of a much more comprehensive model. Such a predictive tool is clearly needed for assessment of atmospheric effects, especially in the vicinity of the Cape Canaveral land-sea interface where sharp contrasts in surface thermal and moisture characteristics exist and significant convective activity occurs.

INTRODUCTION

The National Aeronautics and Space Administration (NASA) has been examining the possible environmental impacts of its Space Shuttle Program for about 8 years. Formal Environmental Impact Statements were published in July 1972 (ref. 1) and April 1978 (ref. 2). One of the potential problem areas cited, atmospheric pollution, stems mainly from the planned use of a solid rocket motor (SRM) booster design. The tropospheric portion of this environmental problem centers on the possible effects of relatively large, localized, low-level releases of SRM exhaust products. For the present discussion, these include more than 60 metric tons of hydrogen chloride (HCl) and about 90 metric tons of aluminum oxide (alumina) particles emitted below 2.5-km altitude per launch.[1]

Environmental impact studies of SRM exhaust clouds in the troposphere have been shaped and focused by three principal concerns. First, gaseous components of the afterburned exhaust (refs. 3 to 5) combined with chloridized alumina particles (refs. 6 to 13), entrained ground debris (refs. 14 to 16), and large amounts of sprayed water used for acoustic baffling and launch pad cooling (refs. 5 and 14), may adversely impact ground receivers, which include both plant and animal life (refs. 1, 2, and 17 to 21). Second, the possibility exists that precipitation scavenging of HCl might lead to localized deposition of unacceptably acidic (mostly hydrochloric acid) rain on nearby land areas or protected waters before atmospheric dispersion has effectively reduced the potential hazard to acceptable limits (refs. 1, 2, 6, and 17 to 24). Third, the potential exists for inadvertent weather modification effects, which conceivably may occur up to a few days after launch (refs. 25 and 26) and may be caused by alumina ice nuclei (refs. 13 and 25 to 29).

The formation, altitude stabilization, and transport with atmospheric dispersion of Space Shuttle and Titan III SRM exhaust clouds have been the subjects of several

---

[1]Note that the stabilized ground cloud is defined in ref. 2 as containing 35 metric tons HCl (20 sec burn up to about 1.1-km altitude), and more recent mission designs (1976) indicate about 44 metric tons HCl exhausted for a 20 sec burn up to 1.2-km altitude. Since the ground cloud definition in ref. 2 was used for evaluating surface level concentrations, additional HCl exhausted at levels higher than 1.2 km would be relatively unimportant. However, for the present Shuttle case (prediction of in-cloud concentrations and eventual acid-rain characteristics), a more conservative resultant source strength (61 metric tons HCl) is being used.

modeling studies (refs. 14 and 30 to 35). Experimental field studies of Titan III clouds (refs. 7, 8, 10 to 13, 27 to 29, and 36 to 48) have attempted to provide cloud geometry and temporal species concentration data for validation and refinement of NASA's Gaussian multilayer diffusion models (refs. 30 to 35) and also for more sophisticated atmospheric dynamics models currently under development (refs. 22, 23, and 49). The field studies, in conjunction with idealized laboratory experiments (refs. 6, 7, and 9), have also provided certain physical-chemical data to allow initial characterizations of cloud composition and important rate processes for calculation of acid-rain formation and weather-modification effects. Although the early Titan III field studies concentrated on obtaining transient-species concentration data at ground level from arrays of stationary and semimobile sites (refs. 36 to 41), more recent efforts have focused mainly on obtaining in-cloud species concentration profiles and particle/aqueous-acid aerosol size distribution measurements from successive figure-eight patterns flown by instrumented aircraft (refs. 39 to 48).

Although most of the published modeling results have focused on defining transient-species concentrations and dosages at ground level, relatively few have dealt with corresponding species concentrations aloft, even though vertical concentration profiles are inherent in the calculations and in-cloud concentrations have been measured. Since studies of potential acidic rain and inadvertent weather-modification effects require information on HCl concentrations (and alumina acid-aerosol characteristics) aloft, an initial objective of this study is to characterize representative sets of downwind vertical HCl concentration profiles that apply to large exhaust clouds over a range of meteorological conditions.

For certain applications, it is both practical and desirable to define integrated vertical burdens, or vertical column densities, of components. For example, optical remote sensing techniques (two-ended or Sun tracking), which lead directly to measurement of column density, have a practical advantage in mapping the source strength characteristics of a polluted cloud since only two-dimensional data in the horizontal plane are required. Thus, calculations of both vertical concentration profiles and column densities may be useful in the consideration of certain remote sensing applications.

At present, however, information about column density in SRM exhaust clouds is needed to calculate acid-rain deposition characteristics. It has been shown, through development of an idealized washout model (refs. 6 and 24), that scavenging of HCl(g) by raindrops is effectively an irreversible absorption process that is linearly dependent on vertical HCl(g) column density σ, regardless of the actual variation in vertical concentration profile below the rainfall source. Thus, useful analytical expressions for predicting HCl(g) washout, rain pH, and ground deposition of HCl can be applied to independently dispersing SRM exhaust clouds if the temporal and spatial variation of σ can be specified in terms of time and ground coordinates.

Accordingly, the primary focus of the present paper is to evaluate vertical HCl column density under a variety of meteorological conditions for input to the refined acid-rain model of reference 24. Some pertinent details of the acid-rain model are first reviewed, however, and then some specifics of the present approach are given.

The analytic rain scavenging model treats the idealized case of an independently generated vertical rainfall that overrides and scavenges HCl(g), by washout processes, from an independently dispersing SRM exhaust cloud. The washout model applies best at low-to-moderate relative humidities for SRM exhaust clouds, where HCl(g) tends to predominate over the aqueous-acid aerosol component after a few minutes of cloud dilution, and at stable stratification conditions in the lower troposphere. The

washout model was first used (ref. 6) to predict the resultant characteristics of acid-rain deposition for a "spring fair weather" (SFW) Space Shuttle SRM exhaust cloud dispersion case, derived independently from application of Model 4, one of the Gaussian multilayer diffusion models (MDM) that were developed at the NASA Marshall Space Flight Center (MSFC). The SFW dispersion case was based on one of seven "standard meteorologies" documented for the Cape Canaveral, Florida, area. These were selected to represent a range of characteristic cases of overland advection with turbulent diffusion in the planetary boundary layer in order to establish an initial basis for assessing the downwind concentration history of HCl at the Earth's surface (refs. 50 and 51).

In the present paper, the Model 4 MDM is applied to nine independent exhaust cloud dispersion cases based on the seven standard meteorological regimes. These cases include the following: (a) An improved version of the SFW Shuttle case; (b) all seven standard meteorological cases for the smaller but chemically similar Titan III SRM-propelled vehicle, which exhausts about 40 percent of the material that the Shuttle does in the 0- to 4.0-km altitude range; and (c) an abnormal (pad-abort) Titan III case. Downwind vertical HCl concentration profiles calculated for these cases provide one basis for comparisons with existing in-cloud data on Titan III launch effluents. They also provide the requisite data for determinations of σ as described below.

A simple approach is used herein for quantitative characterization of σ from extensive arrays of multilayer HCl concentration histories calculated with the MDM. It is then shown that each dispersive decay of σ can be generalized as a function of downwind distance (or time) from launch site through a one-term power-law expression. Sets of two empirically derived constants for each of the nine dispersion cases are shown to characterize the power-law decays of σ within ±10 percent for the entire range of MDM output distances downwind of SRM exhaust cloud stabilization (1 to 100 km). The σ expressions, in terms of the previously developed HCl(g) washout model, are defined as follows (refs. 6 and 24):

$$\sigma = \int_0^{z_{top}} p_{o,z}(HCl)\,dz = p_o(HCl)\,z \simeq \alpha X^{-\beta} \tag{1}$$

where $p_{o,z}(HCl)$ is the prewashout HCl(g) concentration in parts per million by volume at altitude z, $p_o(HCl)$ represents a vertically averaged concentration over z, X is the downwind distance from launch site, and α and β represent empirical constants. These σ expressions are sufficiently simple, when used as inputs for the analytic acid-rain model, that they allow relatively straightforward parametric analyses and characterizations of downwind acidic rainfall for assumed occurrences of rainfall events.

SYMBOLS

$C(HCl)$ calculated average HCl(g + aq) concentration in diluted SRM exhaust cloud, expressed in dimensionless volume/volume units, ppmv

$\hat{C}(HCl)$ peak value of measured in-cloud HCl concentration, expressed in dimensionless volume/volume units, ppmv

m_o initial mass of HCl in SRM exhaust cloud, g HCl

$p(HCl)$ average concentration of HCl(g) in parcel of diluted SRM exhaust, expressed in dimensionless volume/volume units, ppmv

$p_o(HCl)$ initial value of $p(HCl)$ before HCl(g) washout begins at $t = 0$, ppmv

Q_I effective heat release for solid rocket propellant combustion, cal/g propellant (1 cal = 4.184 J)

t elapsed time after launch, hr

U_c mean unidirectional wind speed which describes horizontal motion of SRM exhaust cloud, m/sec

X unidirectional downwind distance from launch site, $X_o + X_{cs}$, km

X_o virtual source distance upwind from SRM cloud stabilization point at $X_{cs} = 0$, km

X_{cs} unidirectional downwind distance from SRM cloud stabilization point, km

Z_m SRM cloud-centroid height, m

z_{top} height of SRM cloud top above ground, m

α, β constants which define power-law decay of HCl(g) column density σ in dispersing SRM exhaust cloud; α is equivalent to ppmv-m at $X = 1$ km, and β is dimensionless exponent of X in equation (1)

θ_c average wind direction, deg

Λ washout coefficient for HCl scavenging by falling raindrops, sec^{-1}

σ vertical HCl(g) column density, ppmv-m

Abbreviations:

CFP cold front passage

FFW fall fair weather

FW, Pre-CF fair weather, pre-cold front

LLSB low-level sea breeze

MDM multilayer diffusion model

Post-CFP post-cold front passage

SB sea breeze

SFW spring fair weather

SRM solid rocket motor

APPLICATION OF THE MULTILAYER DIFFUSION MODEL

The rocket effluent dispersion calculations used in this paper employ the NASA MSFC exhaust cloud rise preprocessor model and the Gaussian multilayer diffusion models (MDM), which are described and documented in references 30 and 31 for operational prediction of toxic fuel hazards. Model 4 (multilayer, diamond-shaped stabilized cloud), Version II (updated enthalpy content) of the MDM code is used throughout this study for dispersion calculations and is designated herein as MDM-4(II). Simultaneous inclusion of the precipitation-scavenging subroutine is indicated by the designation MDM-5(II) (ref. 30).

Model Description

An overview which broadly characterizes the NASA MSFC rocket exhaust diffusion modeling technique is given in section IV.A of reference 33. Specific applications of the cloud rise preprocessor and the variously modified Gaussian multilayer diffusion models to rocket exhaust dispersion for tropospheric air quality predictions at ground level are described in references 14 and 30 to 35. Some of these references focus on the inherent mathematical and physical limitations of this basically statistical analytic approach (ref. 14), parametric studies of the principal variables upon which the MDM's are based (refs. 14 and 32), and comparisons of calculated rocket effluent concentrations at ground level with those obtained from other advective diffusion models (ref. 14).

Standard Meteorological Regimes for Cape Canaveral

The meteorological regimes selected for study consist of the set of standard meteorologies (ref. 50) that were originally provided for calculating atmospheric dispersion of rocket exhaust effluents in the Cape Canaveral, Florida, area (ref. 51). They represent the major types of meteorological conditions which lead to overland transport and are likely to be encountered in the Cape Canaveral area.

The meteorological profiles of temperature, wind speed, and wind direction from references 30 and 51 for all seven meteorological regimes are shown in figures 1(a) to (g). They are based on averages of selected data obtained from Kennedy Space Center (KSC) rawinsonde releases and from the NASA 150-Meter Ground Winds Tower Facility at KSC. The profile data, including pressures, are tabulated[2] in reference 50.

Inspection of the meteorological profiles indicates large differences in the thermal structure and wind characteristics aloft. Furthermore, note that significant deviations occur, at various levels, from the preprocessor-calculated average values (one each) of wind speed U_c and wind direction θ_c that are used in MDM-4(II) to describe average SRM-cloud advective motion after altitude stabilization. Thus, horizontal wind shear effects are not directly accounted for in the MDM-4(II) calculations since individual layers in the multilayer structure are not allowed to advect independently, even though average wind speed values for each layer were specified in

[2]The "KSC Sea Breeze, Normal Launch" case in ref. 50 is the present low-level sea breeze case. The present sea breeze case is not tabulated in ref. 50, but is illustrated in ref. 30.

the program output. Instead, the effects of horizontal and vertical wind shear, relative to average SRM exhaust cloud advective speed and direction, are simulated in each layer by sets of horizontal (cross direction) and vertical turbulence parameters which applied to each layer. These parameters are standard deviations of the wind azimuth and elevation angle fluctuations. In principle, these standard deviations can be obtained from a comprehensive set of local meteorological data, such as those tabulated in part for the Cape Canaveral area on specific launch occasions (refs. 52 to 54). In the absence of direct measurements, the turbulence parameters can be deduced from the simple profile measurements such as those shown in figures 1(a) to (g). The latter procedure was used for the seven standard meteorologies used in this study. The methodology used to deduce these parameters is described in reference 14 and references 30 to 35. The specific values of MDM-4(II) input parameters used in this study are summarized in table A1 in the appendix.

Characteristics of Stabilized SRM Source Clouds

The SRM exhaust cloud rise preprocessor numerically calculates the vertical and horizontal distribution of HCl which results from buoyant cloud rise with turbulent air entrainment under a specified potential temperature gradient (refs. 30 to 35). The vertical source-strength distribution at cloud altitude stabilization is assigned a multilayer structure, based partly on locations of changes in the meteorological profiles. Similarly, the stabilized cloud is assigned a specific geometric shape in the vertical cross section, which characterizes the layer widths, and hence the HCl concentrations, in the stabilized SRM cloud. In the case of Model 4, a conical body of revolution, having a diamond-shaped cross section symmetrical about the vertical centroid axis, is used to bound the horizontal layers. This is shown in figure 2 and is discussed below.

An example of the geometric definition of a Titan III stabilized SRM exhaust cloud is shown in figure 2(a) for the sea breeze (SB) meteorological regime at Cape Canaveral. Resultant layer source strengths are also shown for completeness. The calculated height of the cloud centroid Z_m is 993 m and is based on a currently accepted value for the effective propellant heat release Q_I of 2790 cal/g propellant. The fine-layered definition of the surface mixing layer has an upper bound H_m of 800 m based on the onset of temperature inversion at 800 m as shown in figure 1(d). The "stem" of the so-called column begins at 1680 m and has a radius of 200 m.

A second stabilized SRM exhaust cloud is shown in figure 2(b) for the Post-CFP meteorological regime applied to the case of a normal launch of the Titan III vehicle. In this case, the calculated height of the cloud centroid is 1341 m, compared with 1506 m for the "pad abort" launch case (Post-CFP (pad abort)), and 993 m for the previously discussed SB case. Thus, as expected, both the vertical temperature profile and the input source strength influence the determination of Z_m. Note also that the height of the surface mixing layer (H_m = 1400 m, from fig. 1(g)) is greater than in the SB case but is not defined strictly at the minimum temperature point (1700 m) in figure 1(g). Instead, H_m is defined at the turning point in potential temperature.

A third Titan III SRM exhaust cloud is shown in figure 2(c) for the CFP case. The corresponding vertical temperature gradient in figure 1(f) is not as steep as in the Post-CFP case, resulting in a somewhat lower cloud centroid height (Z_m = 1230 m). However, the temperature profile does not exhibit an inversion up to 2000 m, and thus the surface layer is assigned a height of H_m = 2000 m; the multilayer structure is

arbitrarily terminated at this point. Geometric definitions for the remaining meteorological cases (not shown) are based on application of the same principles as described in the above three cases. Plots of the layer structures and initial vertical distribution of HCl for these remaining cases (Q_I = 2790 cal/g propellant) are similar, based on tabulated values of HCl source strength in each SRM exhaust cloud layer Q(HCl) in the appendix and an entrainment coefficient γ of 0.64 for stabilized Titan III exhaust clouds.

Source-Strength Considerations

Although the vertical-line—source-strength input function (propellant mass burn rate versus altitude) is accurately known for any prescribed Titan III or Space Shuttle mission, the dynamics of cloud rise determine the resultant vertical and horizontal distributions of SRM exhaust mass (and concentrations) in the altitude-stabilized cloud. Thus, the calculated layer source strengths, tabulated in the appendix for the present MDM-subdivided stabilized SRM exhaust clouds, differ from the incremental exhaust input source strengths and are highly dependent on the meteorology considered. Consequently, the resultant cumulative HCl source strength is always smaller than the cumulative input of HCl mass exhausted up to various altitudes. Also, both the resultant layer and cumulative HCl source strengths vary significantly for different potential temperature profiles. Illustrative examples of HCl input and resultant source strengths are discussed in the remainder of this section. A summary of the resultant cumulative HCl source strengths is given in table 1; other quantities in this table are discussed in the next two sections.

A graphical summary of HCl input histories and resultant source strengths for the chemically similar SRM boosters for both the Space Shuttle (Nov. 1973 design) and the Titan III launch vehicles is shown in figure 3(a); figure 3(b) shows the inputs for two more recent Shuttle missions (1976 design). The cumulative HCl mass inputs to the MDM for both the Shuttle and the Titan III cases are based on propellant consumption rates and launch mission trajectories. They differ by a factor of 2.44 up to 2.0-km altitude in figure 3(a). The resultant "preprocessed" fall fair weather (FFW) cumulative HCl source strength in the MDM stabilized cloud for Titan III is also shown in figure 3(a) for altitudes up to 2.0 km, where the calculation was terminated. Resultant layer source strengths are tabulated for all the Titan III cases in the appendix.

The original Space Shuttle spring fair weather (SFW) cumulative source strength for the stabilized cloud, used in previous acid-rain calculations (ref. 6), is shown as a single point in figure 3(a). In view of the Mission 2 November 1973 design (ref. 54) and also the more recent 1976 design (refs. 55 and 56) shown in figure 3(b), it should be reduced to about 60 metric tons of HCl. This figure approximates cumulative HCl exhausted up to 2.5 km and is still consistent with retention of the original, more conservative 4.0-km upper cloud boundary for the Space Shuttle (as opposed to 2.0-km altitude bounds used for the Titan III cases).

Vertical HCl Profiles and Downwind Cloud Dispersion

The maximum centerline HCl concentration for each defined MDM cloud layer is selected from the MDM-4(II) output in order to provide conservative upper limit HCl concentrations for the respective layers, and thus for the vertically integrated column densities. Sets of calculated HCl concentrations thus define vertical profiles

for nine sequentially increasing distances downwind of the SRM cloud stabilization point X_{cs} ranging from 1 to 100 km.

Vertical HCl concentration profiles at six values of X_{cs} are shown in figure 4(a) for the FFW case. The plotted HCl concentrations, which apply mostly at (or very near) the respective centroids of each defined layer, are arbitrarily connected by straight-line segments in this semilog plot. For $X_{cs} \geq 5$ most of the HCl is contained within layers 6 to 10, and the vertical concentration profile in layers 1 to 5 quickly approaches uniformity in this active and well-defined surface mixing layer. A zero-absorption (perfect reflection) surface boundary condition is used throughout this study. The concentration just above layer 10 is shown to be 0.001 ppmv. In actuality, this concentration is zero, since the layers are terminated at 2000 m to define the upper cloud boundary. This boundary is also designated as a perfect reflector. Thus, no mechanism for convective loss at the boundary of the top layer or sorption loss at the surface has been provided.

Graphical representations of the downwind vertical HCl concentration profiles for the remaining seven meteorological cases are shown in figures 4(b) to (h), using the same parametric range for X_{cs} as in figure 4(a). Inspection of these various cases indicates large differences in initial HCl concentration profile at $X_{cs} = 1$, in subsequent downwind decay of concentration within respective layers, in downwind development of a uniform surface mixing layer, and in development of upper cloud layer stratifications which sometimes are relatively nondispersive with respect to decay of HCl concentration. The development of characteristic surface mixing layers can be seen to vary in height from 200 to 2000 m and in the rate of approach to vertically uniform HCl concentration, although uniformity always occurs within $X_{cs} \leq 20$.

For the Titan III launches under the seven standard meteorological regimes at Cape Canaveral and for the pad abort case, table 1 summarizes the SRM exhaust cloud dimensional, advection, altitude-stabilization, and source-strength characteristics for the present MDM-4(II) application. Note that the mean wind speed for the cloud, which correctly relates distance to time in the model, differs from the wind speeds of the individual layers (tabulated in the appendix). The cloud stabilization times, shown from the model output, are used to estimate downwind drift distances from the launch pad to the point where cloud altitude stabilization theoretically occurs. These calculated cloud stabilization drift distances are compared later with empirically determined virtual source distances.

Finally, as indicated earlier, the resultant HCl source strengths for the stabilized SRM exhaust clouds are also summarized in table 1. These apply from the Earth's surface to the MDM upper cloud boundary, and are conserved throughout the SRM cloud dispersion history (in the absence of rain), since no loss terms are applied at the SRM cloud boundaries.

APPLICATION OF CALCULATED HCl PROFILES

Determination of Vertical HCl Column Density

Since the fundamental HCl source parameter in the idealized acid-rain model of references 6 and 24 is vertical column density σ, the MDM-4(II) cloud dispersion results can be incorporated into the acid-rain model but still remain uncoupled, provided that an independently integrated expression for σ can be determined. This effectively allows replacement of a large set of vertically dependent (multilayer)

concentration terms in a three-dimensional acid-rain model with a single expression independent of the vertical coordinate variable.

Initially in this study, single-term power-law expressions for σ were postulated as the simplest conceivable cases, even though significant curvature was found (ref. 6) for the previous SFW Space Shuttle case. These were explicitly dependent on downwind horizontal distance of the cloud centroid from the cloud stabilization point. The problem, therefore, is to determine whether or not the proposed power-law expressions for σ adequately characterize the calculated results for the various meteorological cases in figure 4.

Integrated vertical HCl column densities were obtained as follows. Tabulated vertical profiles of peak centerline HCl concentration, identical to those shown in figure 4 but including three additional downwind distances X_{CS}, were integrated numerically at each X_{CS} by a product summation technique. The resultant summations were numerically equivalent to the area under a linear concentration versus altitude curve obtained by connecting adjacent-layer centerline concentrations with straight-line segments. The σ values were initially plotted on a log-log scale as a function of downwind distance from cloud stabilization (X_{CS} from 1 to 100 km). Significant curvatures were found at $X_{CS} \leq 20$ km for each of the meteorological cases, indicating departures from simple power-law behavior similar to that found in the previously analyzed SFW Space Shuttle case (ref. 6).

In an effort to find a simpler and more useful characterization of σ that would still retain the necessary accuracy, it became evident that addition of a relatively small empirically determined distance X_o to X_{CS} led to a good straight-line fit of $\log \sigma$ versus $\log (X_{CS} + X_o)$ over the entire range of X_{CS} for all the meteorological cases studied. Since all the empirically determined X_o values were positive and reasonably small, falling entirely in the range 2.5 to 5.0 km with a single exception (FFW) requiring 10.0 km, X_o was identified as an effective virtual source distance for cloud stabilization. These results for X_o indicate reasonably good (but not perfect) correspondence with independent estimates of SRM cloud drift between vehicle launch and the MDM-4(II) specified cloud stabilization times. (See table 1.) Accordingly, the corrected distance of the cloud from launch site is defined by $X = X_{CS} + X_o$ for the present study.

Results of Vertical HCl Column Density Determinations

The empirical power-law fits of σ versus X are shown in figures 5(a) to (h) for each of the Titan III cases studied. In addition, the previous (ref. 6) and presently modified SFW Space Shuttle cases are shown in figures 6 and 7. The corresponding decay expressions $\sigma = \alpha(X_{CS} + X_o)^{-\beta}$ are given in each case, along with the resultant HCl source strength m_o and the mean transport wind speed U_c, which correctly relates downwind distance to elapsed time.

The straight-line fits of the calculated data points in figures 5(a) to (h) and 7 are excellent throughout the data range for all the meteorological cases studied. Thus, the demonstration of adequate power-law fits for downwind decay of σ leads to substantial analytic simplification, with respect to the calculation and parameterization of acid-rain characteristics, through application of the previously defined analytic expressions.

In order to examine and compare some of the resultant effects of meteorology on σ, the above-mentioned empirically determined parameters are summarized in table 2 along with other relevant exhaust cloud properties derived from the MDM-4(II) calculations. The corresponding time-dependent expressions for σ, calculated through use of U_c to convert distance to time, are also given.

Although the deduced values of α can be referred to as an HCl column density "source strength" at unit distance, the reader should recognize that α is inherently sensitive to X_o. In turn, X_o is influenced in the MDM-4(II) cloud rise calculations by the vertical profiles of temperature and wind speed, as well as the placement of vertical layer boundaries. Thus, the physical significance of α is not precisely defined.

A noteworthy internal consistency exists for the two Post-CFP meteorological cases, which apply to a normal launch (line source) and a pad abort (point source) situation. The respective X_o and β values are identical, and the ratio of α and σ values (0.71) is identical to the ratio of the m_o values. In the absence of other similar paired calculations for Titan III launches, it is not known whether a simple linear scaling law would apply to other meteorological cases.

A roughly similar comparison can be made between the fully modified Space Shuttle (see fig. 7) and Titan III SFW cases, but it is not as exact since additional multilayer structure bounded at 4000-m altitude is used for calculating the Shuttle case, whereas the Titan III case is terminated at 2000 m. While the respective values of β differ (1.64 and 1.98), the X_o values are the same (4.0 km), and the ratio of values of α (3.85) is fairly close to the ratio of values of m_o (4.21). In terms of corrected distance from launch site, the point at which the ratios of σ and m_o are equal to 4.21 is $X = 1.3$ km, which is still close to the launch site. Thus, the above comparisons between Titan III and Space Shuttle launches for SFW meteorology suggest that approximately linear scaling of σ with source strength applied.

Collective Results for Dispersive Decay of σ and Potential Rain pH

The power-law decays of σ, deduced in figures 5(a) to (h) for the eight Titan III cases, are shown collectively as functions of corrected distance from launch site X in figure 8 and also as corresponding functions of elapsed time after launch $t = X/(3.6U_c)$ in figure 9. The SFW Shuttle case deduced in figure 7 is shown as a dashed line in each figure. Rain pH values shown in figures 8 and 9 were calculated from reference 24 and are discussed later.

The most noticeable feature of figures 8 and 9 is that the dispersive decays of σ differ greatly among the seven standard meteorological regimes. A range of more than two orders of magnitude in σ is spanned at $X \geq 100$ km downwind and/or $t \geq 2.0$ hr. At shorter distances and times the total span in σ is somewhat less, but still exceeds an order of magnitude for $X > 10$ km and/or $t > 0.2$ hr. These results tend to confirm our earlier expectations of large variations in atmospheric dispersion under widely different meteorological conditions, and they help to emphasize the need for developing a comprehensive atmospheric dynamics model (e.g., see refs. 22 and 49) in order to deal effectively with this large source of variability.

A second important feature of figures 8 and 9 is that relatively large σ values and low potential rain pH's are shown to be possible out to relatively large downwind distances and correspondingly long elapsed times. For example, a $pH \leq 1.5$ is considered environmentally significant for single exposures (refs. 19 and 20). If we accept the validity of the two meteorological cases which tend to define upper bounds for σ (FFW and FW, Pre-CF), initial rain pH's between 1.0 and 1.5 (depending on rainfall rate) could occur at downwind distances up to 50 km and elapsed times of nearly 5 hours, based on $\sigma \geq 6000$ ppmv-m (ref. 24). Although these estimates are derived from the two least-dispersive meteorological cases, they are not considered excessively conservative. For example, somewhat more severe stagnation conditions are possible, and no estimated uncertainty bounds have been imposed. Although the predictions in figures 8 and 9 also indicate $\sigma > 2000$ ppmv-m and potential rain pH's of 2.0 or less at downwind distances up to 200 km and elapsed times exceeding 10 hr, we must recognize that the validity of these longer range results becomes less certain with increasing distance and time.

Some competing effects, which both reduce and increase σ, are now identified. First, since convective loss of HCl from the SRM exhaust cloud's upper boundary, HCl sorption at ground level, and variable advection (wind speed and direction) for the respective MDM cloud layers are not accounted for in the present model calculations, inclusion of these processes would tend to reduce σ systematically at progressively large distances. Second, the variances used in the present MDM-4(II) calculations were originally based on field data which applied to relatively small-scale atmospheric turbulence (ref. 51). It is well known (ref. 57), however, that as the relevant turbulence scale increases for atmospheric dispersion of very large plumes, the appropriate variances and overall dispersion rates tend to become weaker power-law functions of the characteristic scale size (e.g., source cloud diameter) and downwind distance. Thus, the exponent β, which characterizes the decay of σ with X, could systematically decrease to about 0.50 at large values of X under some meteorological conditions. This would occur in a fashion similar to that observed in large-scale dispersion studies (ref. 57) and that actually observed for Titan III exhaust clouds (ref. 48). The most extreme and best documented example out of eight Titan III cases observed thus far was for the September 5, 1977, launch (ref. 48). For this launch, 45 data points for maximum in-cloud HCl concentration $\hat{C}(HCl)$, obtained over the postlaunch period of 3 to 300 minutes, are well characterized by $\beta = 0.54$ in the empirical expression

$$\hat{C}(HCl) = 55t^{-0.54}, \text{ ppmv HCl}$$

An inclusive envelope is shown in figure 10 which characterizes the previously discussed (fig. 8) range of dispersive decay of σ and potential rain pH that might be expected for Titan III launches. This envelope encompasses all seven standard meteorological conditions at Cape Canaveral, but does not include additional uncertainty bounds to account for the above-mentioned effects. The shaded area beyond $X = 200$ km is meant to denote an additional level of uncertainty, as discussed above. The purpose of the envelope is to define a regime of most probable σ based on the present modeling results.

Dispersive Decays of In-Cloud HCl Concentration and Comparison With Measurements

Dispersive decays of corresponding vertically averaged HCl concentrations C(HCl) were deduced for the eight Titan III cases, and the results are shown as functions of X and elapsed time in figures 11 and 12. These averaged peak-centerline HCl concentrations were computed from expressions for σ by estimating effective cloud thickness which applies in figures 4(a) to (h) for $X_{CS} \geq 5$ km, as indicated in table 1, and by dividing the appropriate expressions for σ in table 1 by the corresponding cloud thickness.

Since the dispersive decays of C(HCl) in figures 11 and 12 correspond to decays of potential rain pH in figures 8 and 9, comparisons of these figure sets facilitate preliminary estimates of acid-rain potential based on measurements of in-cloud HCl. Such comparisons have proven useful in correlating in-cloud HCl concentrations with simultaneous rain composition data. (See ref. 48.)

A comparison of the calculated results in figure 12 with experimental measurements of peak in-cloud HCl concentrations for eight Titan III launches is illustrated in figure 13 (reproduced from ref. 48). Since the calculated dispersion results are derived from a set of standard meteorologies for the Cape Canaveral area, they have no direct relationships to the actual launch cases. Thus, no one-to-one comparisons are possible. However, certain first order features of the respective sets are in agreement, as discussed below.

First, to a good approximation all the experimental in-cloud HCl concentration data are shown in reference 48 to be adequately characterized by single-term power-law decay expressions, such as those shown to apply for the modeled temporal results. Next, the total range of measured HCl concentrations is approximately bounded by the total range of predicted concentrations after about 0.2 hr (lower limit of model validity) up to the indicated termination of each launch data fit (at 0.5 to 5.0 hr). Moreover, the respective HCl ranges at various times are large; for example, the ratios of highest to the lowest HCl concentration are about 100 for both sets and increase after 1.0 hr postlaunch. Despite this apparent intersection of the respective experimental and calculated sets of HCl decay histories, four of the measured in-cloud peak HCl concentrations decayed significantly slower with time than the slowest calculated concentration ($\beta = 0.83$ for FFW). Notably, the worst-case model calculations of HCl concentration (highest values) are partially confirmed experimentally. The apparent tendency of the dispersion model to overpredict the rate of decay of peak HCl concentration is consistent with the derivation of MDM empirical dispersion coefficients, which are essentially based on correlations of relatively small-scale turbulence measurements. Thus, while there is surprisingly good overall agreement with respect to HCl concentrations, the present MDM application appears somewhat deficient in that it fails to account for the reduced effect of large-scale turbulent diffusion, bounded by an inversion layer, that applies to large stabilized SRM exhaust clouds several minutes after launch.

Reduction of σ as a Result of Precipitation Scavenging

The use of MDM-5(II) to calculate in-cloud HCl concentrations during progressive HCl(g) washout is checked by comparing MDM-5(II) concentration profiles with similar

"no rain" results from MDM-4(II) through application of the idealized HCl(g) washout model developed in references 6 and 24. The FFW meteorological case is selected, a HCl(g) washout coefficient Λ corresponding to 7.7 mm rainfall per hour is specified ($\Lambda = 4.68 \times 10^{-4}$ sec^{-1}), and the elapsed time for onset of rain after cloud stabilization t_1 is defined ($t_1 = 394$ sec). (See ref. 24 for details of the washout model.) Two otherwise identical calculations of vertical HCl(g) profiles are needed for each downwind distance, one with MDM-5(II) that allows evaluation of σ with rain and a reference calculation with MDM-4(II) that defines σ with no rain. The MDM-4(II) gives results equivalent to results presented earlier in figures 5(a) to (h). Equating the ratio of σ (with rain) to σ (no rain) with the ratio of p(HCl) to p_o(HCl) and plotting selected values as a function of distance from cloud stabilization X_{cs} gives the results shown in figure 14(a). The straight line, which agrees very well with the calculated points, was obtained from the washout model in reference 24, that is,

$$p(HCl)/p_o(HCl) = \exp\left[-\Lambda\left(1000\,\frac{X_{cs}}{U_c} - t_1\right)\right]$$

Note that $p(HCl)/p_o(HCl) = 1$ at $X_{cs} = 2.41$ km, which corresponds to onset of rain at $t_1 = 394$ sec. Results of a similar test of MDM-5(II) using the SFW meteorology are shown in figure 14(b) and indicate equally good agreement. The difference in downwind HCl(g) washout histories between figures 14(a) and (b) is entirely due to the difference in average SRM cloud speed U_c.

The above comparisons demonstrate that the calculated reduction of σ as a result of HCl washout, using the numerical outputs of MDM-4(II) and MDM-5(II), is quantitatively equivalent to that evaluated with the analytic washout model. However, the simplicity of the analytic model, which requires only a single determination of σ decay in the absence of rain, allows subsequent evaluations of σ and various HCl washout and deposition characteristics with greatly reduced computational effort. Thus, a comprehensive matrix of lengthy MDM-5(II) calculations is no longer required in order to evaluate the effects of various combinations of assumed rain onset time and washout coefficient corresponding to an assumed rainfall intensity. This technique could prove useful for real-time predictions and probability assessments of acid-rain hazards during prelaunch countdowns.

SUMMARY OF RESULTS

Some important features of the collective results are now summarized. First, the dispersive decays of σ and C(HCl) differ greatly for the seven standard meteorological regimes tested at Cape Canaveral, Florida. A range of more than two orders of magnitude in σ and C(HCl) is spanned at $X \geq 100$ km downwind and $t \geq 2.0$ hr. At shorter distances and times, the total span in σ and C(HCl) is somewhat less, but still exceeds an order of magnitude for $X > 10$ km and $t > 0.2$ hr. These results are consistent with our working hypothesis that various representative meteorological conditions at Cape Canaveral lead to widely different exhaust cloud dispersion rates.

Second, significantly large values of σ and correspondingly large values of C(HCl) are shown to be possible out to relatively large downwind distances and times from launch site. This is especially true for the two least dispersive Titan III cases, which had the largest in-cloud concentrations. Here, for example,

$\sigma \geq 6000$ ppmv-m and $C(HCl) \geq 5$ ppmv were calculated at $X = 50$ km and $t = 5.0$ hr. Note that HCl concentrations at ground level are much smaller. Application of a previously developed HCl washout model indicates that the above σ could lead to rainwater pH ≤ 1.5, which is considered environmentally significant for a single exposure on certain plants. A pH of 1.5 for rainwater is more than 1000 times more acidic than average rain in the Cape Canaveral area (pH = 4.6), which itself is 10 times more acidic than unpolluted rain. Thus, the σ values for the two worst-case conditions suggest that atmospheric dispersion may not be rapid enough under some conditions to avoid significant environmental consequences downwind if rainfall occurs.

Next, the calculated decays of $C(HCl)$ were compared with published analyses of available in-cloud peak HCl concentration data obtained from eight Titan III launches. Four major features are noted. First, details of the in-cloud data presented elsewhere indicate that straight-line fits of $\log C(HCl)$ versus $\log t$ are entirely adequate representations of the data, which extend beyond $t = 2.0$ hr for three of the eight launches. Thus, the data are in reasonable agreement with the power-law characteristics of the present model. Second, the various in-cloud data exhibit a spread of two orders of magnitude for $t \geq 1.0$ hr, depending on launch date and meteorology. Thus, the natural variability is large. Third, an inclusive $C(HCl)$ envelope bounding the calculated decays of $C(HCl)$ versus t is found to bound nearly all the in-cloud HCl concentration data for $t \geq 0.2$ hr. In fact, the total span of in-cloud data at 1.0 hr postlaunch is 0.3 to 20 ppmv HCl (allowing small extrapolations) for the eight Titan III launches, which is nearly identical to the calculated span for the seven meteorological regimes. Fourth, the power-law decays of the in-cloud data tend to be less dispersive than those calculated for the eight Titan III cases. More specifically, values of β for the in-cloud data vary principally from 1.25 to 0.54 for the six best defined cases, whereas values of β for the calculated decays of σ and $C(HCl)$ vary from 1.98 to 0.83 for the seven standard meteorological regimes.

Thus, while some apparent differences exist among the above collective sets of experimental in-cloud data and model-calculated values of $C(HCl)$, there is still a significant level of overall agreement observed. In effect, this provides a first order validation of the model as an assessment tool. However, the present results do not allow detailed model-prediction versus experimental-measurement comparisons, since the calculated results are based on standard meteorological regimes rather than meteorological data for the specific launches.

Finally, several factors are identified that affect the validity of the calculated values of σ and $C(HCl)$ with respect to the real atmosphere, especially at large X and t. First, the model assumes stable stratification conditions in the lower troposphere, and hence, lack of vertical convective motion. Obviously this is an oversimplification that can significantly invalidate the results under some conditions. Second, neglect of convective loss of HCl from the SRM exhaust cloud's upper boundary, HCl sorption at ground level, and variable advection for the respective MDM layers tends to result in unrealistically large values of σ and $C(HCl)$ at large downwind distances. Neglect of these factors, however, is a convenient means of allowing the model to predict somewhat high at large X so as to err on the safe side. Finally, the use of variances in the model based on relatively small-scale (compared to SRM cloud size) atmospheric turbulence measurements tends to result in overestimation of dispersion at large distances and, hence, underestimation of σ and $C(HCl)$. The previously cited in-cloud HCl measurement results are considered evidence for this effect.

CONCLUDING REMARKS

The atmospheric dispersion results for large solid rocket motor exhaust clouds calculated with the present multilayer diffusion model indicate wide variability with meteorological conditions and sufficiently slow dispersion under some conditions to warrant continued environmental concern and further study. In view of these results, and since the basic formulation of modified Gaussian dispersion models is statistical-analytical in nature and does not treat the essential physics of atmospheric motion in the troposphere, it is apparent that a much more comprehensive dynamics model is needed. Such a model would provide a more accurate predictive tool for assessment of atmospheric transport, dispersion, precipitation scavenging, and dry/wet deposition effects. Such a model is especially needed in the vicinity of the Cape Canaveral, Florida, area, where sharp contrasts in surface thermal and moisture characteristics tend to control convective activity.

Langley Research Center
National Aeronautics and Space Administration
Hampton, VA 23665
November 25, 1981

APPENDIX

SUMMARY OF MDM-4(II) INPUT PARAMETERS

The MDM-4(II) input parameters, used for calculating Titan III dispersion cases under each of the seven standard meteorological regimes, are summarized in table A1. Note that the present calculations are based on a corrected value for total heat release Q_I of 2790 cal/g of propellant (see ref. 33) rather than the earlier, unrealistic value of 691 cal/g used in reference 30. The cloud centroid height Z_m, shown in parentheses, stemmed from the outdated Q_I value and is presently retained as an identifier. The unbracketed Z_m was calculated directly from the Q(HCl) versus $(Z_{BK} + Z_{TK})/2$ data. Note that H, which is defined as the effective source-cloud release height for a Model 3 calculation, compares approximately to Z_m. Other Titan III parameters used were a fuel expenditure rate of 4.17 Mg/s (ref. 30); a time after ignition t_R in seconds defined as a function of altitude Z(m) by $t_R = 0.6346\ Z^{0.4837}$; a 20.8 weight-percent HCl exhaust composition; and an entrainment coefficient of 0.64, used for calculating the width of stabilized Titan III exhaust clouds. The Titan III on-pad abort case was also the same as that defined in reference 30. The symbols used in table A1 are defined as follows:

H	effective source-cloud release height for a Model 3 calculation
p	pressure, millibars (1 millibar = 100 Pa)
Q(HCl)	HCl source strength in each defined SRM exhaust cloud layer, kg HCl
T	temperature, K
U	mean wind speed, m/sec
U_{RK}	wind speed at reference height, m/sec
Z	height, m
Z_m	ground-cloud stabilization height, m
Z_{RK}	reference height of 2 m
α_K	lateral diffusion exponent
β_K	vertical diffusion exponent
θ	mean wind direction, deg
σ_A	standard deviation of wind azimuth angle, deg
σ_{AR}	standard deviation of wind azimuth angle at reference height, deg
σ_E	standard deviation of wind elevation angle, deg
σ_{ER}	standard deviation of wind elevation angle at reference height, deg
σ_{xo}	standard deviation of alongwind distribution at source, meters
σ_{yo}	standard deviation of crosswind distribution at source, meters

σ_{zo} standard deviation of vertical distribution at source, meters

τ_K cloud-stabilization time, sec

τ_{oK} sampling time for standard-deviation calculations, sec

Φ potential temperature $\left[T\left(\frac{1000}{p}\right)^{0.286}\right]$, K

Subscripts:

BK bottom of Kth layer

TK top of Kth layer

APPENDIX

TABLE A1.- MDM-4(II) MODEL INPUT VALUES FOR STANDARD METEOROLOGICAL REGIMES AT KENNEDY SPACE CENTER

(a) *Fall fair weather regime*

Parameter	Units	Input values for SRM exhaust cloud layer -									
		1	2	3	4	5	6	7	8	9	10
z_{BK}	m	2	200	400	600	800	1000	1200	1400	1600	1800
z_{TK}	m	200	400	600	800	1000	1200	1400	1600	1800	2000
z_m	m					(915)		1322			
U_{BK}	m/sec	3.80	5.97	6.39	6.65	6.85	7.00	6.70	6.45	6.18	5.90
U_{TK}	m/sec	5.97	6.39	6.65	6.85	7.00	6.70	6.45	6.18	5.90	5.60
θ_{BK}	deg	90	95.8	101.6	107.4	113.2	119.0	121.5	124.0	126.0	129.0
θ_{TK}	deg	95.8	101.6	107.4	113.2	119.0	121.5	124.0	126.0	129.0	131.0
Φ_{BK}	K	297.9	298.2	298.6	298.6	299.2	299.0	300.3	301.6	302.9	304.3
Φ_{TK}	K	298.2	298.6	298.6	299.2	299.0	300.3	301.6	302.9	304.3	305.6
p_{BK}	millibars	1013	994	972	949	926	906	885	865	844	824
p_{TK}	millibars	994	972	949	926	906	885	865	844	824	805
$\sigma_{E_{BK}}$	deg	10.86	6.88	6.42	6.17	6.00	5.86	.10	.10	.10	.10
$\sigma_{E_{TK}}$	deg	6.88	6.42	6.17	6.00	5.86	.10	.10	.10	.10	.10
$\sigma_{A_{BK}}$	deg	12.00	7.60	7.10	6.82	6.63	6.48	.50	.50	.50	.50
$\sigma_{A_{TK}}$	deg	7.60	7.10	6.82	6.63	6.48	.50	.50	.50	.50	.50
τ_K	sec	364									
τ_{oK}	sec	600									
z_{RK}	m	18									
U_{RK}	m/sec	4.7									
σ_{AR}	deg	12.0									
σ_{ER}	deg	6.6									
σ_{xo}	m	29.77	89.3	148.8	208.4	267.9	327.4	370.7	311.2	251.7	192.1
σ_{yo}	m	29.77	89.3	148.8	208.4	267.9	327.4	370.7	311.2	251.7	192.1
σ_{zo}	m	57.16	57.74	57.74	57.74	57.74	57.74	57.74	57.74	57.74	57.74
α_K		1	1	1	1	1	1	1	1	1	1
β_K		1	1	1	1	1	1	1	1	1	1
H	m	1273									
Q(HCl)	kg	28.6	101.5	333.4	833.2	1586	2298	3116	2989	2167	1423

TABLE A1.- Continued

(b) Spring fair weather regime

Parameter	Units	Input values for SRM exhaust cloud layer -									
		1	2	3	4	5	6	7	8	9	10
Z_{BK}	m	2	200	400	600	800	1000	1200	1400	1600	1800
Z_{TK}	m	200	400	600	800	1000	1200	1400	1600	1800	2000
Z_m	m				(795)			1380			
U_{BK}	m/sec	5.41	6.72	6.95	7.08	7.18	7.26	7.32	7.37	7.42	7.46
U_{TK}	m/sec	6.72	6.95	7.08	7.18	7.26	7.32	7.37	7.42	7.46	7.50
θ_{BK}	deg	100	108	116	124	132	140	148	156	164	172
θ_{TK}	deg	108	116	124	132	140	148	156	164	172	180
Φ_{BK}	K	298.9	299.2	299.4	300.0	300.5	300.9	301.0	301.0	301.8	302.0
Φ_{TK}	K	299.2	299.4	300.0	300.5	300.9	301.0	301.0	301.8	302.0	302.4
p_{BK}	millibars	1013	994	972	949	926	906	885	865	844	824
p_{TK}	millibars	994	972	949	926	906	885	865	844	824	805
$\sigma_{E_{BK}}$	deg	6.51	5.23	5.36	4.97	4.90	4.85	4.81	4.77	4.74	4.72
$\sigma_{E_{TK}}$	deg	5.23	5.36	4.97	4.90	4.85	4.81	4.77	4.74	4.72	4.69
$\sigma_{A_{BK}}$	deg	7.00	5.63	5.45	5.35	5.27	5.22	5.17	5.14	5.10	5.08
$\sigma_{A_{TK}}$	deg	5.63	5.45	5.35	5.27	5.22	5.17	5.14	5.10	5.08	5.05
τ_K	sec	416									
τ_{oK}	sec	600									
Z_{RK}	m	18									
U_{RK}	m/sec	6									
σ_{AR}	deg	7									
σ_{ER}	deg	3.8									
σ_{xo}	m	29.77	89.30	148.8	208.4	267.9	327.4	387.0	370.1	310.6	251.1
σ_{yo}	m	29.77	89.30	148.8	208.4	267.9	327.4	387.0	370.1	310.6	251.1
σ_{zo}	m	57.16	57.74	57.74	57.74	57.74	57.74	57.74	57.74	57.74	57.74
α_K		1	1	1	1	1	1	1	1	1	1
β_K		1	1	1	1	1	1	1	1	1	1
H	m	1372									
Q(HCl)	kg	26.21	84.03	263.5	653.1	1279	1980	2550	3201	2596	1842

TABLE A1.- Continued

(c) Low-level sea breeze regime

Parameter	Units	Input values for SRM exhaust cloud layer -						
		1	2	3	4	5	6	7
Z_{BK}	m	2	150	300	500	700	1000	1500
Z_{TK}	m	150	300	500	700	1000	1500	2000
Z_m	m				(567)	959		
U_{BK}	m/sec	2.51	7.90	9.50	5.60	4.00	2.70	2.90
U_{TK}	m/sec	7.90	9.50	5.60	4.00	2.70	2.90	3.10
θ_{BK}	deg	140	145	150	162	173	190	240
θ_{TK}	deg	145	150	162	173	190	240	250
Φ_{BK}	K	292.2	293.3	293.6	295.5	297.7	300.6	303.2
Φ_{TK}	K	293.3	293.6	295.5	297.7	300.6	303.2	306.0
p_{BK}	millibars	1013	1000	983	961	937	906	855
p_{TK}	millibars	1000	983	961	937	906	855	805
$\sigma_{E_{BK}}$	deg	9.63	3.06	2.54	.10	.10	.10	.10
$\sigma_{E_{TK}}$	deg	3.06	2.54	.10	.10	.10	.10	.10
$\sigma_{A_{BK}}$	deg	12.0	3.81	3.17	.50	.50	.50	.50
$\sigma_{A_{TK}}$	deg	3.81	3.17	.50	.50	.50	.50	.50
τ_K	sec	199						
τ_{oK}	sec	600						
Z_{RK}	m	18						
U_{RK}	m/sec	4.5						
σ_{AR}	deg	12						
σ_{ER}	deg	9.9						
σ_{xo}	m	22.33	66.98	119.1	178.6	253.0	168.2	93.0
σ_{yo}	m	22.33	66.98	119.1	178.6	253.0	168.2	93.0
σ_{zo}	m	42.72	43.30	57.74	57.74	86.60	144.3	144.3
α_K		1	1	1	1	1	1	1
β_K		1	1	1	1	1	1	1
H	m	908						
Q(HCl)	kg	34.80	132.5	545.6	1587	3137	2363	834.9

TABLE A1.- Continued

(d) Sea breeze regime

Parameter	Units	Input values for SRM exhaust cloud layer -										
		1	2	3	4	5	6	7	8	9	10	11
Z_{BK}	m	2	100	200	300	400	500	600	700	800	1300	1800
Z_{TK}	m	100	200	300	400	500	600	700	800	1300	1800	2200
Z_m	m								(832)	993		
U_{BK}	m/sec	6.0	8.9	9.6	9.9	10.2	10.4	10.6	10.8	10.9	10.0	11.9
U_{TK}	m/sec	8.9	9.6	9.9	10.2	10.4	10.6	10.8	10.9	10.0	11.9	13.0
θ_{BK}	deg	150	150	150	152	153	157	160	170	180	228	240
θ_{TK}	deg	150	150	152	153	157	160	170	180	228	240	250
Φ_{BK}	K	289.4	288.2	287.2	286.1	285.2	284.3	283.5	282.8	282.2	287.2	284.2
Φ_{TK}	K	288.2	287.2	286.1	285.2	284.3	283.5	282.8	282.2	287.2	284.2	280.2
P_{BK}	millibars	1013	1004	994	983	972	961	949	937	926	875	824
P_{TK}	millibars	1004	994	983	972	961	949	937	926	875	824	768
$\sigma_{E_{BK}}$	deg	6.70	4.54	4.24	4.07	3.95	3.87	3.80	3.74	3.69	.10	.10
$\sigma_{E_{TK}}$	deg	4.54	4.24	4.07	3.95	3.87	3.80	3.74	3.69	.10	.10	.10
$\sigma_{A_{BK}}$	deg	8.00	5.42	5.06	4.86	4.72	4.62	4.53	4.46	4.40	.50	.50
$\sigma_{A_{TK}}$	deg	5.42	5.06	4.86	4.72	4.62	4.53	4.46	4.40	.50	.50	.50
τ_K	sec	247										
τ_{oK}	sec	600										
Z_{RK}	m	2										
U_{RK}	m/sec	6.0										
σ_{AR}	deg	8.0										
σ_{ER}	deg	7.6										
σ_{xo}	m	14.9	44.7	74.4	104.2	134.0	163.7	193.5	223.3	300.6	151.8	93.0
σ_{yo}	m	14.9	44.7	74.4	104.2	134.0	163.7	193.5	223.3	300.6	151.8	93.0
σ_{zo}	m	28.3	28.9	28.9	28.9	28.9	28.9	28.9	28.9	144.3	144.3	115.5
α_K		1	1	1	1	1	1	1	1	1	1	1
β_K		1	1	1	1	1	1	1	1	1	1	1
H	m	1030										
Q(HCl)	kg	26.2	46.3	111.2	240.0	466.5	815.8	1284	1818	2985	1587	739.6

TABLE A1.- Continued

(e) Fair weather, pre-cold front regime

Parameter	Units	Input values for SRM exhaust cloud layer -							
		1	2	3	4	5	6	7	8
Z_{BK}	m	2	65	218	400	600	800	1076	1200
Z_{TK}	m	65	218	400	600	800	1076	1200	1400
Z_m	m			(397)			875		
U_{BK}	m/sec	1.5	3.5	3.0	3.0	3.0	2.5	2.0	2.0
U_{TK}	m/sec	3.5	3.0	3.0	3.0	2.5	2.0	2.0	2.0
θ_{BK}	deg	253	238	194	198	199	211	235	229
θ_{TK}	deg	238	194	198	199	211	235	229	215
Φ_{BK}	K	290.6	295.6	297.7	298.1	298.9	299.8	300.0	300.1
Φ_{TK}	K	295.6	297.7	298.1	298.9	299.8	300.0	300.1	300.7
p_{BK}	millibars	1018	1011	994	974	951	929	900	887
p_{TK}	millibars	1011	994	974	951	929	900	887	867
$\sigma_{E_{BK}}$	deg	5.37	3.21	2.69	.10	.10	.10	.10	.10
$\sigma_{E_{TK}}$	deg	3.21	2.69	.10	.10	.10	.10	.10	.10
$\sigma_{A_{BK}}$	deg	7.00	4.19	3.50	.50	.50	.50	.50	.50
$\sigma_{A_{TK}}$	deg	4.19	3.50	.50	.50	.50	.50	.50	.50
τ_K	sec	160							
τ_{oK}	sec	600							
Z_{RK}	m	18							
U_{RK}	m/sec	2.6							
σ_{AR}	deg	7.0							
σ_{ER}	deg	5.1							
σ_{xo}	m	9.70	42.1	92.0	148.8	208.4	198.6	139.1	93.0
σ_{yo}	m	9.70	42.1	92.0	148.8	208.4	198.6	139.1	93.0
σ_{zo}	m	18.19	44.17	52.54	57.74	57.74	79.67	35.80	57.74
α_K		1	1	1	1	1	1	1	1
β_K		1	1	1	1	1	1	1	1
H	m	803							
Q(HCl)	kg	30.49	76.98	405.2	1447	2829	3655	2155	1293

TABLE A1.- Continued

(f) Cold front passage regime

Parameter	Units	Input values for SRM exhaust cloud layer -										
		1	2	3	4	5	6	7	8	9	10	11
Z_{BK}	m	2	125	250	400	613	800	1000	1200	1400	1600	1800
Z_{TK}	m	125	250	400	613	800	1000	1200	1400	1600	1800	2000
Z_m	m					(675)			1230			
U_{BK}	m/sec	5.60	13.0	15.0	15.0	15.0	13.7	12.0	11.3	10.4	8.8	8.0
U_{TK}	m/sec	13.0	15.0	15.0	15.0	13.7	12.0	11.3	10.4	8.8	8.0	7.0
θ_{BK}	deg	41.0	44.5	48.0	49.0	51.0	54.0	59.0	66.0	73.5	80.0	86.5
θ_{TK}	deg	44.5	48.0	49.0	51.0	54.0	59.0	66.0	73.5	80.0	86.5	91.0
Φ_{BK}	K	295.3	295.9	296.9	296.9	297.1	297.7	298.5	299.3	300.0	300.7	301.3
Φ_{TK}	K	295.9	296.9	296.0	297.1	297.7	298.5	299.3	300.0	300.7	301.3	302.4
p_{BK}	millibars	1018.6	1007.5	990.5	974.0	950.0	929.5	908.4	887.5	866.5	846.0	827.0
p_{TK}	millibars	1007.5	990.5	974.0	950.0	929.5	908.4	887.5	866.5	846.0	827.0	807.5
$\sigma_{E_{BK}}$	deg	8.71	7.64	7.47	7.36	7.26	7.20	7.15	7.11	7.07	7.04	7.02
$\sigma_{E_{TK}}$	deg	7.64	7.47	7.36	7.26	7.20	7.15	7.11	7.07	7.04	7.02	6.99
$\sigma_{A_{BK}}$	deg	100.0	8.77	8.58	8.45	8.34	8.27	8.21	8.16	8.12	8.09	8.06
$\sigma_{A_{TK}}$	deg	8.77	8.58	8.45	8.34	8.27	8.21	8.16	8.12	8.09	8.06	8.03
τ_K	sec	301										
τ_{oK}	sec	600										
Z_{RK}	m	18										
U_{RK}	m/sec	8.8										
σ_{AR}	deg	10.0										
σ_{ER}	deg	8.8										
σ_{xo}	m	18.6	55.8	96.7	150.8	210.3	267.9	327.4	294.4	234.9	175.4	115.8
σ_{yo}	m	18.6	55.8	96.7	150.8	210.3	267.9	327.4	294.4	234.9	175.4	115.8
σ_{zo}	m	35.5	36.08	43.30	61.49	53.98	57.74	57.74	57.74	57.74	57.74	57.74
α_K		1	1	1	1	1	1	1	1	1	1	1
β_K		1	1	1	1	1	1	1	1	1	1	1
H	m	1145										
Q(HCl)	kg	25.79	53.96	154.5	483.8	1184	2061	2891	3301	2404	1518	989.2

TABLE A1.- Concluded

(g) Post-cold front passage regime

Parameter	Units	Input values for SRM exhaust cloud layer -									
		1	2	3	4	5	6	7	8	9	10
z_{BK}	m	2	125	250	400	600	800	1000	1200	1400	1700
z_{TK}	m	125	250	400	600	800	1000	1200	1400	1700	2000
z_m	m					(751)			1341		
U_{BK}	m/sec	4.30	8.20	9.00	9.60	10.0	11.0	11.0	11.0	10.4	8.6
U_{TK}	m/sec	8.20	9.00	9.60	10.0	11.0	11.0	11.0	10.4	8.6	6.0
θ_{BK}	deg	80.0	80.5	82.0	80.0	78.0	75.0	71.0	65.0	57.0	40.5
θ_{TK}	deg	80.5	82.0	80.0	78.0	75.0	71.0	65.0	57.0	40.5	9.0
Φ_{BK}	K	294.0	294.7	295.8	295.7	295.2	295.6	295.6	295.6	295.9	297.8
Φ_{TK}	K	294.7	295.8	295.7	295.2	295.6	295.6	295.6	295.9	297.8	303.7
p_{BK}	millibars	1022	1009	993.7	977.0	954.0	932.0	910.6	890.0	868.0	838.0
p_{TK}	millibars	1009	993.7	977.0	954.0	932.0	910.6	890.0	868.0	838.0	808.0
$\sigma_{E_{BK}}$	deg	8.47	4.85	4.42	4.14	3.92	3.77	3.66	3.57	3.50	.10
$\sigma_{E_{TK}}$	deg	4.85	4.42	4.14	3.92	3.77	3.66	3.57	3.50	.10	.10
$\sigma_{A_{BK}}$	deg	9.00	5.15	4.69	4.41	4.17	4.01	3.89	3.80	3.72	.50
$\sigma_{A_{TK}}$	deg	5.15	4.69	4.41	4.17	4.01	3.89	3.80	3.72	.50	.50
τ_K	sec	442									
τ_{oK}	sec	600									
z_{RK}	m	18									
U_{RK}	m/sec	6.0									
σ_{AR}	deg	9.0									
σ_{ER}	deg	8.23									
σ_{xo}	m	18.6	55.8	96.7	148.8	208.4	267.9	327.4	387.0	384.0	294.7
σ_{yo}	m	18.6	55.8	96.7	148.8	208.4	267.9	327.4	387.0	384.0	294.7
σ_{zo}	m	35.51	36.08	43.30	57.74	57.74	57.74	57.74	57.74	86.60	86.60
α_K		1	1	1	1	1	1	1	1	1	1
β_K		1	1	1	1	1	1	1	1	1	1
H	m	1420									
Q(HCl)	kg	22.46	34.92	85.76	231.1	569.1	1125	1784	2271	2999	2174
^{a}Q(HCl)	kg	1.50	3.76	13.28	56.37	221.7	683.7	1654	3139	4917	5169
$^{a}z_m$	m							(1132)		1506	

[a]With pad abort.

REFERENCES

1. Environmental Statement for the Space Shuttle Program - Final Statement. NASA TM X-68541, 1972.

2. Environmental Impact Statement - Space Shuttle Program. NASA TM-82278, 1978.

3. Stewart, Roger B.; and Gomberg, Richard I.: The Production of Nitric Oxide in the Troposphere as a Result of Solid-Rocket-Motor Afterburning. NASA TN D-8137, 1976.

4. Gomberg, Richard I.; and Stewart, Roger B.: A Computer Simulation of the Afterburning Processes Occurring Within Solid Rocket Motor Plumes in the Troposphere. NASA TN D-8303, 1976.

5. Gomberg, Richard I.; and Wilmoth, Richard G.: Effects of Entrained Water and Strong Turbulence on Afterburning Within Solid Rocket Motor Plumes. NASA TP-1111, 1978.

6. Pellett, G. L.: Washout of HCℓ and Application to Solid Rocket Exhaust Clouds. Precipitation Scavenging (1974), ERDA Symp. Ser. 41 (CONF-741003), June 1977, pp. 437-465.

7. Dawbarn, R.; Kinslow, M.; and Watson, D. J.: Analysis of the Measured Effects of the Principal Exhaust Effluents From Solid Rocket Motors. NASA CR-3136, 1980.

8. Varsi, G.: Appendix E - Particulate Measurements. Proceedings of the Space Shuttle Environmental Assessment Workshop on Stratospheric Effects, Andrew E. Potter, compiler, NASA TM X-58198, 1977, pp. E-1 - E-12.

9. Cofer, W. R., III; and Pellett, G. L.: Adsorption and Chemical Reaction of Gaseous Mixtures of Hydrogen Chloride and Water on Aluminum Oxide and Application to Solid-Propellant Rocket Exhaust Clouds. NASA TP-1105, 1978.

10. Woods, D. C.: Rocket Effluent Size Distributions Made With a Cascade Quartz Crystal Microbalance. Proceedings of the 4th Joint Conference on Sensing of Environmental Pollutants, American Chem. Soc., c.1978, pp. 716-718.

11. Chuan, R. L.; and Woods, D. C.: Morphology and Elemental Composition Analysis by Size of Rocket Particulate Effluent. Proceedings of the 4th Joint Conference on Sensing of Environmental Pollutants, American Chem. Soc., c.1978, pp. 610-613.

12. Woods, David C.; and Chuan, Raymond L.: Aerosol Characterization With a Quartz Crystal Microbalance Cascade Impactor. Proceedings: Advances in Particle Sampling and Measurement (Daytona Beach, FL, October 1979), W. B. Smith, ed., EPA-600/9-80-004, Jan. 1980, pp. 130-145. (Available from NTIS as PB80-187487.)

13. Parungo, Farn P.; and Allee, Paul A.: Rocket Effluent: Its Ice Nucleation Activity and Related Properties. J. Appl. Meteorol., vol. 17, no. 12, Dec. 1978, pp. 1856-1863.

14. Hwang, Bao Chuan; and Gould, Robert K.: Rocket Exhaust Ground Cloud/Atmospheric Interactions. NASA CR-2978, 1978.

15. Pellett, G. L.; Spangler, L. W.; Storey, R. W.; and Bendura, R. J.: Characterization of Soil From Cape Canaveral Launch Complex, Postlaunch Pad Debris Particulates, and Interaction of Soil With Aqueous HCℓ. Paper presented at Space Shuttle Environmental Effects Program Review (NASA Kennedy Space Center, Fla.), March 1978.

16. Kang, Yoonok; Pellett, G. L.; Skiles, Jean Ann; and Wightman, J. P.: Interaction of Gaseous Hydrogen Chloride and Water With Sandy Soil. J. Colloid & Interface Sci., vol. 75, no. 2, June 1980, pp. 313-321.

17. Environmental Impact Statement for the Kennedy Space Center - 1978-1979 Revision. NASA TM-81015, 1979.

18. Dept. of the Air Force: Environmental Impact Analysis Process - Environmental Impact Statement, Space Shuttle Program, Vandenberg AFB, California. Jan. 1978. (Available from DTIC as AD A060 462.)

19. Granett, A. L.; and Taylor, O. C.: The Effect of Designated Pollutants on Plant Species. AMRL-TR-79-73, U.S. Air Force, Dec. 1979. (Available from DTIC as AD A078 933.)

20. Heck, Walter W.; Knott, William M.; Stahel, Edward P.; Ambrose, John T.; McCrimmon, James N.; Engle, Madeleine; Romanow, Louse A.; Sawyer, Alan G.; and Tyson, James D.: Response of Selected Plant and Insect Species to Simulated Solid Rocket Exhaust Mixtures and to Exhaust Components From Solid Rocket Fuels. NASA TM-74109, 1980.

21. Potter, Andrew E.: Environmental Effects of the Space Shuttle. J. Environ. Sci., vol. XXI, no. 2, Mar./Apr. 1978, pp. 15-21.

22. Dingle, A. Nelson: Rain Scavenging of Solid Rocket Exhaust Clouds. NASA CR-2928, 1978.

23. Dingle, A. N.: Acid Rain: Microphysical Model. Proceedings of Shuttle Environmental Effects Program Review, Andrew E. Potter, ed., NASA CP-2110, 1980, pp. 65-82.

24. Pellett, G. L.: Analytic Model for Washout of HCℓ(g) From Dispersing Rocket Exhaust Clouds. NASA TP-1801, 1981.

25. Bollay, Eugene; Bosart, Lance; Droessler, Earl; Jiusto, James; Lala, G. Garland; Mohnen, Volker; Schaefer, Vincent; and Squires, Patrick: Position Paper on the Potential of Inadvertent Weather Modification of the Florida Peninsula Resulting From the Stabilized Ground Cloud. NASA CR-151199, 1976.

26. Bollay, Eugene; Bosart, Lance; Droessler, Earl; Jiusto, James; Lala, G. Garland; Mohnen, Volker; Schaefer, Vincent; and Squires, Patrick: Position Paper on the Potential of Inadvertent Weather Modification of the Florida Peninsula Resulting From Neutralization of Space Shuttle Solid Rocket Booster Exhaust Clouds. NASA CR-3091, 1979.

27. Hindman, Edward E., II; Garvey, Dennis M.; Langer, Gerhard; Odencrantz, F. Kirk; and Gregory, Gerald L.: Laboratory Investigations of Cloud Nuclei From Combustion of Space Shuttle Propellant. J. Appl. Meteorol., vol. 19, no. 2, Feb. 1980, pp. 175-184.

28. Hindman, Edward E., II; and Radke, Lawrence F.: Cloud Nuclei From Launches of Liquid and Solid Fueled Rockets. Seventh Conference on Inadvertent and Planned Weather Modification (Extended Abstracts), American Meteorol. Soc., c.1979, pp. 18-19.

29. Garvey, Dennis M.; Finnegan, William G.; and Grant, Lewis O.: Ice Nucleating Properties of Rocket Propellant Exhausts. Seventh Conference on Inadvertent and Planned Weather Modification (Extended Abstracts), American Meteorol. Soc., c.1979, pp. 20-21.

30. Dumbauld, R. K.; Bjorklund, J. R.; and Bowers, J. F.: NASA/MSFC Multilayer Diffusion Models and Computer Program for Operational Prediction of Toxic Fuel Hazards. NASA CR-129006, 1973.

31. Dumbauld, R. K.; and Bjorklund, J. R.: NASA/MSFC Multilayer Diffusion Models and Computer Programs - Version 5. NASA CR-2631, 1975.

32. Stewart, Roger B.; and Grose, William L.: Parametric Studies With an Atmospheric Diffusion Model That Assesses Toxic Fuel Hazards Due to the Ground Clouds Generated by Rocket Launches. NASA TN D-7852, 1975.

33. Stephens, J. Briscoe; and Stewart, Roger B.: Rocket Exhaust Effluent Modeling for Tropospheric Air Quality and Environmental Assessments. NASA TR R-473, 1977.

34. Stephens, J. Briscoe; and Hamilton, P. A.: Diffusion Algorithms and Data Reduction Routine for Onsite Launch Predictions for the Transport of Titan III C Exhaust Effluents. NASA TN D-7862, 1974.

35. Stephens, J. Briscoe, ed.: Atmospheric Diffusion Predictions for the Exhaust Effluents From the Launch of a Titan III C, Dec. 13, 1973. NASA TM X-64925, 1974.

36. Gregory, Gerald L.; and Storey, Richard W., Jr.: Effluent Sampling of Titan III C Vehicle Exhaust. NASA TM X-3228, 1975.

37. Stewart, Roger B.; Sentell, Ronald J.; and Gregory, Gerald L.: Experimental Measurements of the Ground Cloud Effluents and Cloud Growth During the February 11, 1974 Titan-Centaur Launch at Kennedy Space Center. NASA TM X-72820, 1976.

38. Bendura, Richard J.; and Crumbly, Kenneth H.: Ground Cloud Effluent Measurements During the May 30, 1974, Titan III Launch at the Air Force Eastern Test Range. NASA TM X-3539, 1977.

39. Gregory, Gerald L.; Wornom, Dewey E.; Bendura, Richard J.; and Wagner, H. Scott: Hydrogen Chloride Measurements From Titan III Launches at the Air Force Eastern Test Range, FL, 1973 Through 1975. NASA TM X-72832, 1976.

40. Wornom, Dewey E.; and Woods, David C.: Effluent Monitoring of the December 10, 1974, Titan III-E Launch at Air Force Eastern Test Range, Florida. NASA TM-78735, 1978.

41. Gregory, Gerald L.; and Storey, Richard W., Jr.: Experimental Measurements of the Ground Cloud Effluents and Cloud Growth for the May 20, 1975, Titan IIIC Launch at Air Force Eastern Test Range, Florida. NASA TM-74044, 1977.

42. Gregory, Gerald L.; Bendura, Richard J.; and Woods, David C.: Launch Vehicle Effluent Measurements During the May 12, 1977, Titan III Launch at Air Force Eastern Test Range. NASA TM-78753, 1979.

43. Woods, David C.; Bendura, Richard J.; and Wornom, Dewey E.: Launch Vehicle Effluent Measurements During the August 20, 1977, Titan III Launch at Air Force Eastern Test Range. NASA TM-78778, 1979.

44. Hindman, E. E., II; Ala, G. G.; Parungo, F. P.; Willis, P. T.; Bendura, R. J.; and Woods, D.: Airborne Measurements of Cloud-Forming Nuclei and Aerosol Particles in Stabilized Ground Clouds Produced by Solid Rocket Booster Firings. NASA CR-160357, 1978.

45. Gregory, G. L.; Emerson, Burt R., Jr.; and Hudgins, Charles H.: Summary of Airborne Chlorine and Hydrogen Chloride Gas Measurements for August 20 and September 5, 1977 Voyager Launches at Air Force Eastern Test Range, Florida. NASA TM-78673, 1978.

46. Wornom, Dewey E.; Bendura, Richard J.; and Gregory, Gerald L.: Launch Vehicle Effluent Measurements During the September 5, 1977, Titan III Launch at Air Force Eastern Test Range. NASA TM-80065, 1979.

47. Sebacher, Daniel I.; Bendura, Richard J.; and Wornom, Dewey E.: Hydrochloric Acid Aerosol and Gaseous Hydrogen Chloride Partitioning in a Cloud Contaminated by Solid Rocket Exhaust. Atmos. Environ, vol. 14, no. 5, 1980, pp. 543-547.

48. Pellett, G. L.; Sebacher, D. I.; Bendura, R. J.; and Wornom, D. E.: HCl in Rocket Exhaust Clouds: Atmospheric Dispersion, Acid Aerosol Characteristics, and Acid Rain Deposition. [Preprint] 80-49.6, Air Pollut. Control Assoc., June 1980.

49. Hsu, Hpiao-Ming: Numerical Simulations of Mesoscale Precipitation Systems. Ph. D. Diss., Univ. of Michigan, Feb. 1979.

50. Susko, Michael; and Stephens, J. Briscoe: Baseline Meteorological Soundings for Parametric Environmental Investigations at Kennedy Space Center and Vandenberg Air Force Base. NASA TM X-64986, 1976.

51. Susko, Michael; Hill, C. Kelly; and Kaufman, John W.: Downwind Hazard Calculations for Space Shuttle Launches at Kennedy Space Center and Vandenberg Air Force Base. NASA TM X-3162, 1974.

52. Stephens, J. Briscoe; Adelfang, S. I.; and Goldford, A. I.: Compendium of Meteorological Data for the Titan III C (AF-777) Launch in May 1975. NASA TM X-73338, 1976.

53. Stephens, J. B.; Adelfang, S. I.; and Goldford, A. I.: Compendium of Meteorological Data for the Viking A Launch in August 1975. NASA TM X-73339, 1976.

54. Stephens, J. B.; Adelfang, S. I.; and Goldford, A. I.: Compendium of Meteorological Data for the Viking B Launch in September 1975. NASA TM X-73340, 1976.

55. Solid Propellant Eng. Staff: Nozzle Exit Exhaust Products From Space Shuttle Boost Vehicle (November 1973 Design). Tech. Memo. 33-712, Jet Propul. Lab., California Inst. Technol., Feb. 1, 1975. (Available as NASA CR-136747.)

56. Bowyer, J. M.: Rocket Motor Exhaust Products Generated by the Space Shuttle Vehicle During Its Launch Phase (1976 Design Data). Publ. 77-9, Jet Propul. Lab., California Inst. Technol., Mar. 1, 1977. (Available as NASA CR-154107.)

57. Pasquill, F.: Atmospheric Diffusion. D. Van Nostrand Co., Ltd., c.1962, pp. 165-178.

TABLE 1.- SRM EXHAUST CLOUD CHARACTERISTICS, AS DEFINED FROM APPLICATION OF MDM-4(II) TO TITAN III

LAUNCHES, FOR SEVEN STANDARD METEOROLOGICAL CASES AT CAPE CANAVERAL, FLORIDA

Meteorological regime	Meteorology abbreviation	Cloud-centroid height, Z_m, m	Surface mixing-layer depth, m	MDM upper cloud boundary, m	Effective cloud thickness at X ≥ 5 km, m	Mean wind speed for cloud, U_c, m/s	Mean wind direction (North ≡ 0°), deg	Cloud stabilization time, sec	Calculated distance, pad to cloud stabilization (from U_c), km	Empirical virtual source distance, X_o, km	HCl source strength, m_o, g
Fall fair weather	FFW	1322	1000	2000	1000	6.127	105	364	2.23	10	14.88×10^6
Spring fair weather	SFW	1380	2000	2000	2000	7.0314	140	416	2.93	4.0	14.48
Low-level sea breeze	LLSB	959	300	2000	1700	6.752	145	199	1.34	3.5	8.634
Sea breeze	SB	993	800	2200	1400	9.923	165	247	2.45	5.0	10.12
Fair weather, pre-cold front	FW, Pre-CF	875	200	1400	1180	2.453	224	160	.39	3.0	11.89
Cold front passage	CFP	1230	2000	2000	2000	6.696	66	301	2.02	4.0	15.07
Post-cold front passage	Post-CFP	1341	1400	2000	600	8.712	69	442	3.85	2.5	11.30
Post-cold front passage (pad abort)	Post-CFP (pad abort)	1506	1400	2000	600	9.284	69	342	3.18	2.5	15.86

TABLE 2.- EMPIRICAL SRM EXHAUST CLOUD PROPERTIES CHARACTERIZING DOWNWIND DISPERSIVE DECAY OF VERTICAL HCl COLUMN DENSITY

[Deduced from application of MDM-4(II) to Titan III launches for seven standard meteorological cases at Cape Canaveral, Florida; the present power-law-decay-modified SFW Shuttle case is shown for both originally used source strength $m_o = 89 \times 10^6$ g HCl (ref. 6) and presently reduced source strength $m_o = 61 \times 10^6$ g HCl consistent with more recent Shuttle mission design (ref. 55)]

Meteorology abbreviation	Cloud-centroid height, Z_m, m	MDM upper cloud boundary, m	Effective cloud thickness at $X_{cs} \geq 5$ km, m	Mean wind speed for cloud, U_c, m/s	HCl source strength, m_o, 10^6 g	Empirical parameters for vertical HCl column density, σ, ppmv-m					
						$\sigma = \alpha(X_{cs} + X_o)^{-\beta} = \alpha x^{-\beta}$			$\sigma = \alpha(t_{cs} + t_o)^{-\beta} = \alpha t^{-\beta}$		
						α, ppmv-m	X_o, km	β	α, ppmv-m	t_o, hr	β
Titan III cases											
FFW	1322	2000	1000	6.127	14.88	1.6×10^5	10	0.84	11.9×10^3	0.453	0.84
SFW	1380	2000	2000	7.0314	14.48	2.6	4.0	1.98	.433	.158	1.98
LLSB	959	2000	1700	6.752	8.634	4.3	3.5	1.32	6.35	.144	1.32
SB	993	2200	1400	9.923	10.12	14.0	5.0	1.81	2.17	.140	1.81
FW, Pre-CF	875	1400	1180	2.453	11.89	2.0	3.0	.93	26.3	.340	.93
CFP	1230	2000	2000	6.696	15.07	4.5	4.0	1.93	.968	.166	1.93
Post-CFP	1341	2000	600	8.712	11.30	.60	2.5	1.13	1.22	.080	1.13
Post-CFP (pad abort)	1506	2000	600	9.284	15.86	.85	2.5	1.13	1.65	.075	1.13
Space Shuttle cases											
SFW (original source strength)	----	4000	----	7.50	89.0	14.6	4.0	1.64	6.56	0.148	1.64
SFW (modified source strength)	----	4000	----	7.50	61.0	10.0	4.0	1.64	4.49	.148	1.64

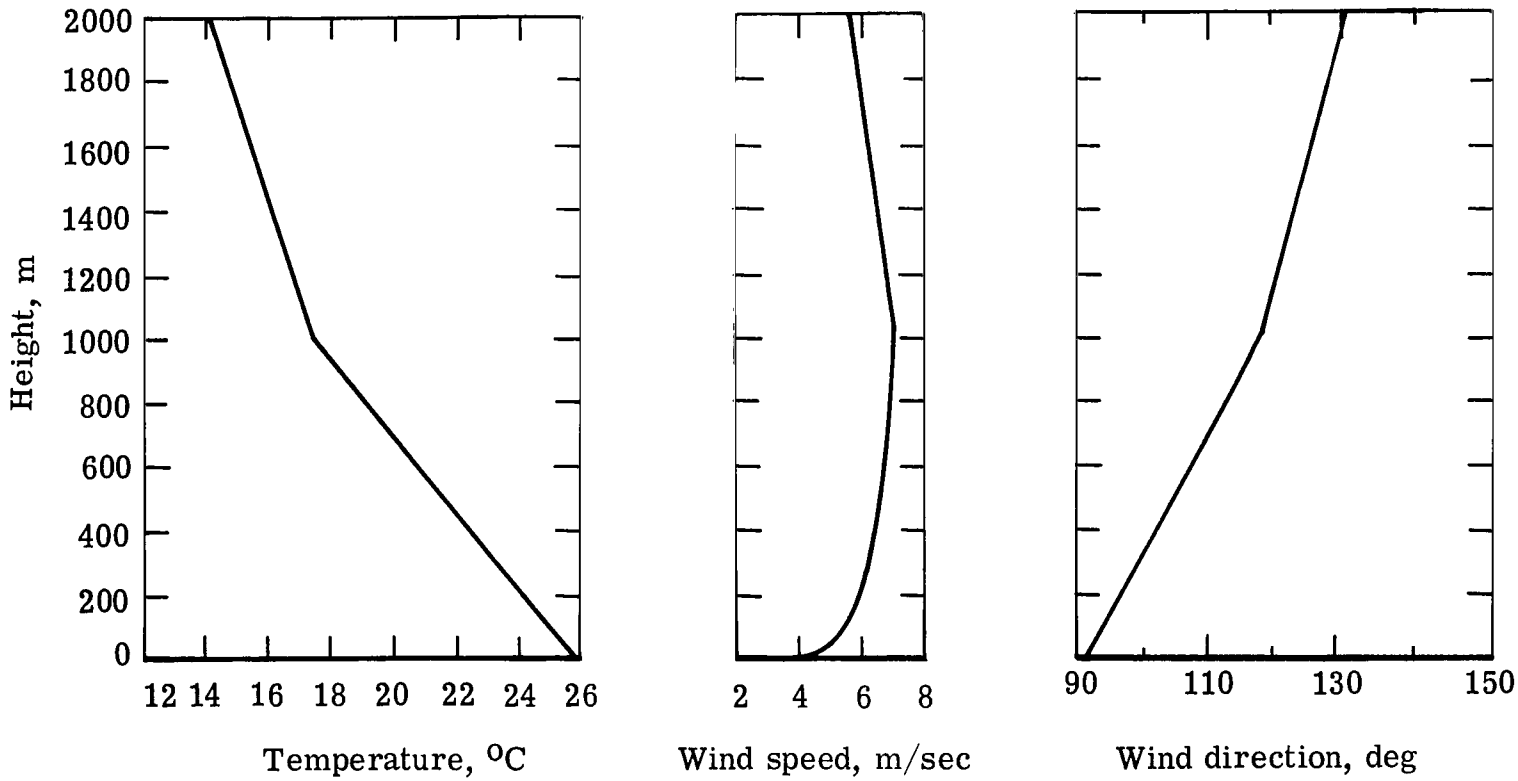

(a) Fall fair weather (FFW) regime (from ref. 51).

Figure 1.- Vertical profiles of temperature, wind speed, and wind direction for standard meteorological regimes at Cape Canaveral, Florida.

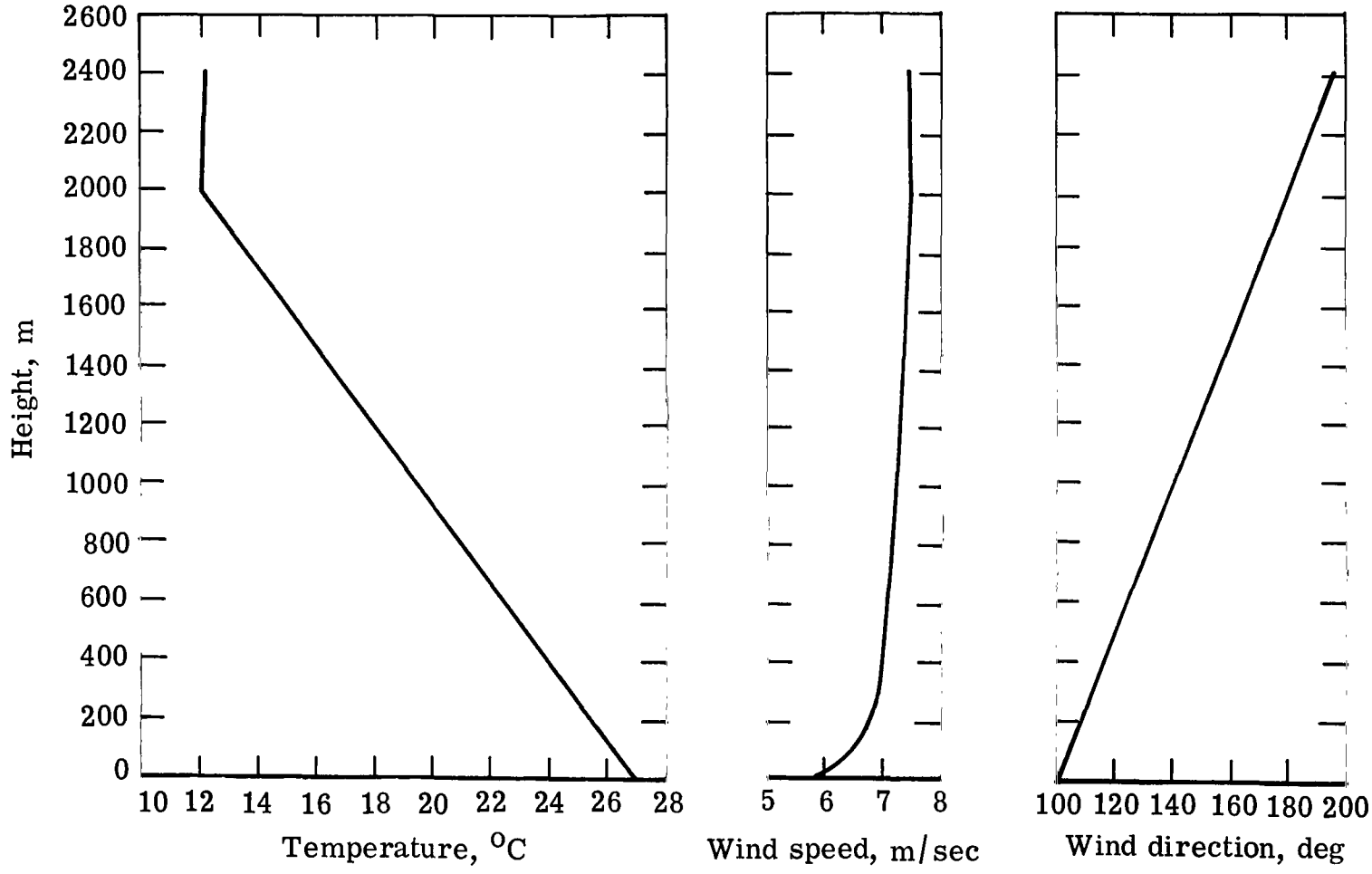

(b) Spring fair weather (SFW) regime (from ref. 51).

Figure 1.- Continued.

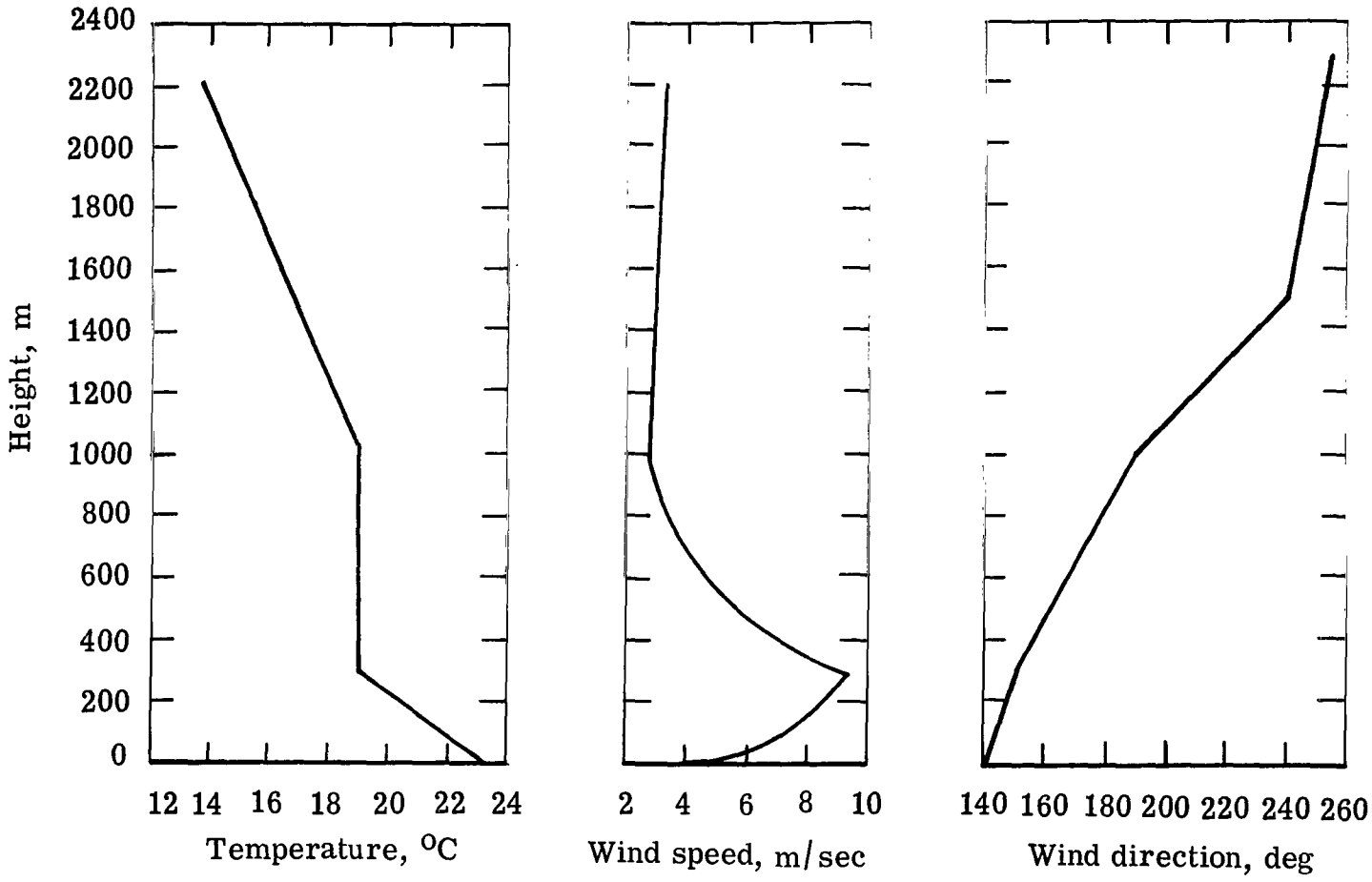

(c) Low-level sea breeze (LLSB) regime (from ref. 51).

Figure 1.- Continued.

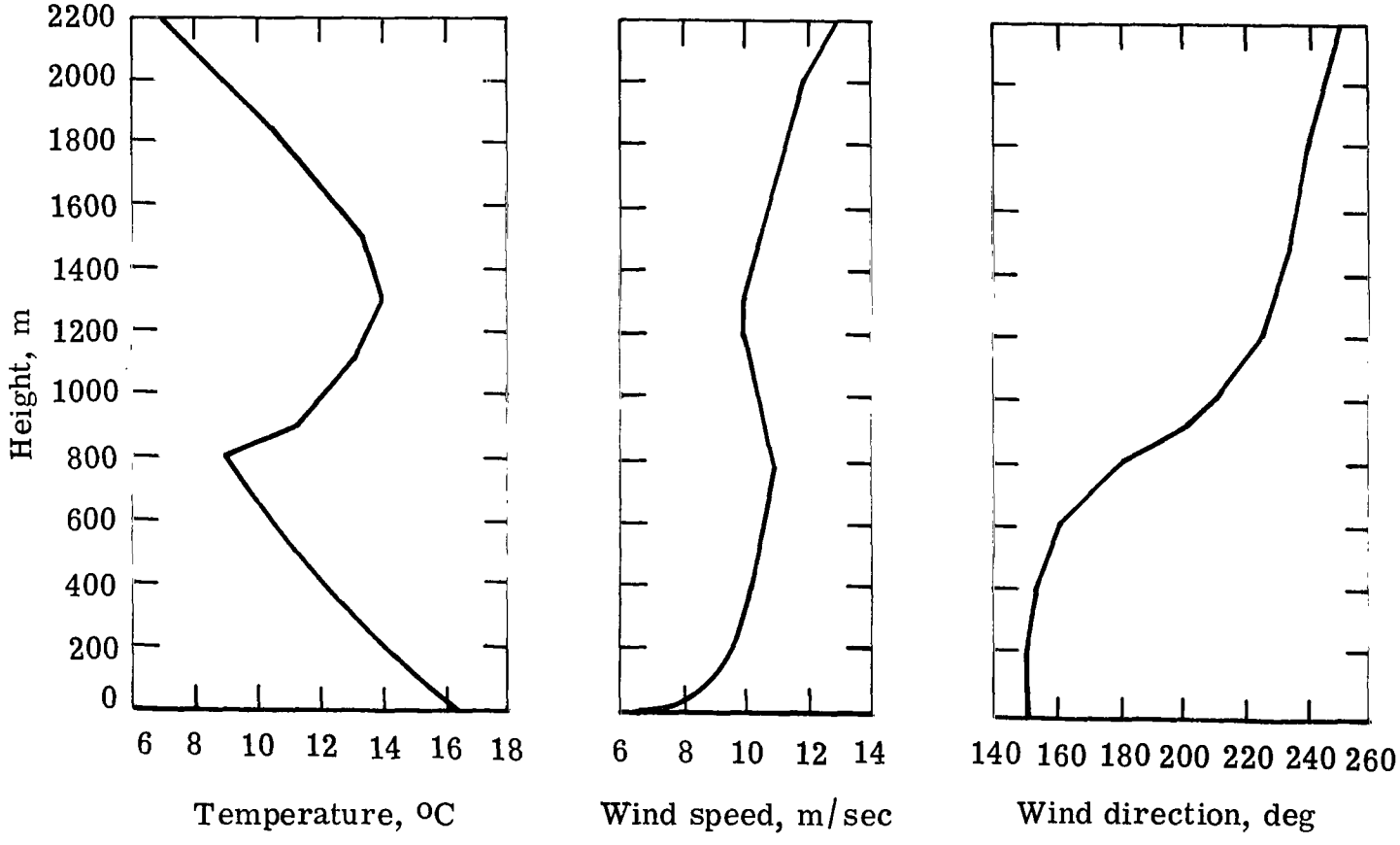

(d) Sea breeze (SB) regime (from ref. 30).

Figure 1.- Continued.

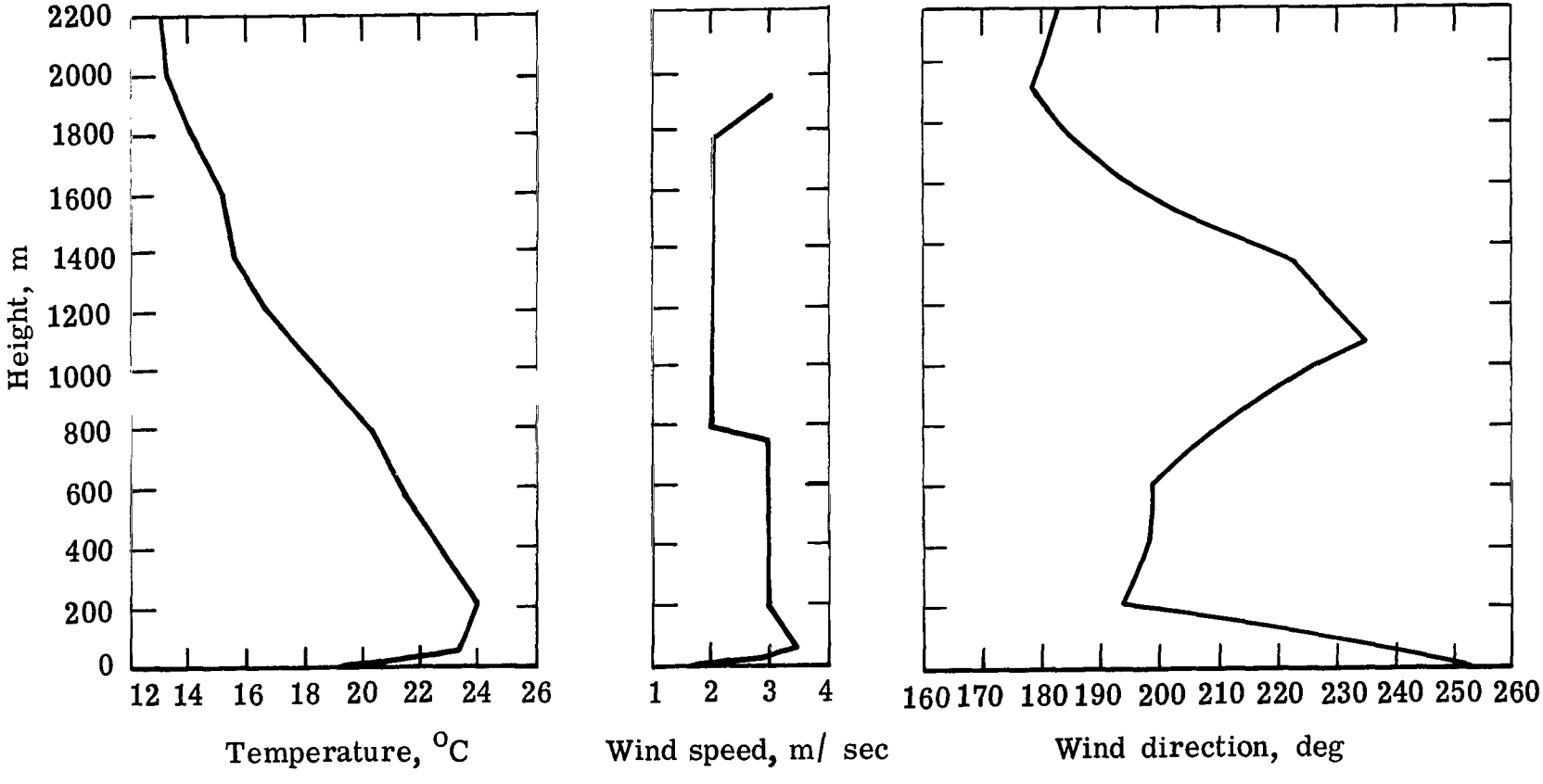

(e) Fair weather, pre-cold front (FW, Pre-CF) regime (from ref. 51).

Figure 1.- Continued.

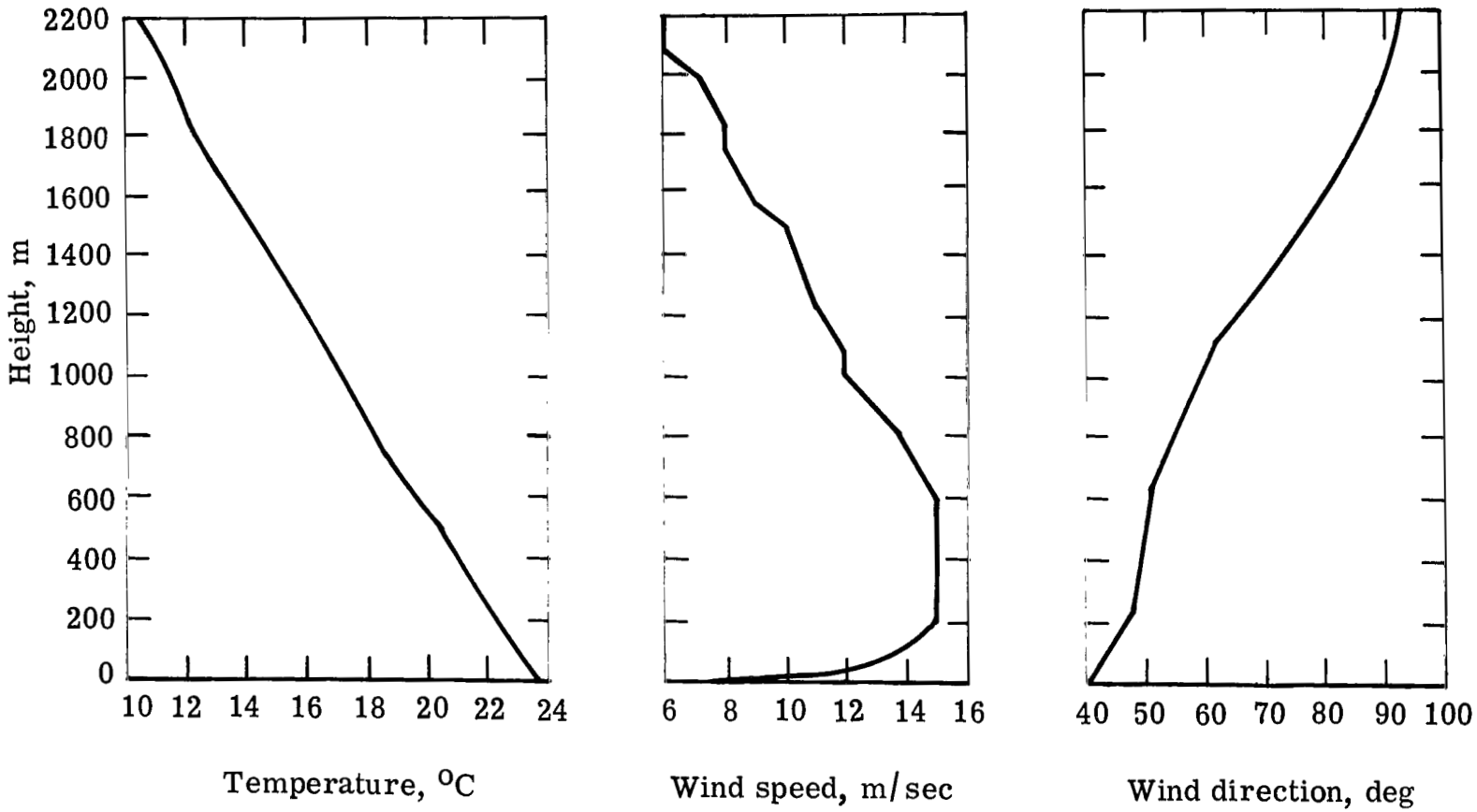

(f) Cold front passage (CFP) regime (from ref. 51).

Figure 1.- Continued.

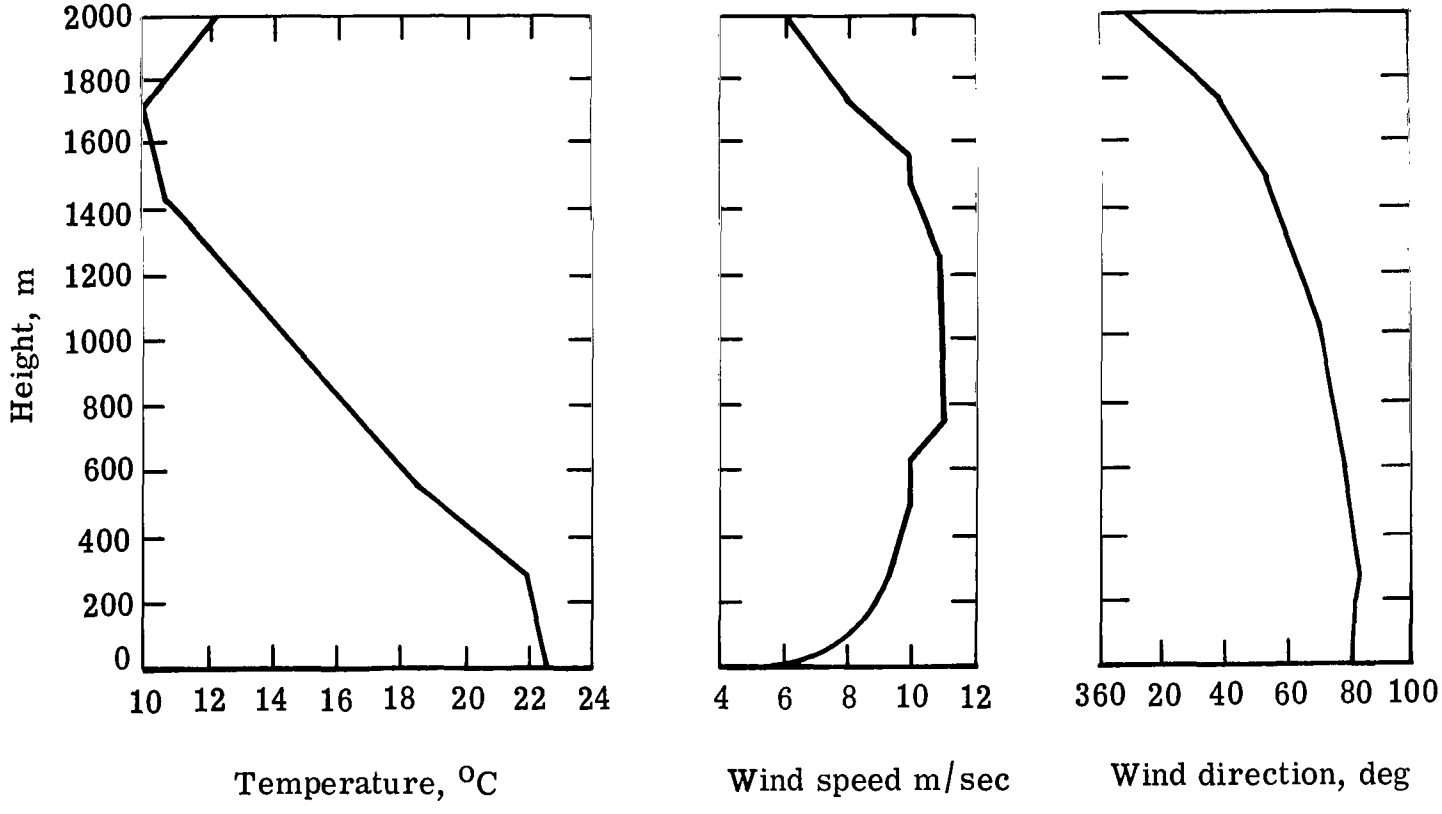

(g) Post-cold front passage (Post-CFP) regime (from ref. 51).

Figure 1.- Concluded.

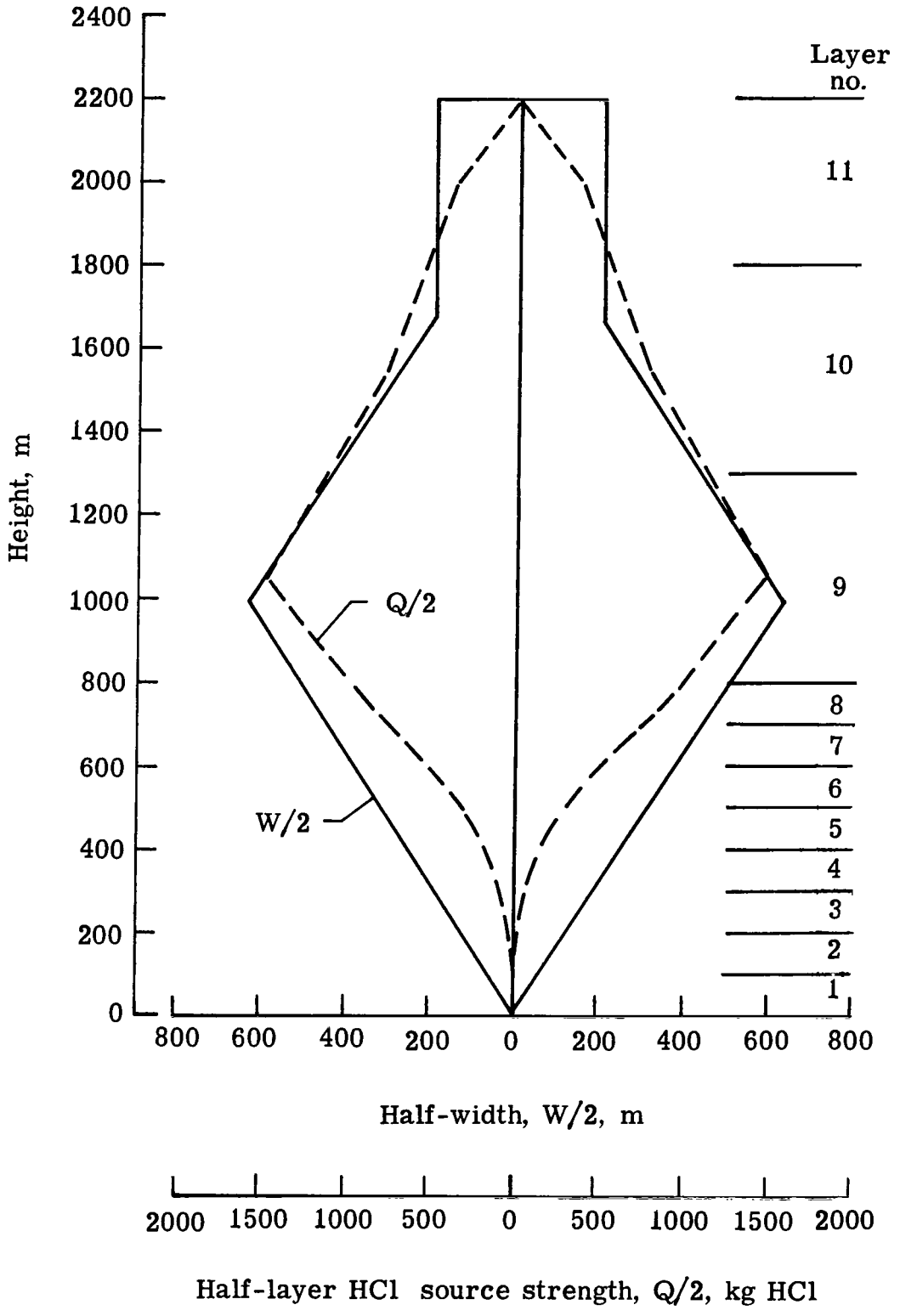

(a) Sea breeze (SB) meteorological regime. Surface mixing layer depth is 800 m and Z_m = 993 m.

Figure 2.- Dimensions and layer source strengths of the stabilized ground cloud of Titan III exhaust products for Q_I = 2790 cal/g propellant.

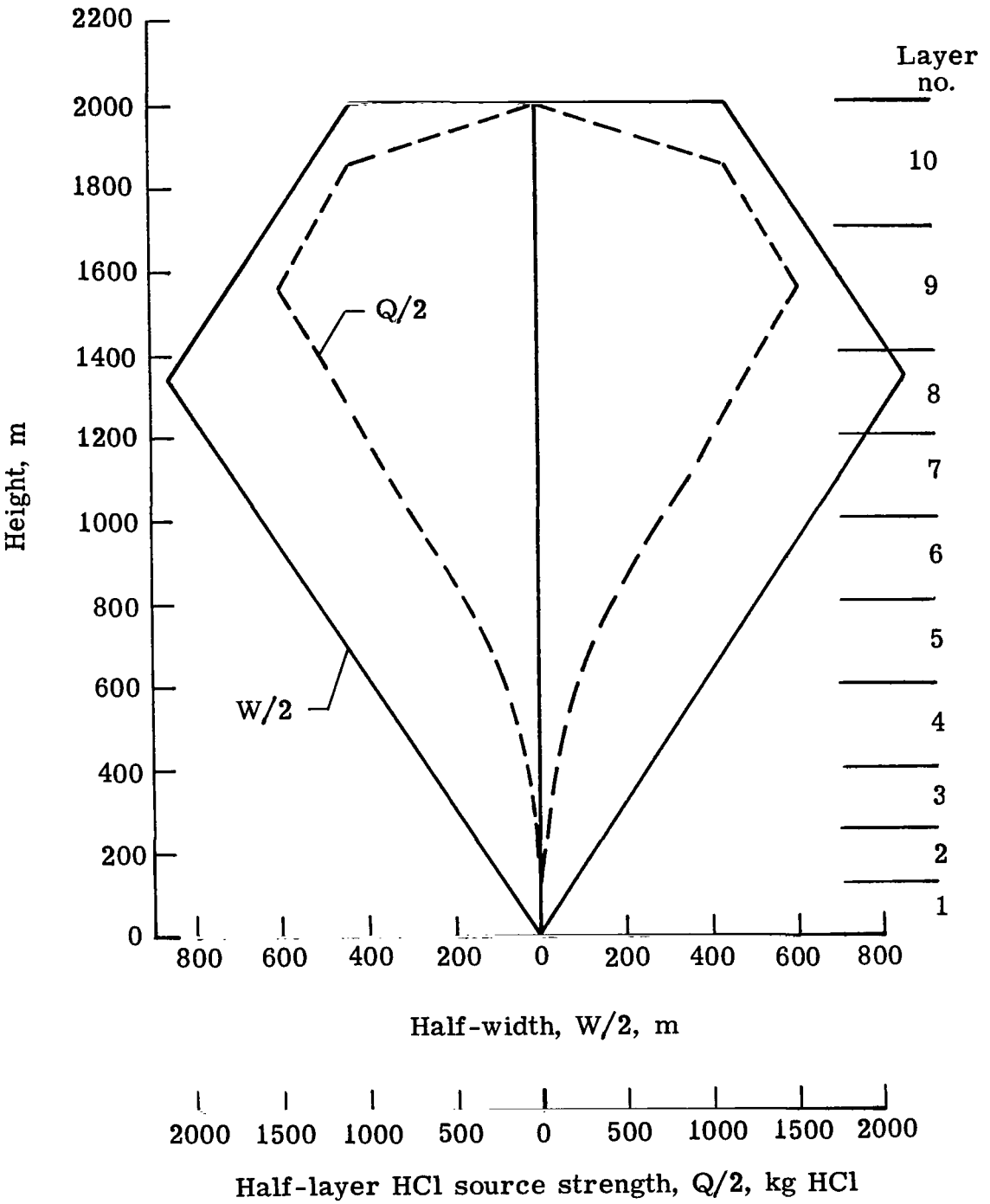

(b) Post-cold front passage (Post-CFP) meteorological regime. Surface mixing layer depth is 1400 m and Z_m = 1341 m.

Figure 2.- Continued.

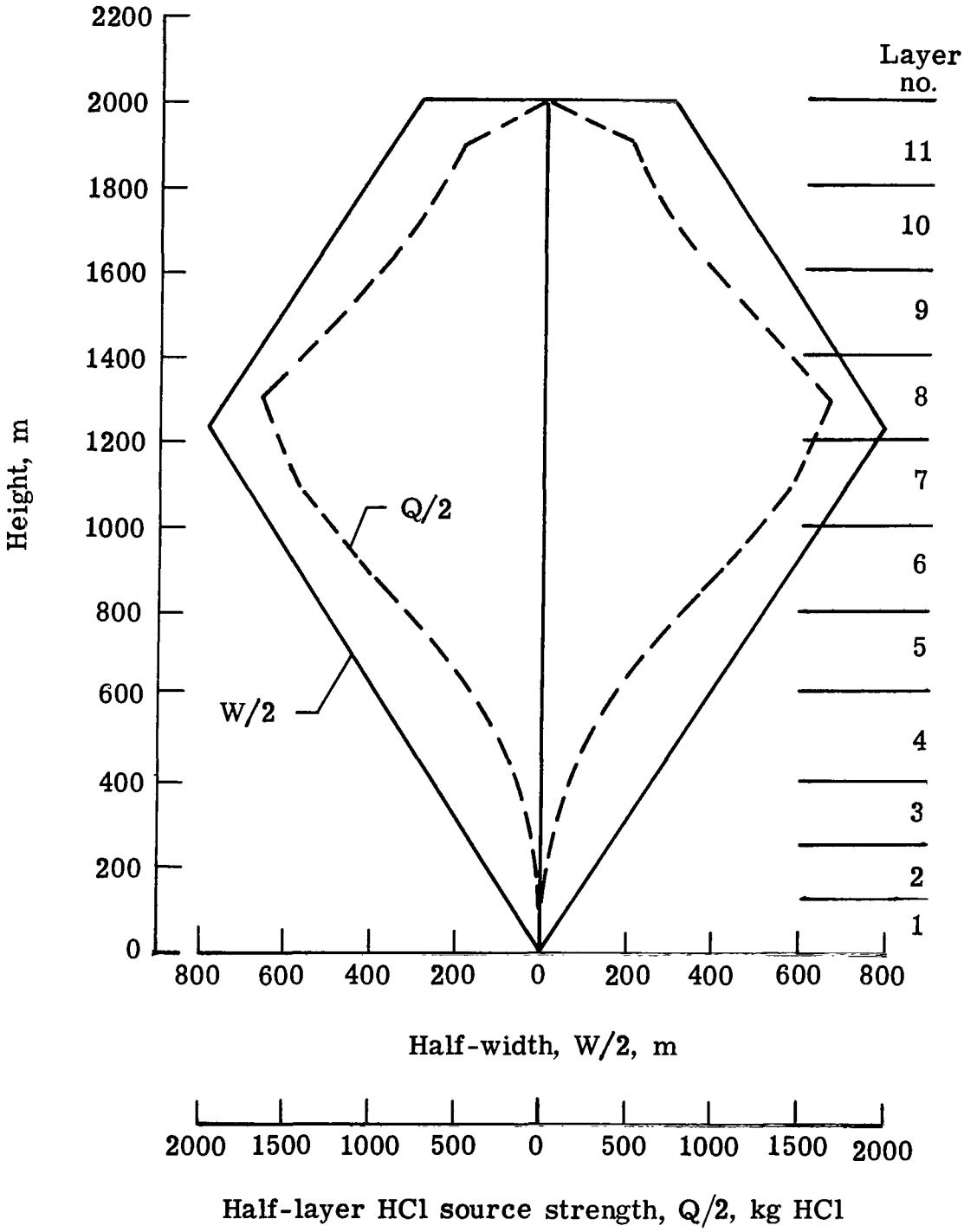

(c) Cold front passage (CFP) meteorological regime. Surface mixing layer depth is 2000 m and Z_m = 1230 m.

Figure 2.- Concluded.

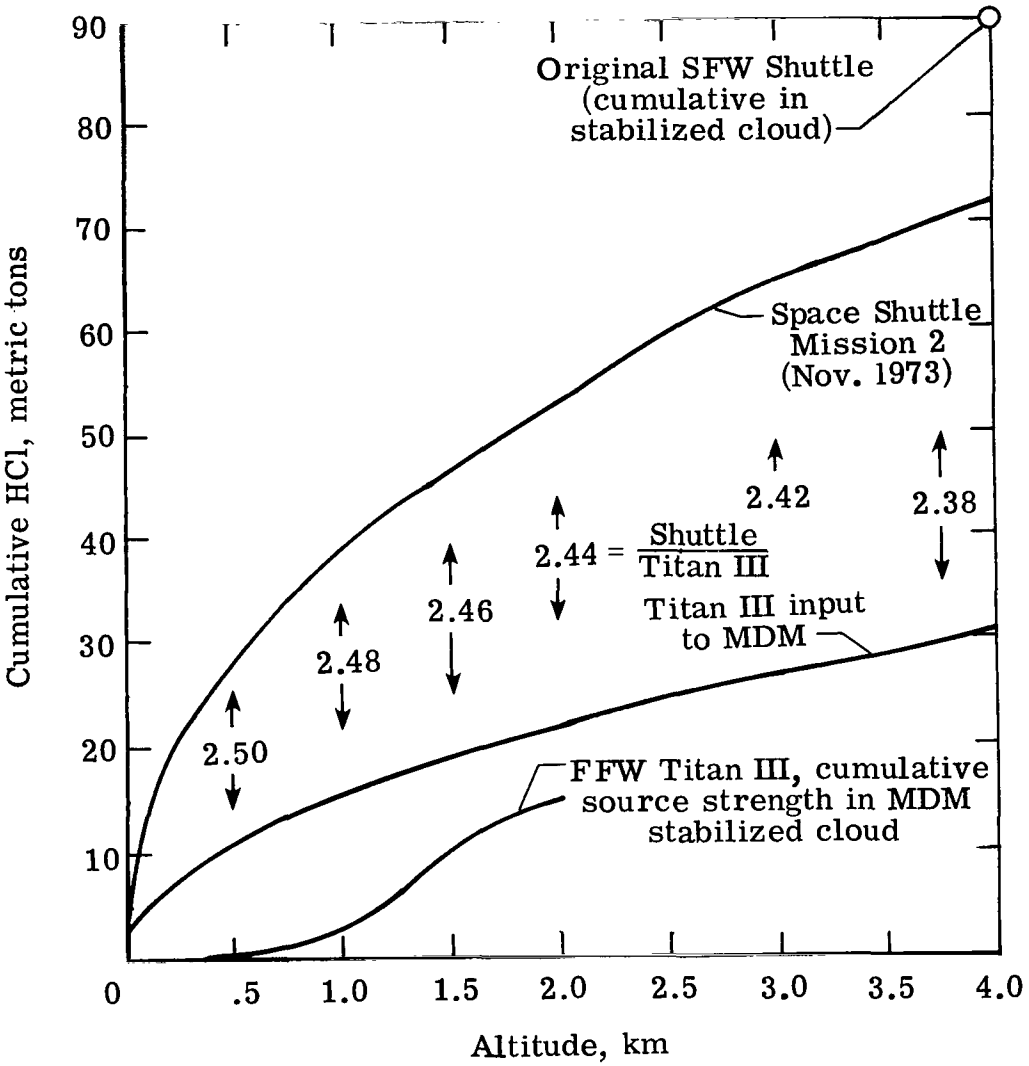

(a) Space Shuttle and Titan III launches.

Figure 3.- Summary of some HCl source strength characteristics.

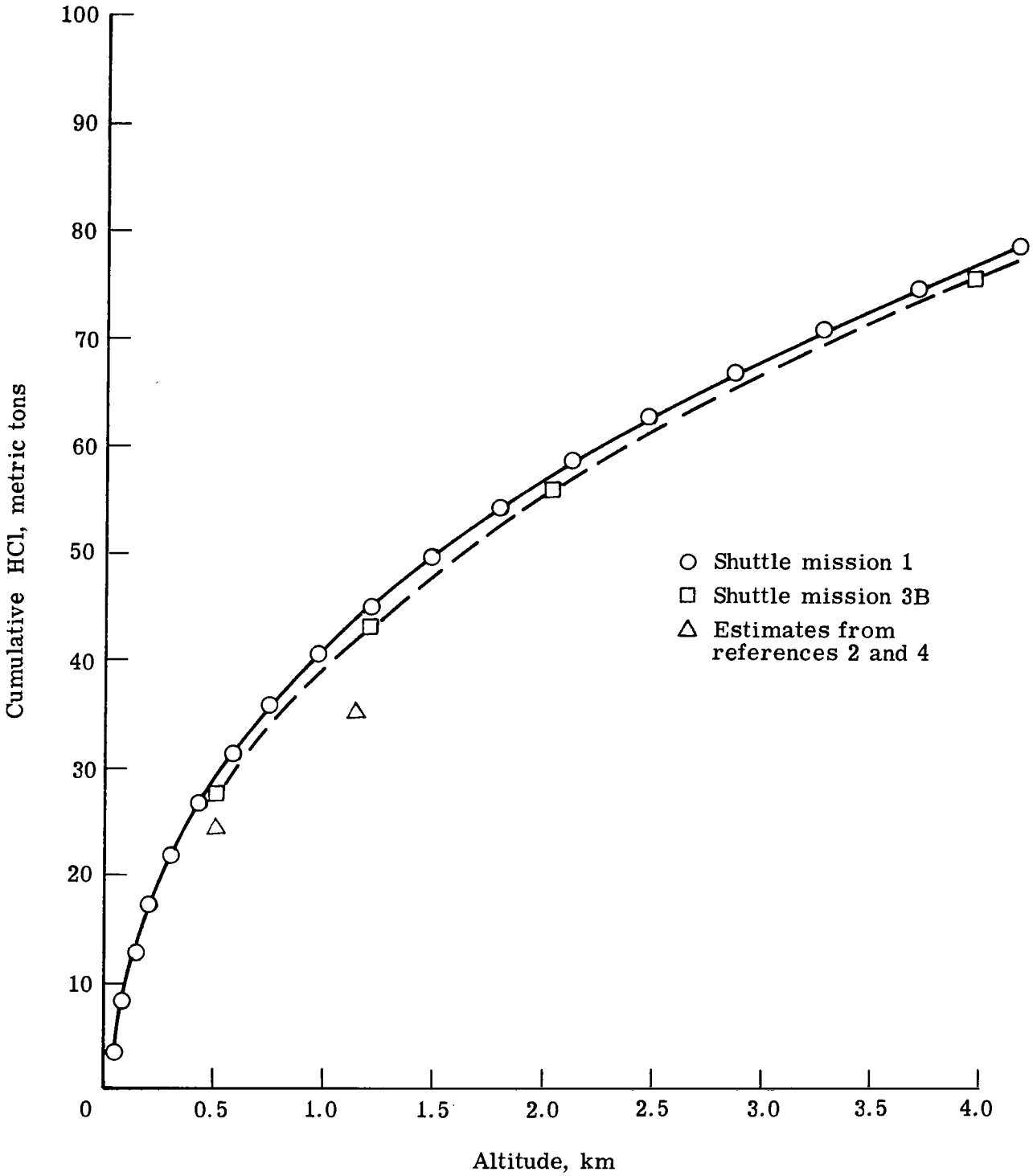

(b) Revised Space Shuttle launches (refs. 55 and 56) compared with earlier estimates (refs. 2 and 4).

Figure 3.- Concluded.

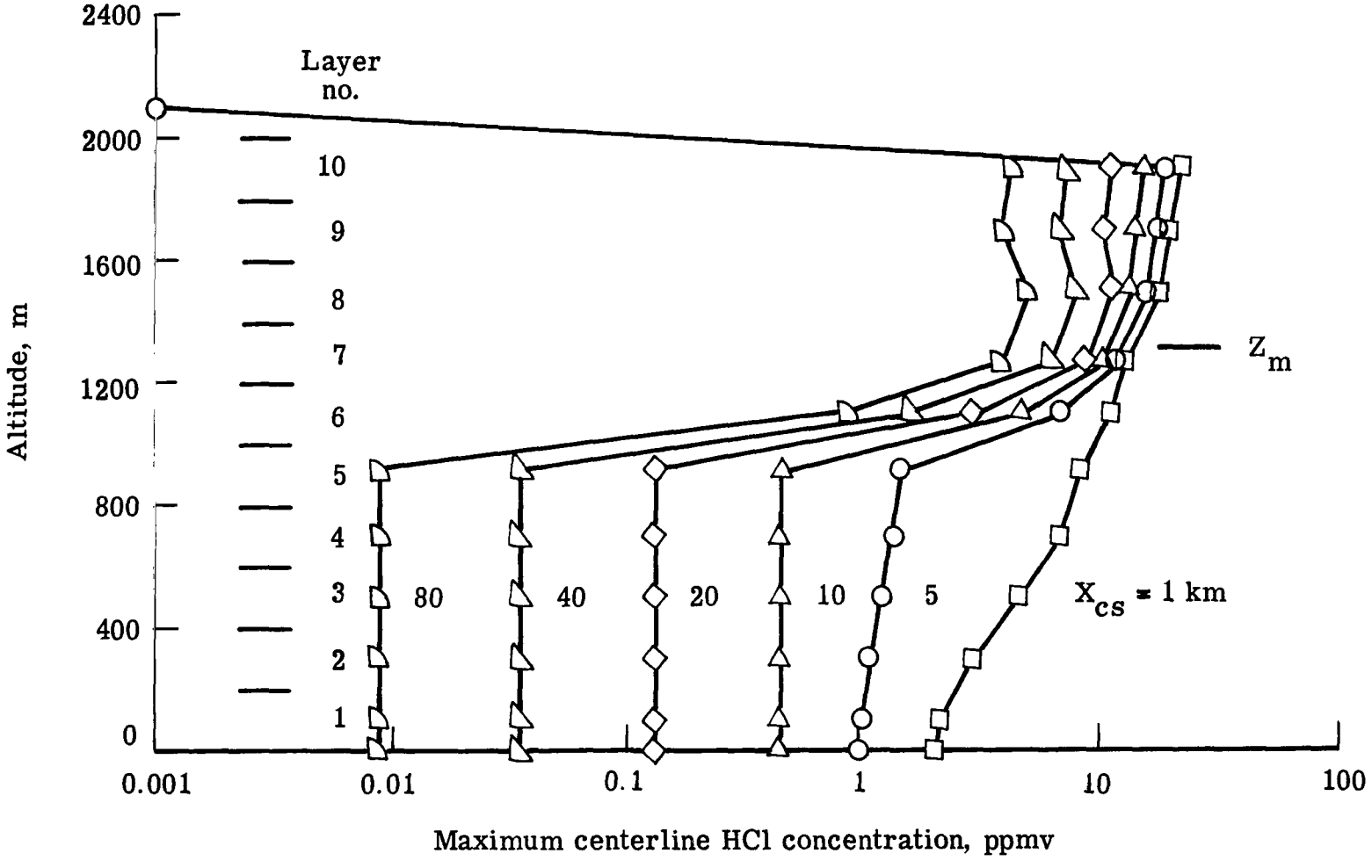

(a) Fall fair weather (FFW) meteorological regime.

Figure 4.- Vertical distribution of HCl at various downwind distances from SRM exhaust cloud altitude stabilization X_{cs} for Titan III launches under seven standard meteorological regimes at Cape Canaveral, Florida. Profiles represent maximum centerline HCl concentrations calculated from application of MDM-4(II).

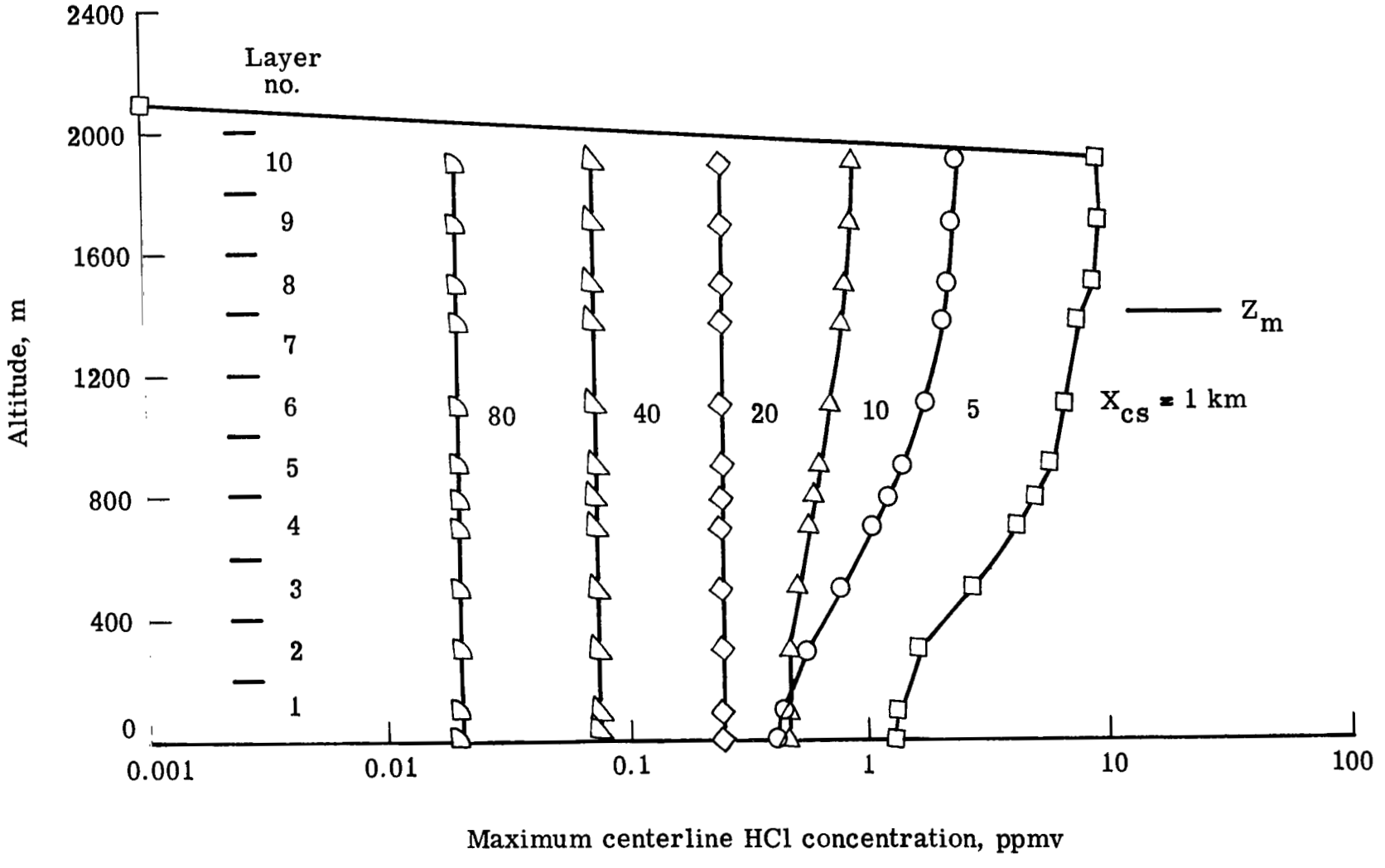

(b) Spring fair weather (SFW) meteorological regime.

Figure 4.- Continued.

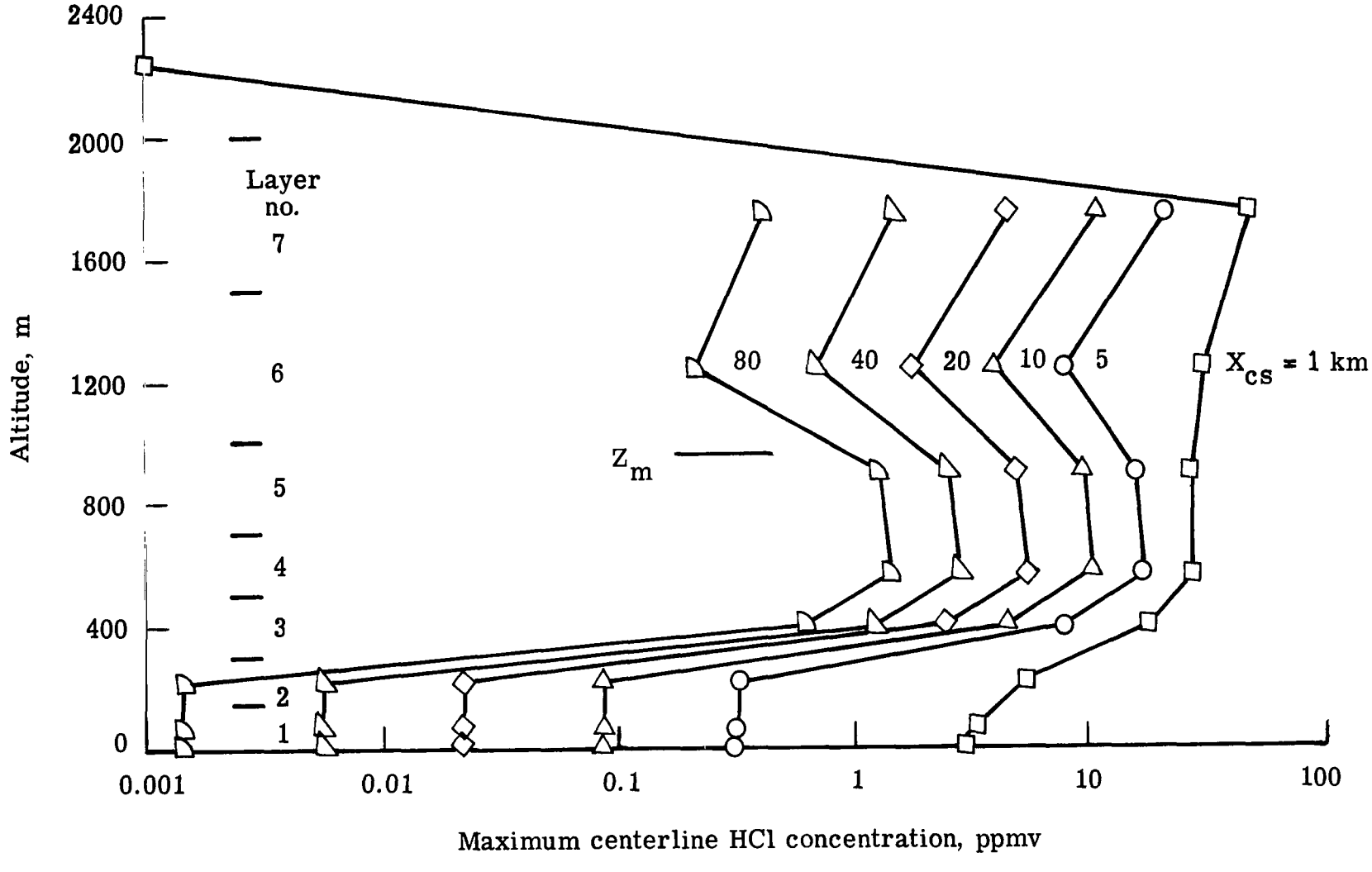

(c) Low-level sea breeze (LLSB) meteorological regime.

Figure 4.- Continued.

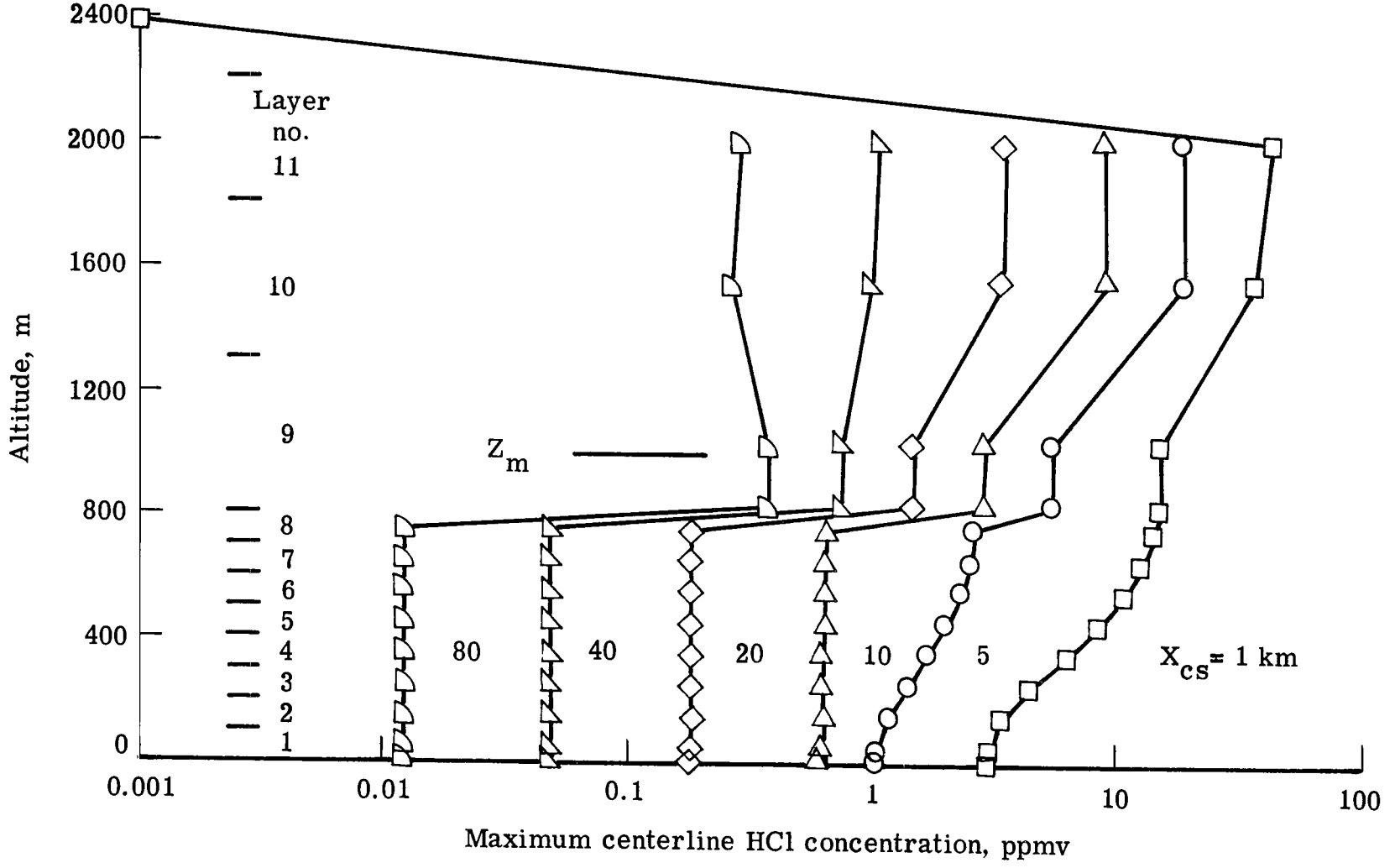

(d) Sea breeze (SB) meteorological regime.

Figure 4.- Continued.

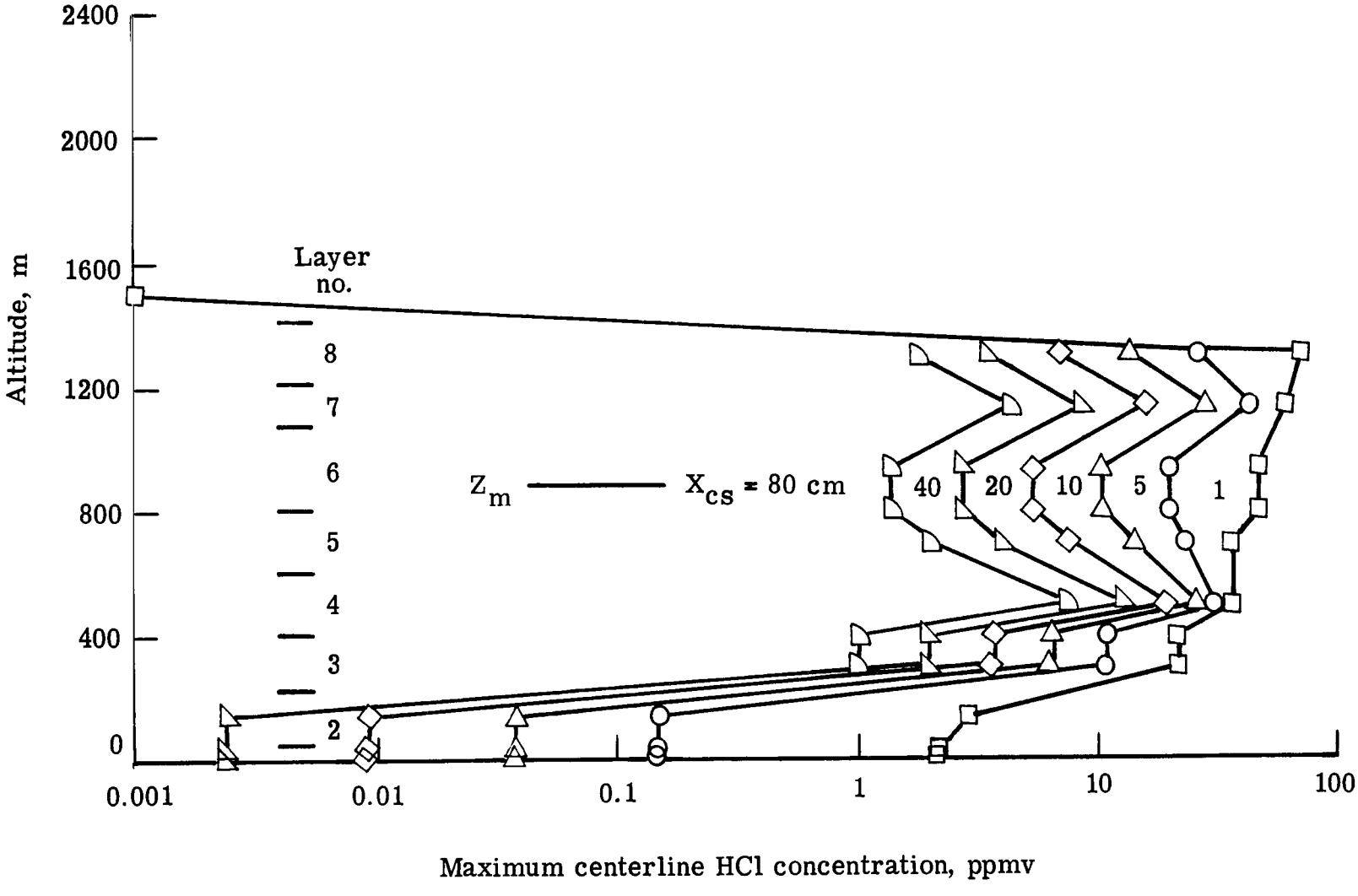

(e) Fair weather, pre-cold front (FW, Pre-CF) meteorological regime.

Figure 4.- Continued.

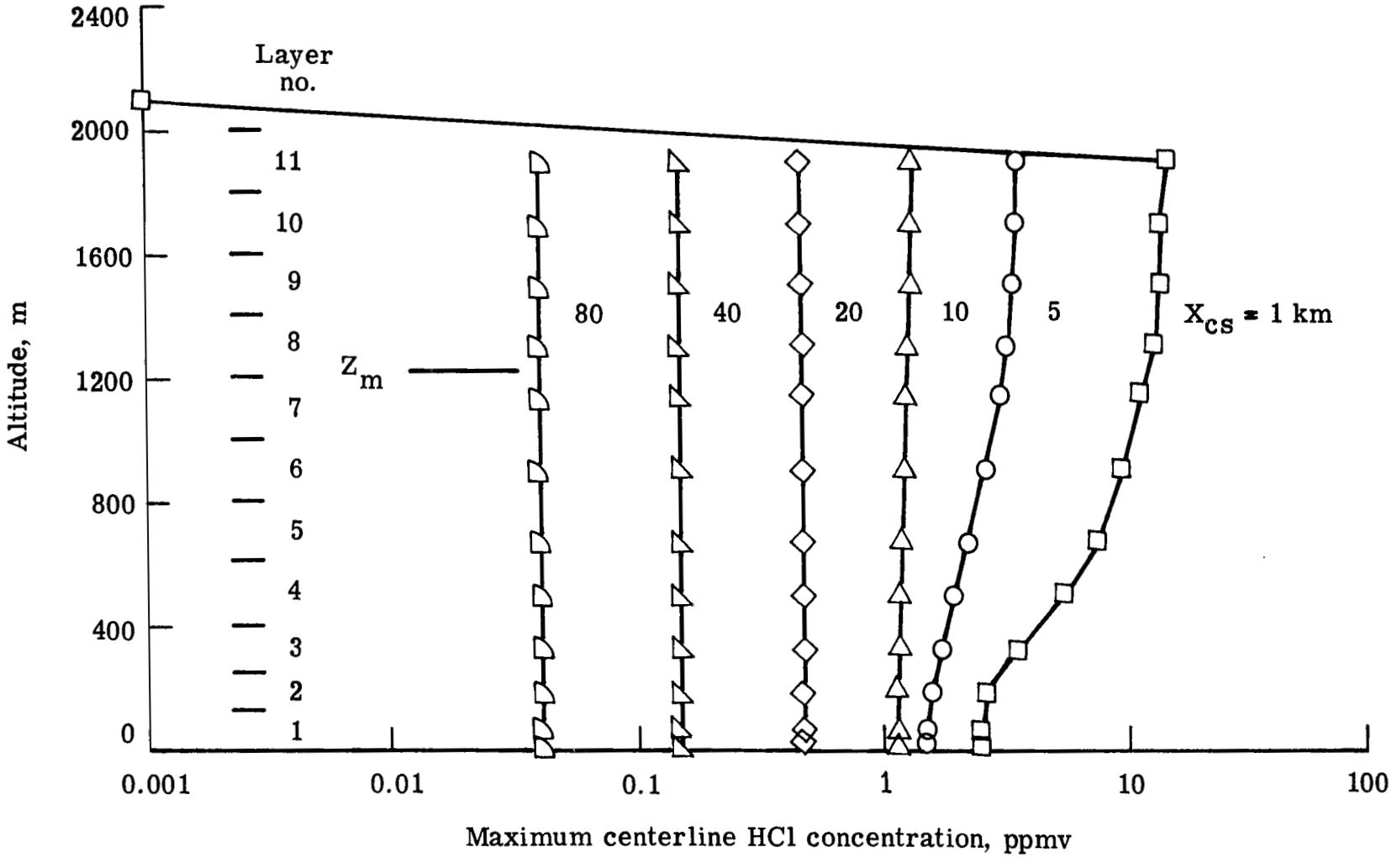

(f) Cold front passage (CFP) meteorological regime.

Figure 4.- Continued.

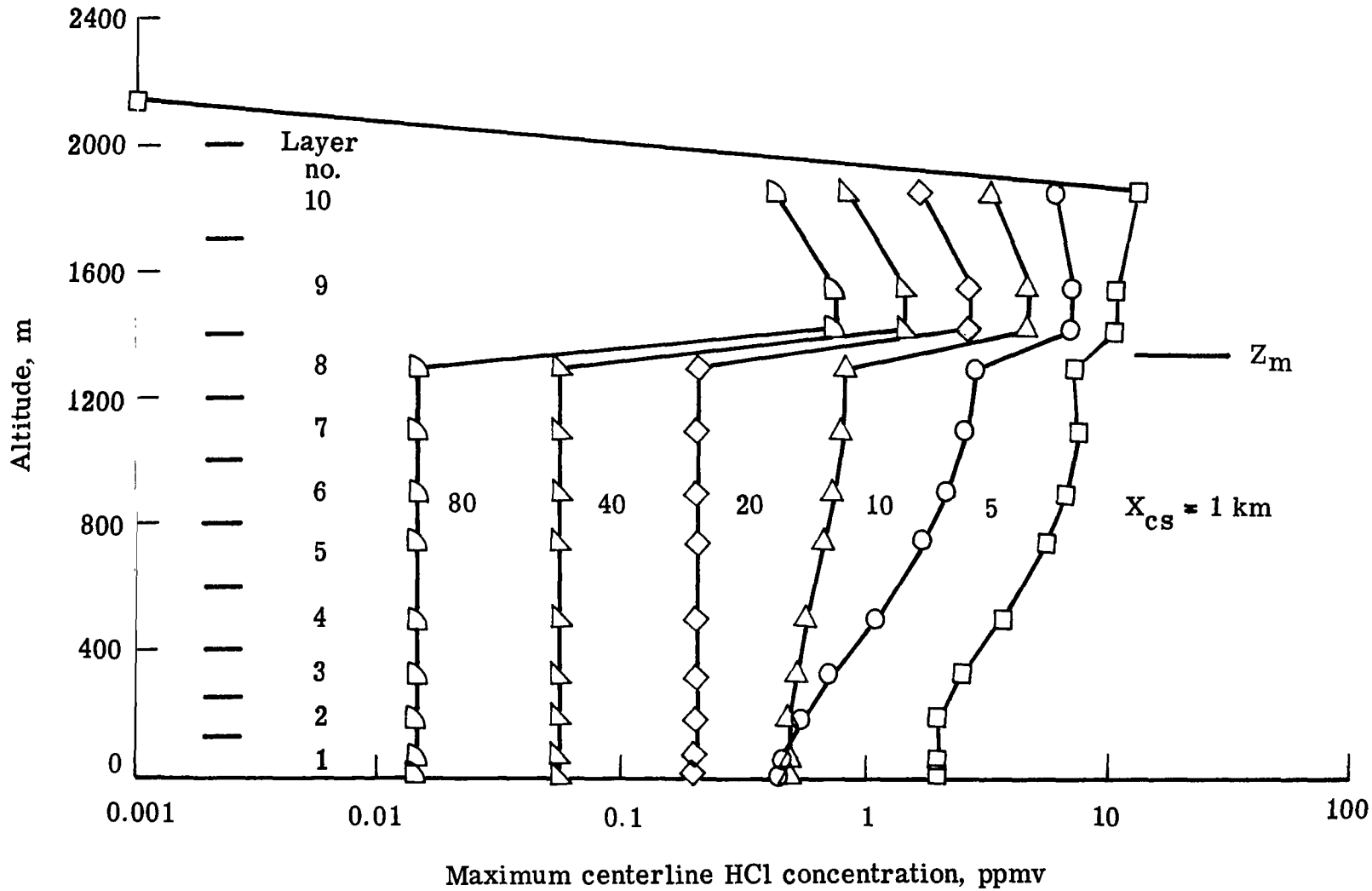

(g) Post-cold front passage (Post-CFP) meteorological regime with a normal launch.

Figure 4.- Continued.

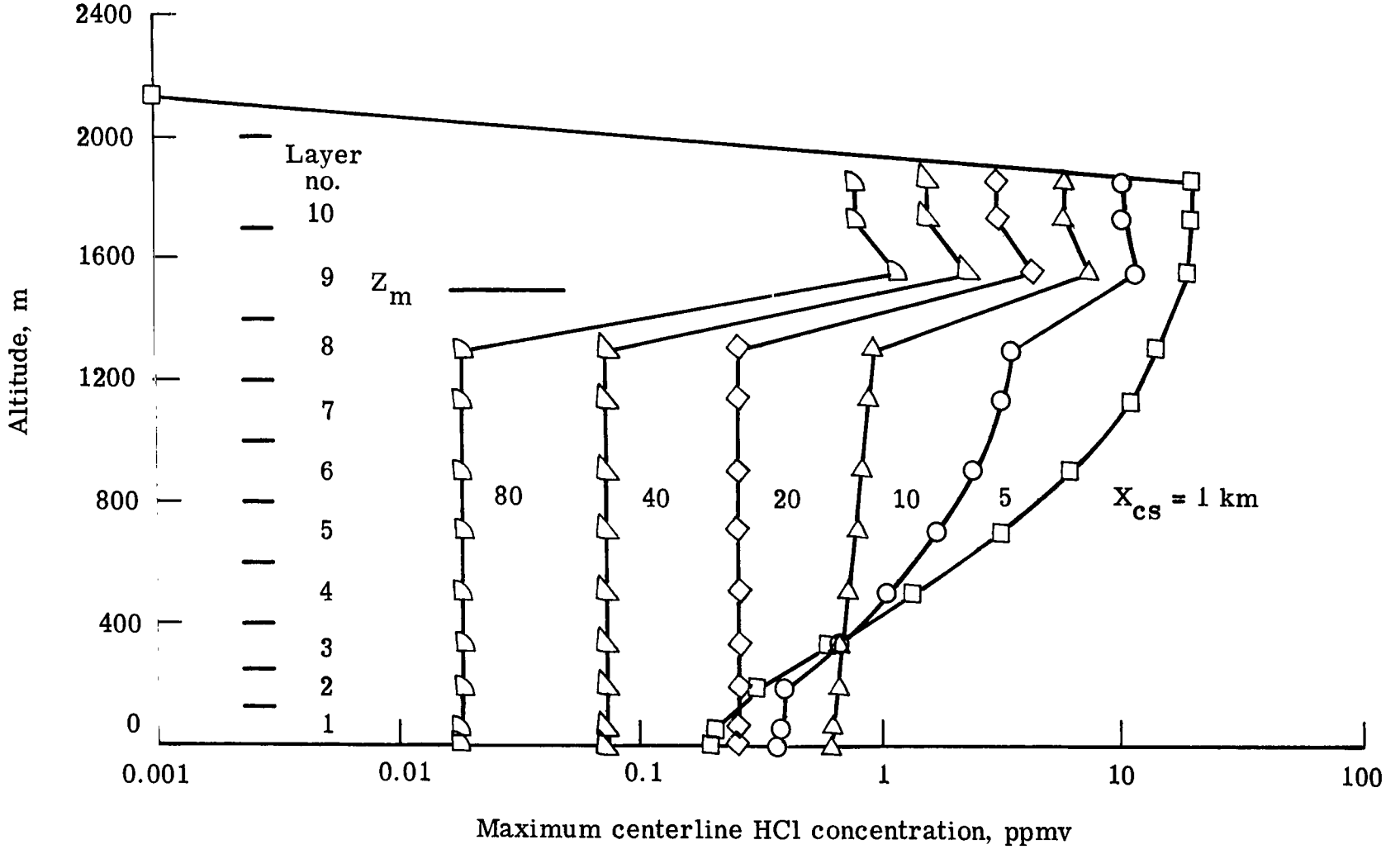

(h) Post-cold front passage meteorological regime with an abnormal (one motor burn on pad) launch (Post-CFP (pad abort)).

Figure 4.- Concluded.

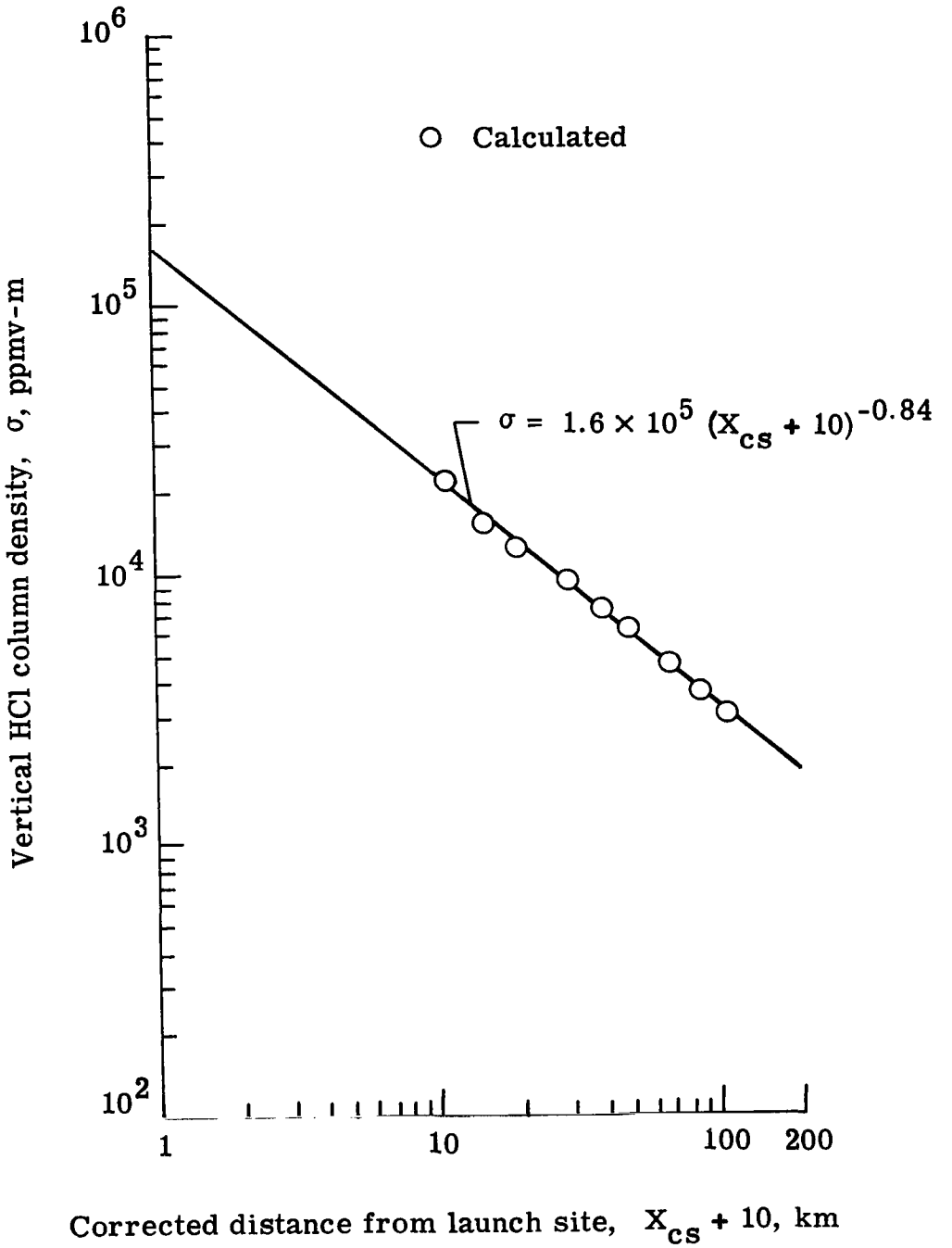

(a) For FFW meteorological regime. $m_o = 14.9 \times 10^6$ g HCl up to 2.0-km altitude; $U_c = 6.127$ m/sec.

Figure 5.- Empirically corrected fits of downwind decays of vertical HCl column density calculated for Titan III launches under seven standard meteorological conditions at Cape Canaveral, Florida.

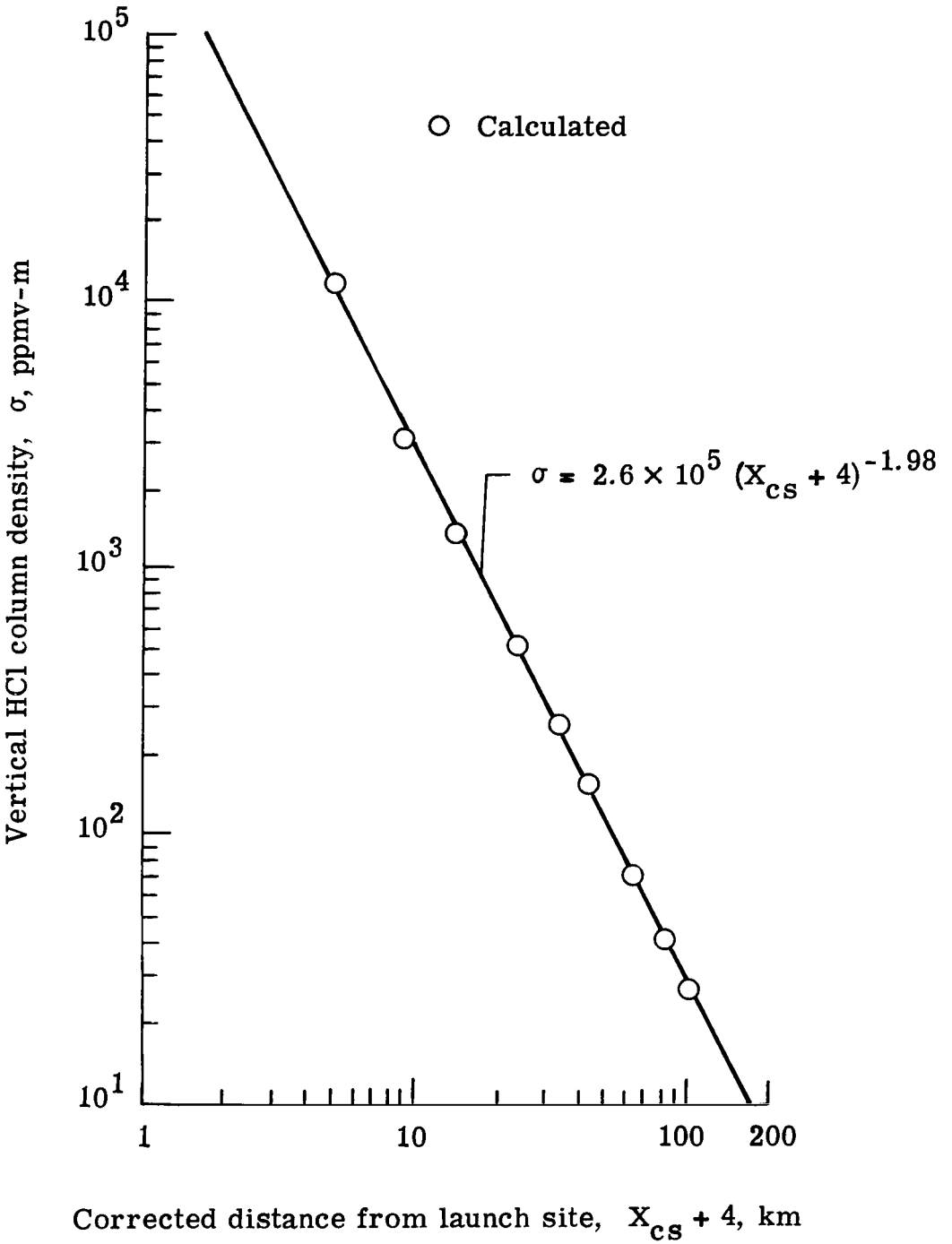

(b) For SFW meteorological regime. m_o = 14.5 × 10^6 g HCl up to 2.0-km altitude; U_c = 7.031 m/sec.

Figure 5.- Continued.

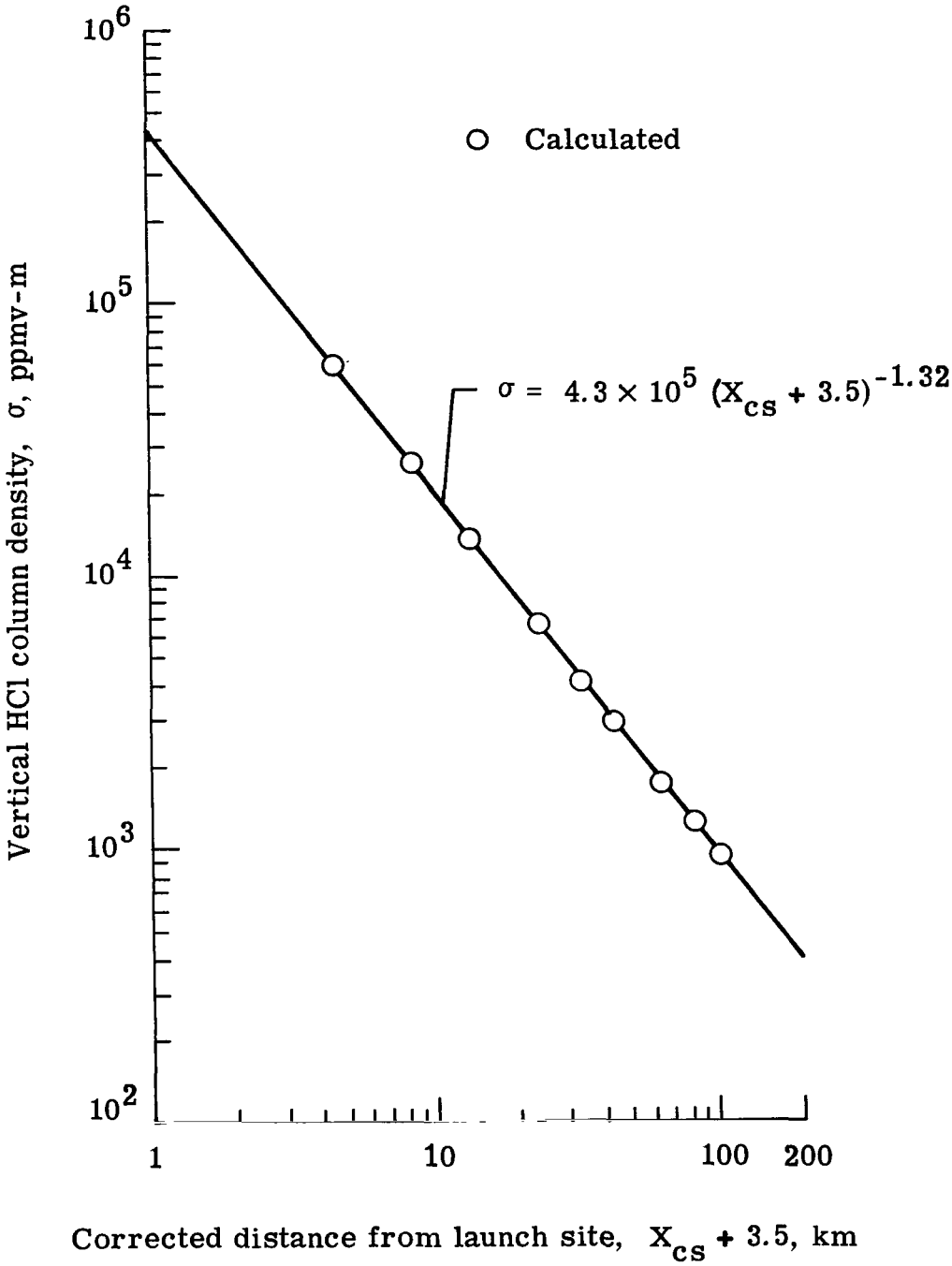

(c) For LLSB meteorological regime. $m_o = 8.63 \times 10^6$ g HCl up to 2.0-km altitude; $U_c = 6.752$ m/sec.

Figure 5.- Continued.

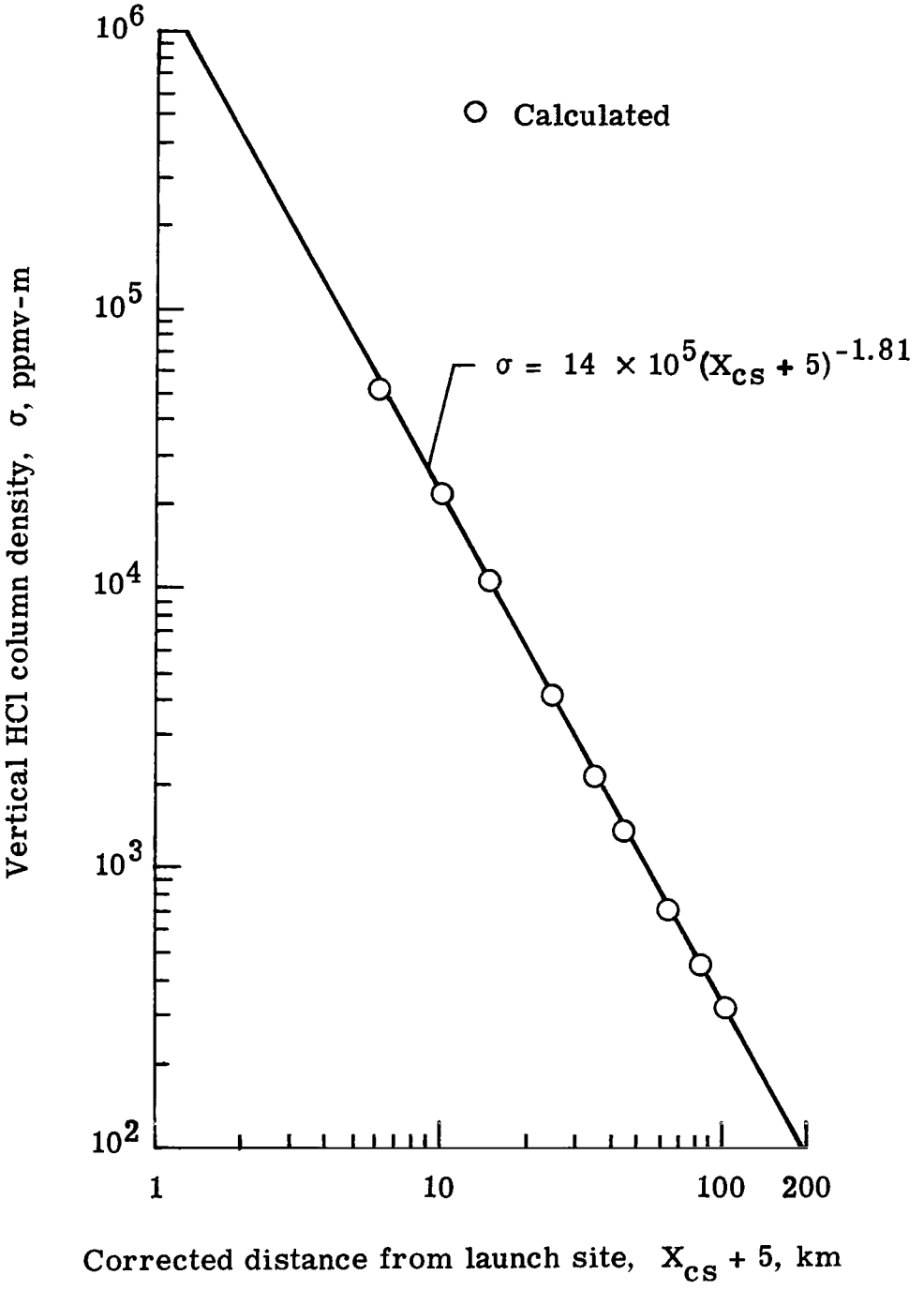

(d) For SB meteorological regime. $m_o = 10.1 \times 10^6$ g HCl up to 2.2-km altitude; $U_c = 9.923$ m/sec.

Figure 5.- Continued.

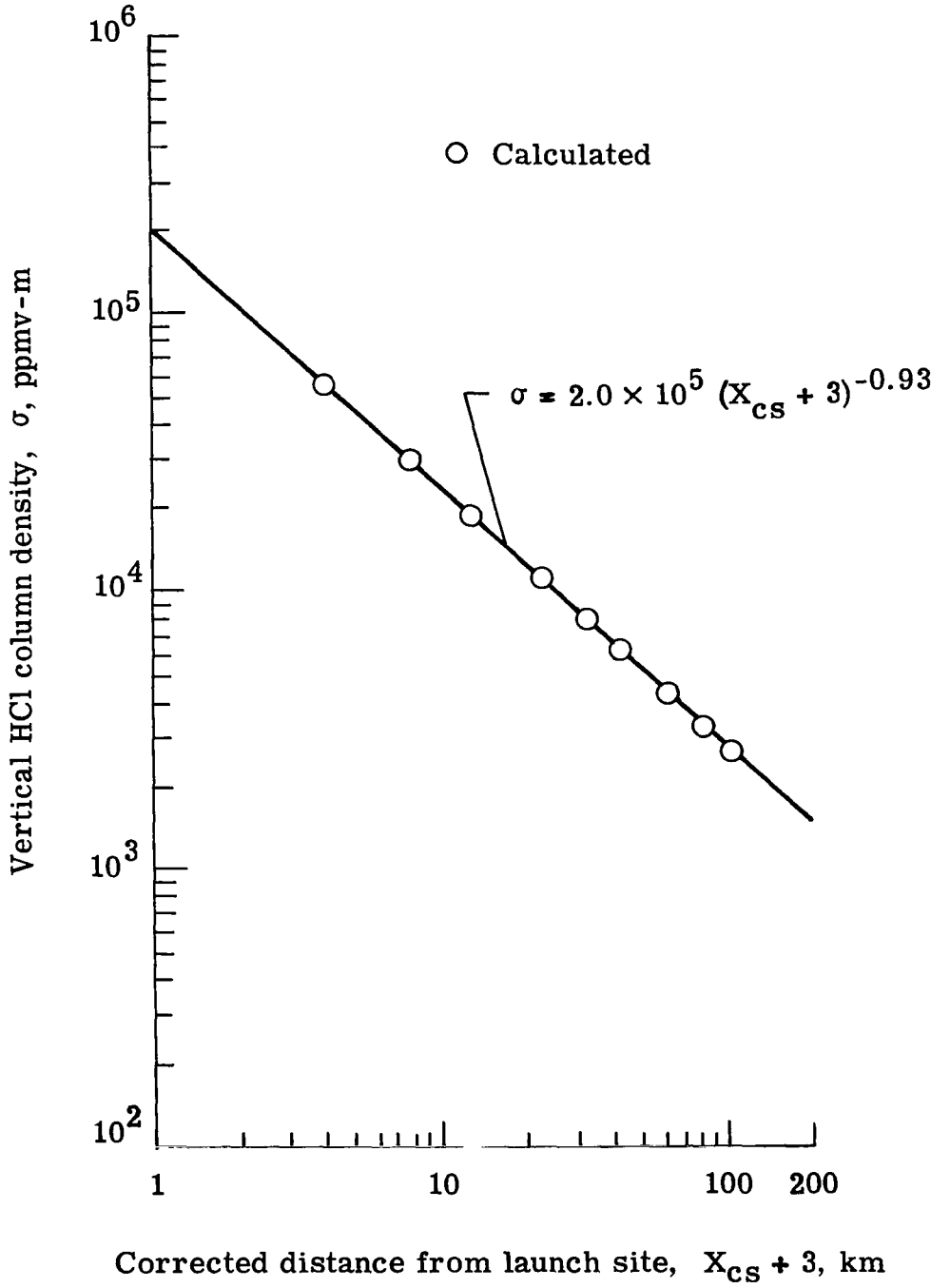

(e) For FW, pre-CF meteorological regime. $m_o = 11.9 \times 10^6$ g HCl up to 1.4-km altitude; $U_c = 2.453$ m/sec.

Figure 5.- Continued.

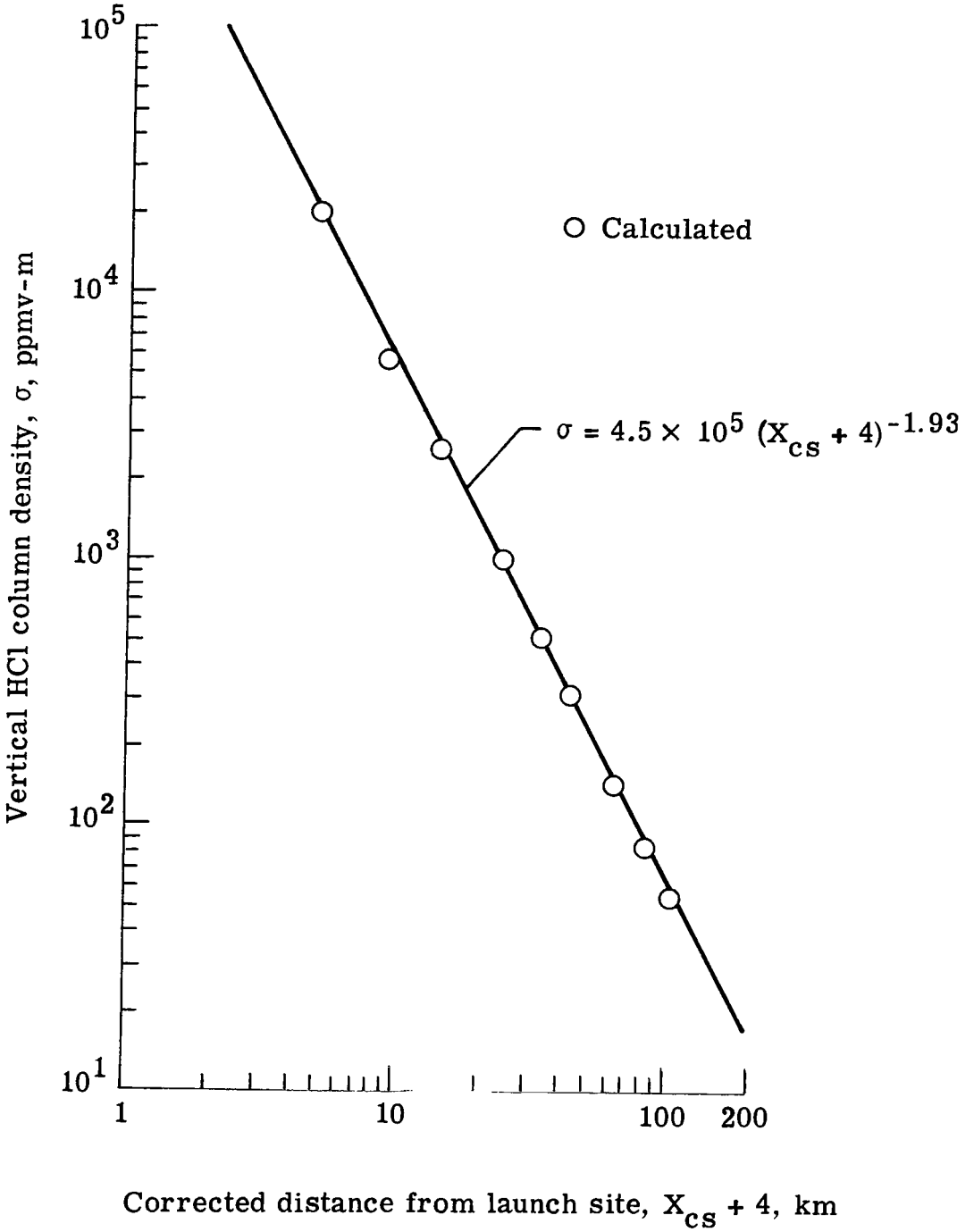

(f) For CFP meteorological regime. m_o = 15.1 × 10^6 g HCl up to 2.0-km altitude; U_c = 6.696 m/sec.

Figure 5.- Continued.

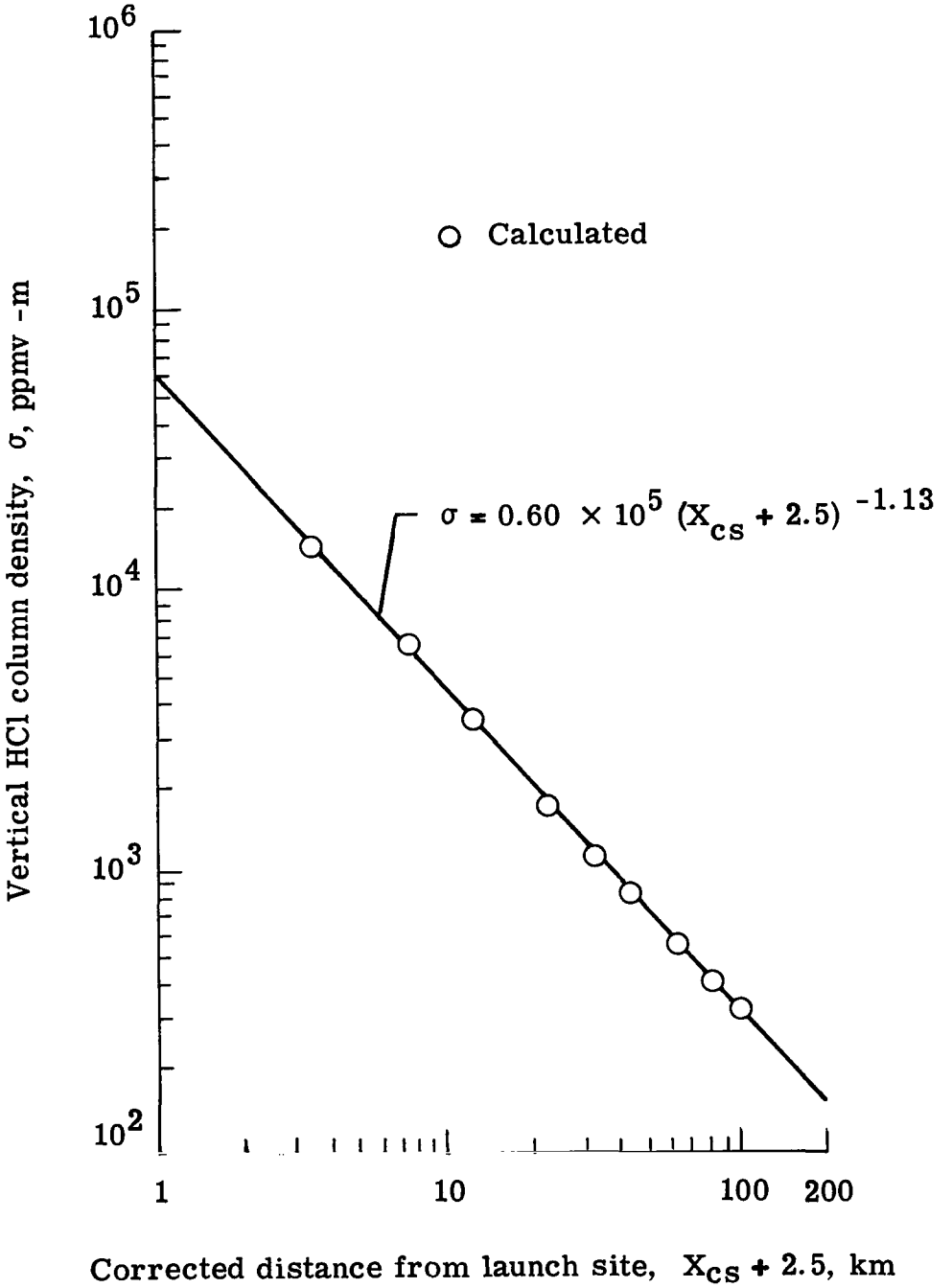

(g) For Post-CFP meteorological regime with a normal launch. m_o = 11.3 × 10^6 g HCl up to 2.0-km altitude; U_c = 8.712 m/sec.

Figure 5.- Continued.

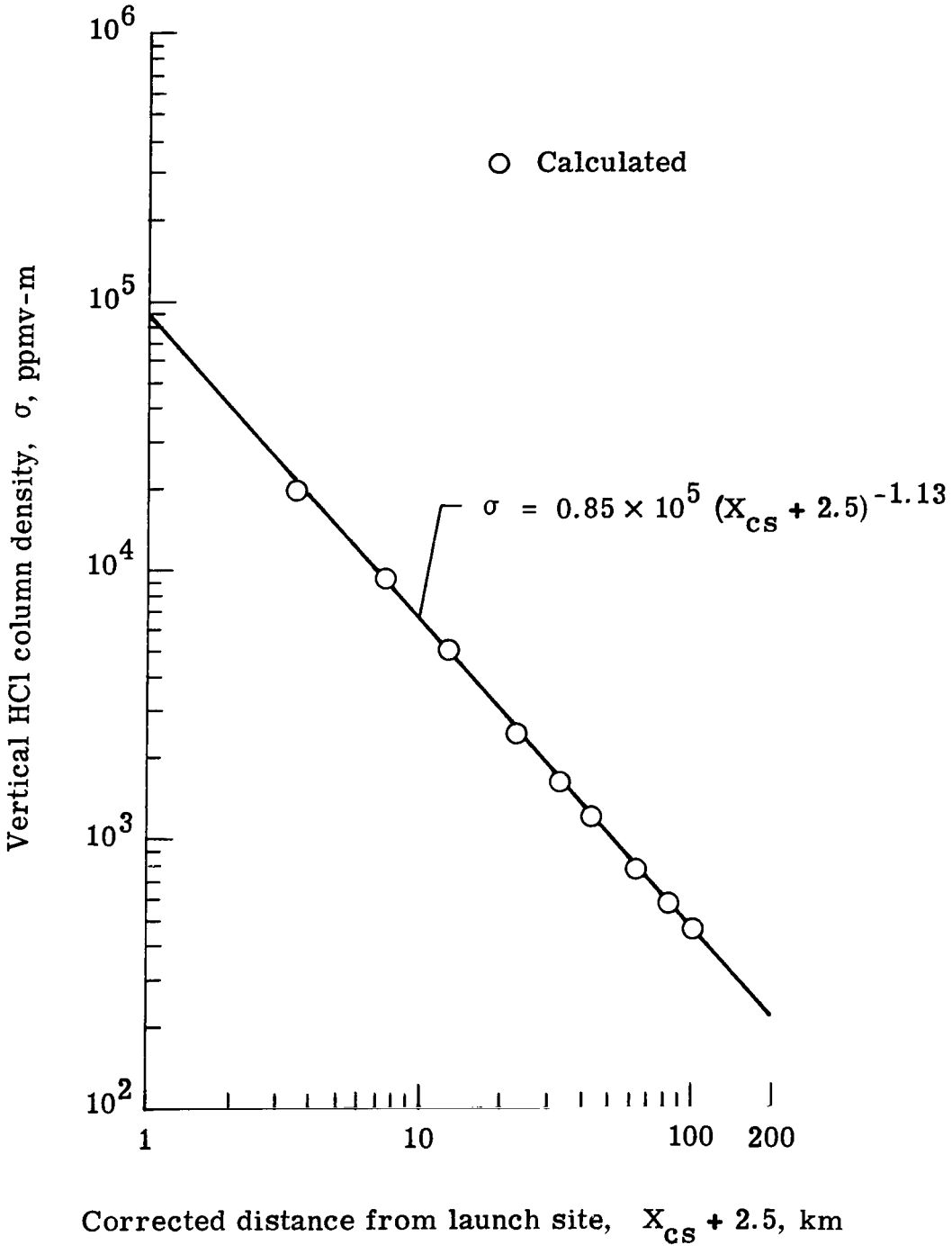

(h) For Post-CFP meteorological regime with an abnormal (one motor burn on pad) launch. $m_o = 15.9 \times 10^6$ g HCl up to 2.0-km altitude; $U_c = 9.284$ m/sec.

Figure 5.- Concluded.

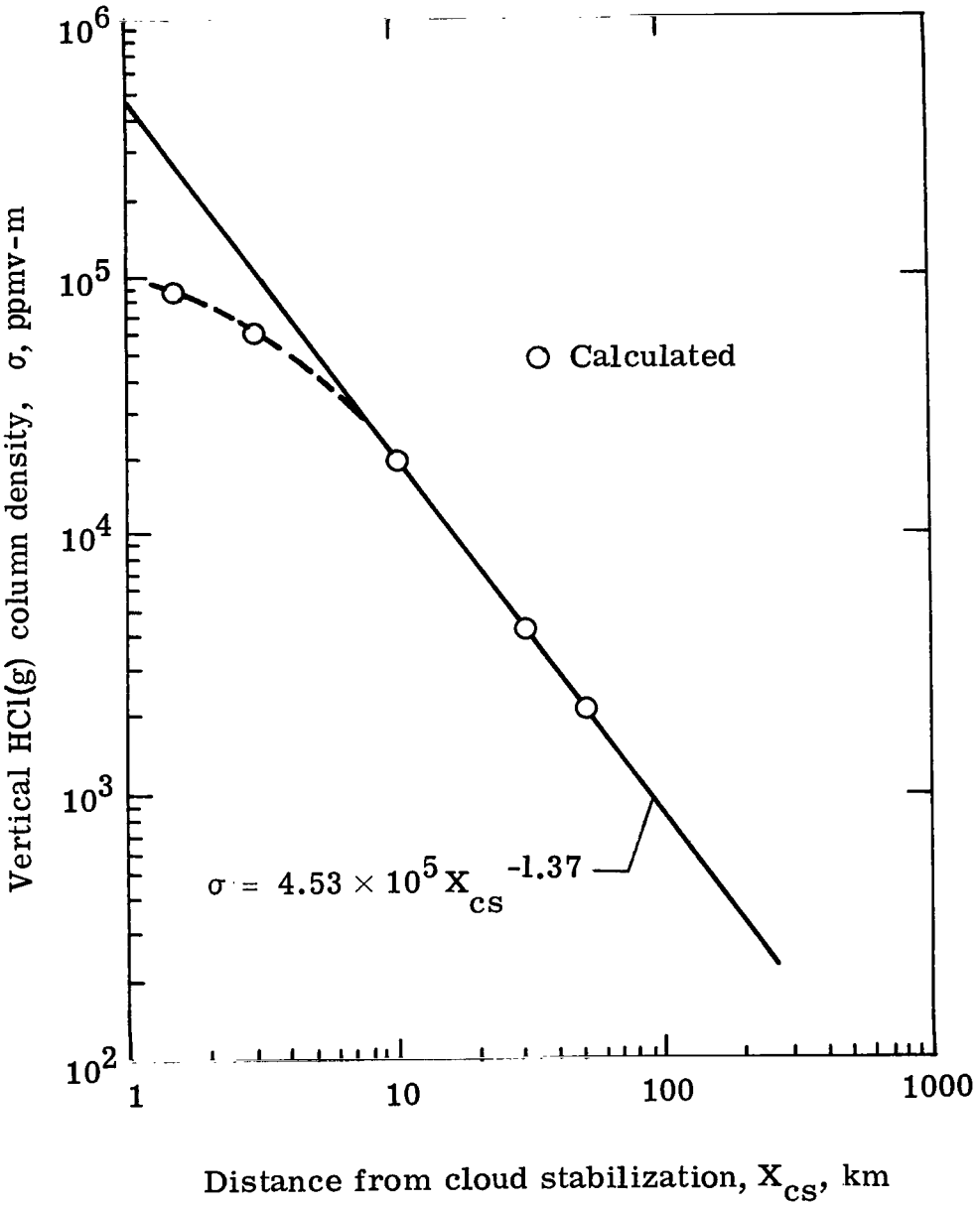

Figure 6.- Functional relationship used in reference 6 to characterize downwind dispersive decay of σ for a Space Shuttle SRM exhaust cloud under SFW meteorological regime. $m_o = 89 \times 10^6$ g HCl.

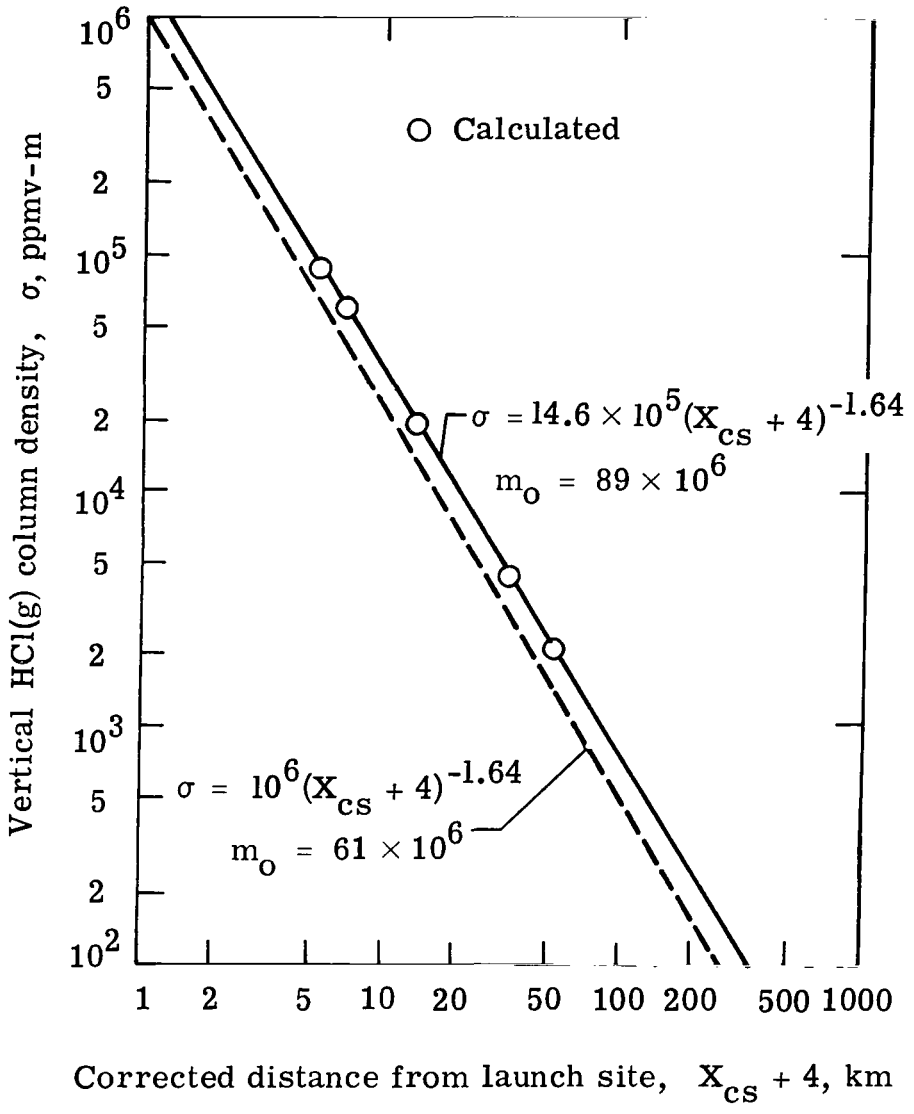

Figure 7.- Virtual-source-distance corrected empirical functions which characterize the modified downwind dispersive decay of σ for a Space Shuttle SRM exhaust cloud under SFW meteorological regime. Functions are shown for both the reference 3 (89×10^6 g HCl) source strength, and the present stabilized-cloud source strength (61×10^6 g HCl) consistent with reference 55.

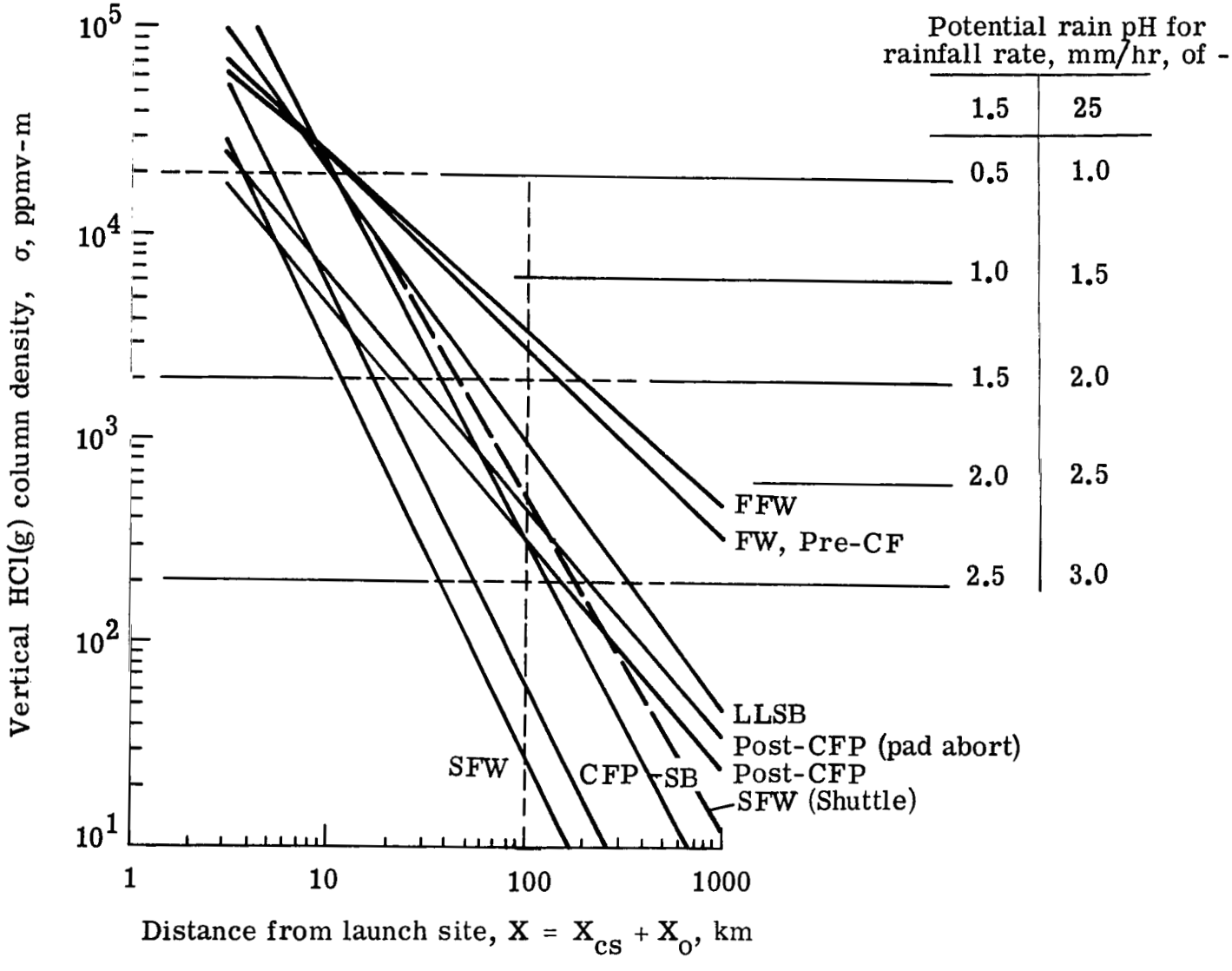

Figure 8.- Dispersive decay of σ and potential rain pH as a function of downwind distance for eight Titan III cases (solid line) and one Space Shuttle case (dashed line) of exhaust cloud dispersion. Results are based on application of MDM-4(II) to the seven standard meteorological regimes. (See table 2.)

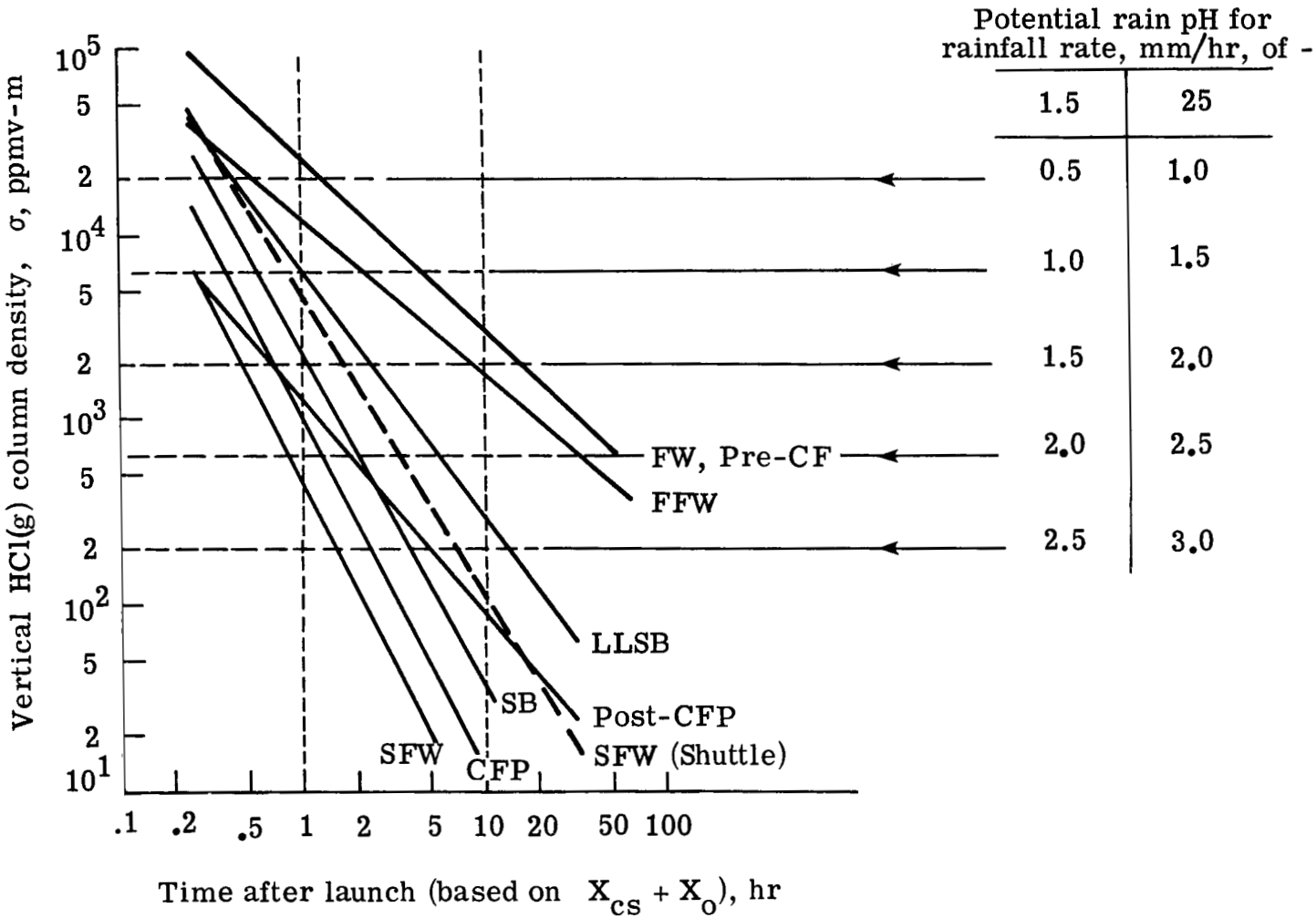

Figure 9.- Dispersive decay of σ and potential rain pH as a function of downwind drift time for seven Titan III cases (solid line) and one Space Shuttle case (dashed line) of exhaust cloud dispersion. Results are based on application of MDM-4(II) to the seven standard meteorological regimes. (See table 2.)

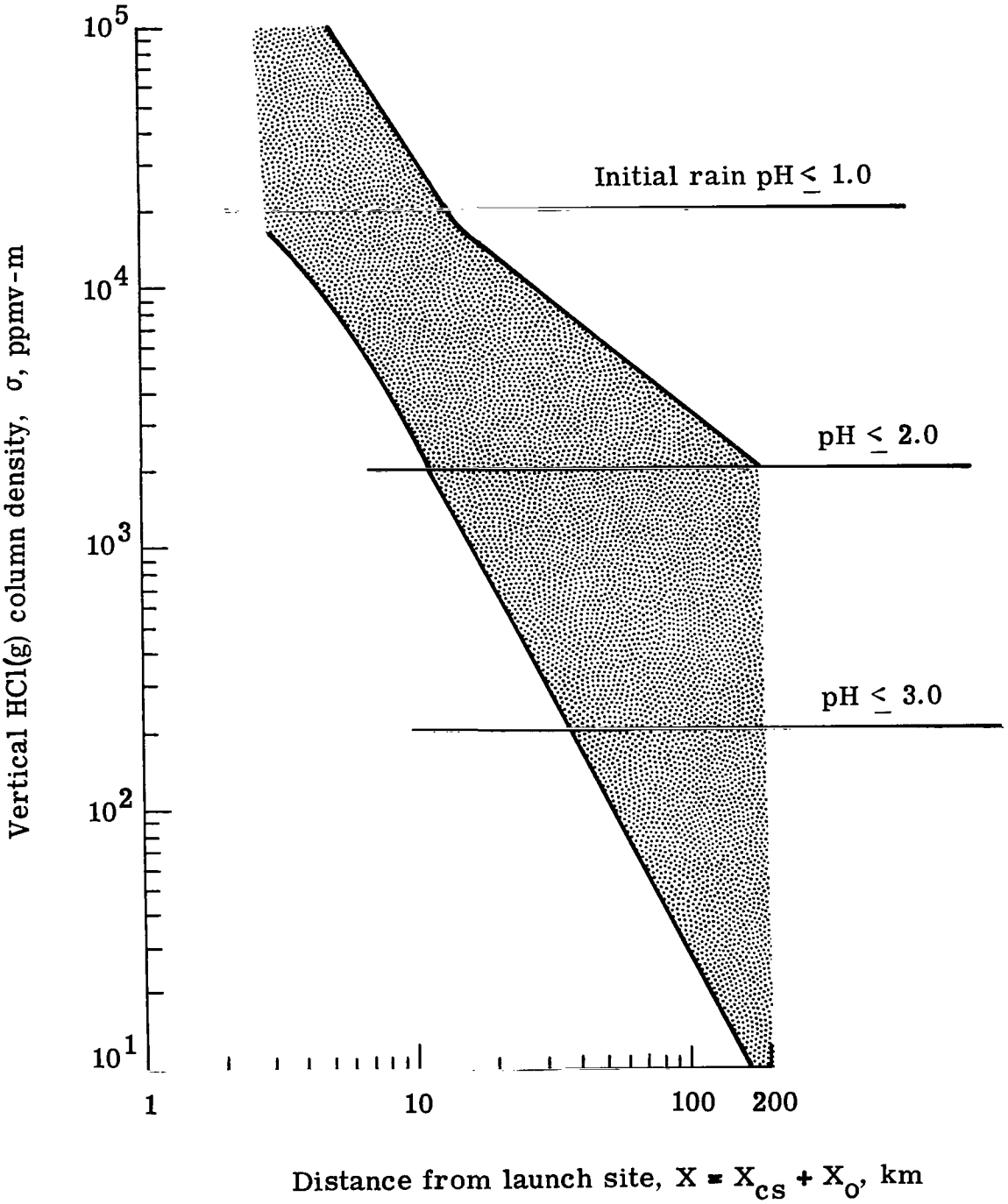

Figure 10.- Envelope for calculated dispersive decay of σ and potential rain pH for all seven Titan III meteorological cases for overland transport in the Cape Canaveral, Florida, area. The indicated potential rain pH ranges correspond to rainfall rates of up to 25 mm/hr.

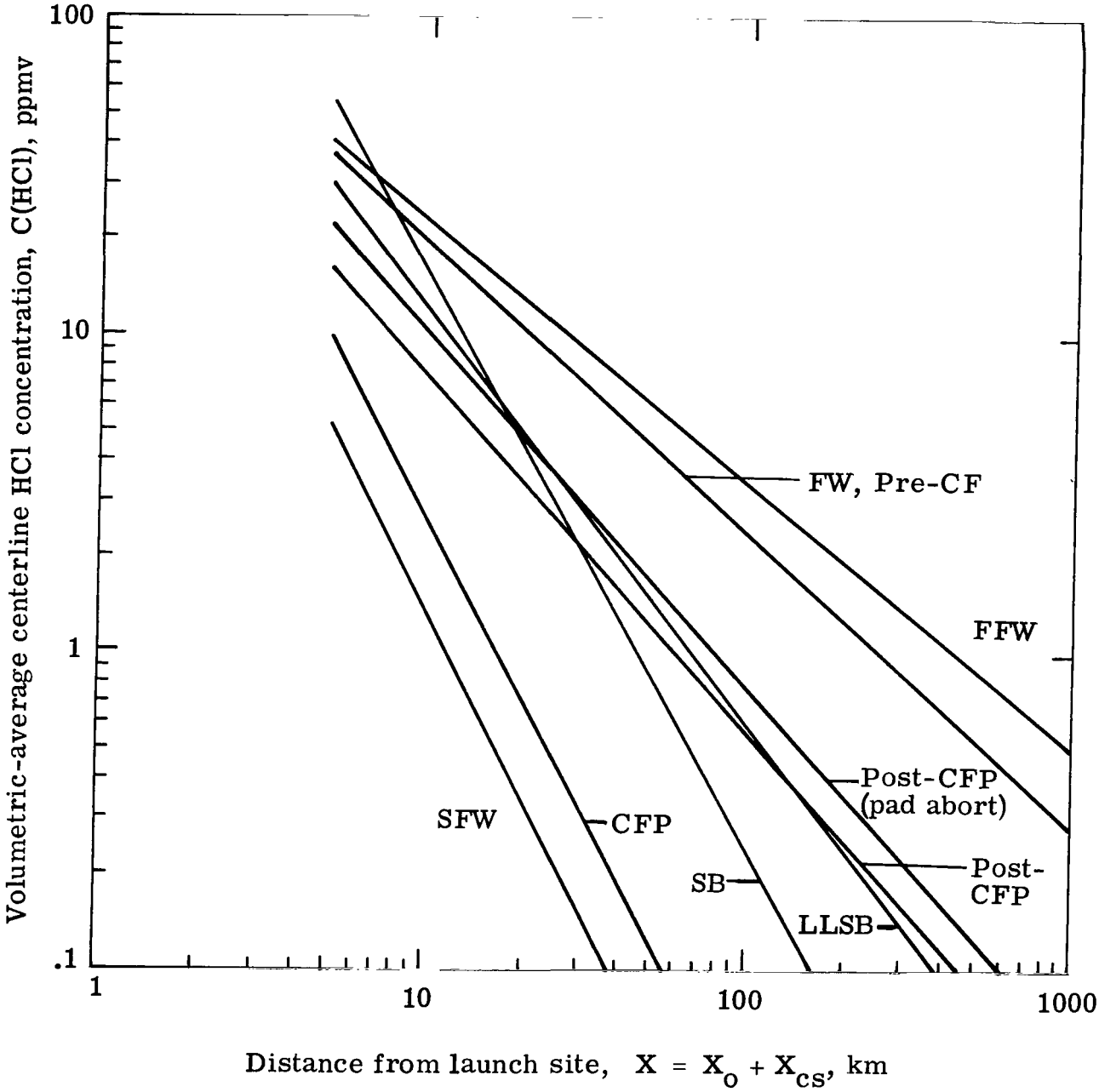

Figure 11.- Dispersive decays of volumetric-average HCl concentration calculated as functions of downwind distance for Titan III SRM exhaust clouds for seven standard meteorological conditions at Cape Canaveral, Florida.

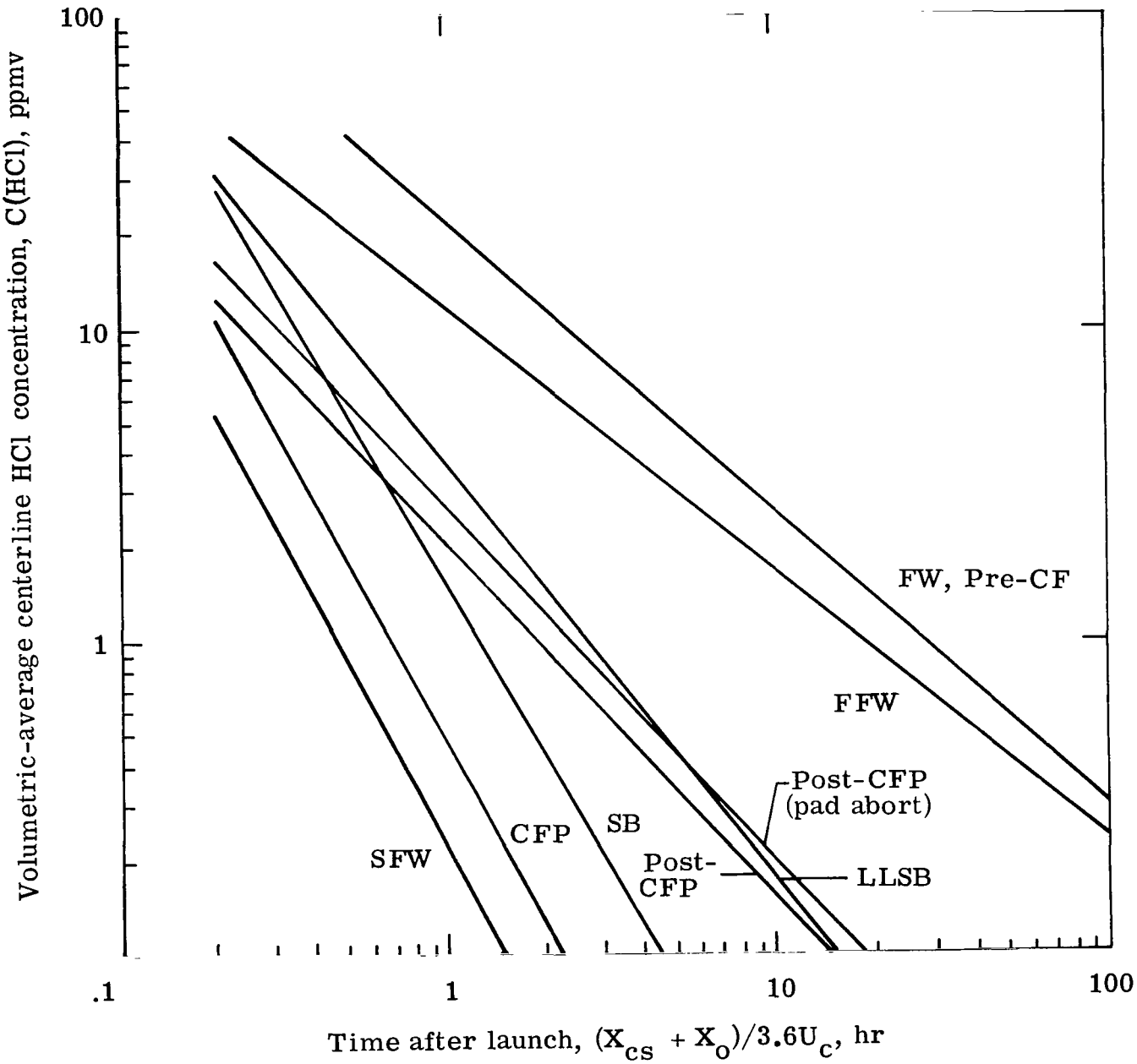

Figure 12.- Dispersive decays of volumetric-average HCl concentration calculated as functions of downwind drift time for Titan III SRM exhaust clouds for seven standard meteorological conditions at Cape Canaveral, Florida.

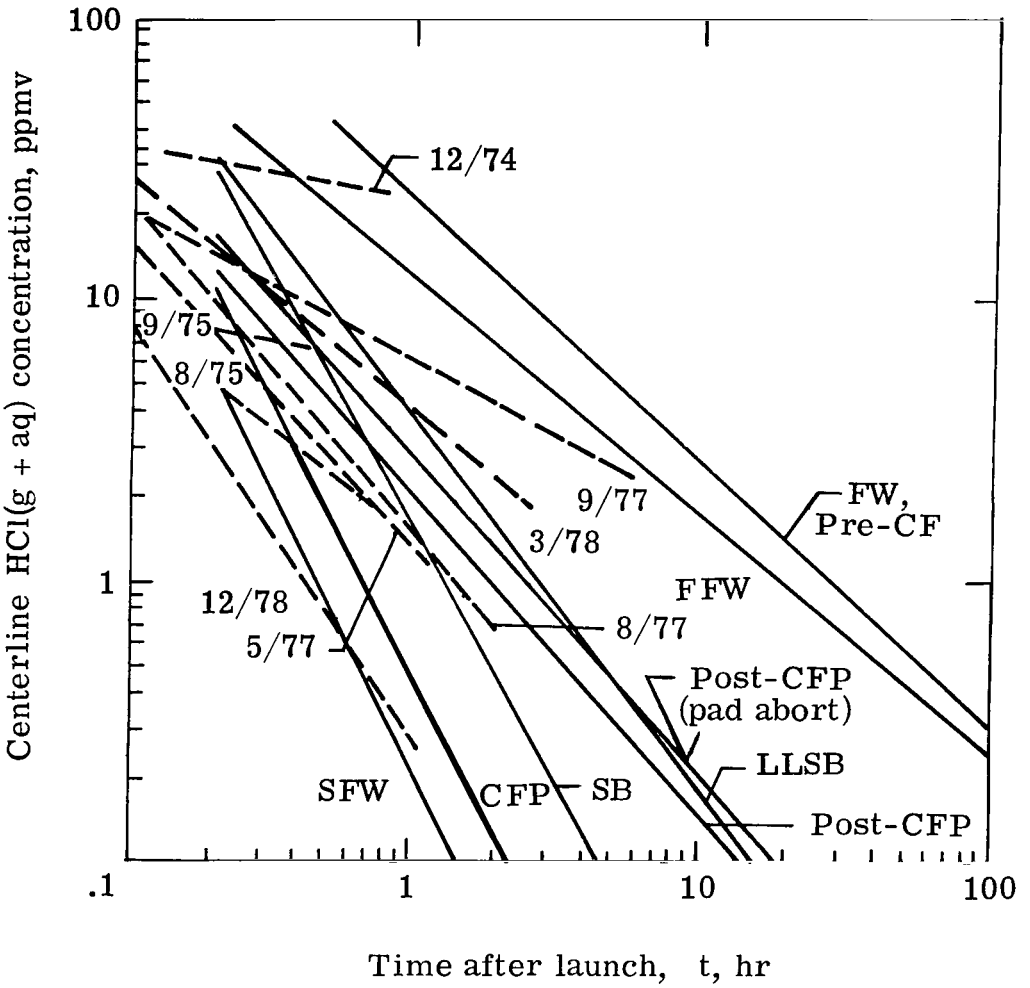

Figure 13.- Calculated decays (solid line) of in-cloud HCl concentration (vertical average, cloud centerline) compared with empirical fits of experimental measurements (dashed line) of peak ($\geq$1 sec) in-cloud HCl for eight Titan III launches at Cape Canaveral, Florida. Note that the various calculated and experimental HCl decays are not comparable on a one-to-one basis, since the respective input and actual launch meteorologies differed. (From ref. 48.)

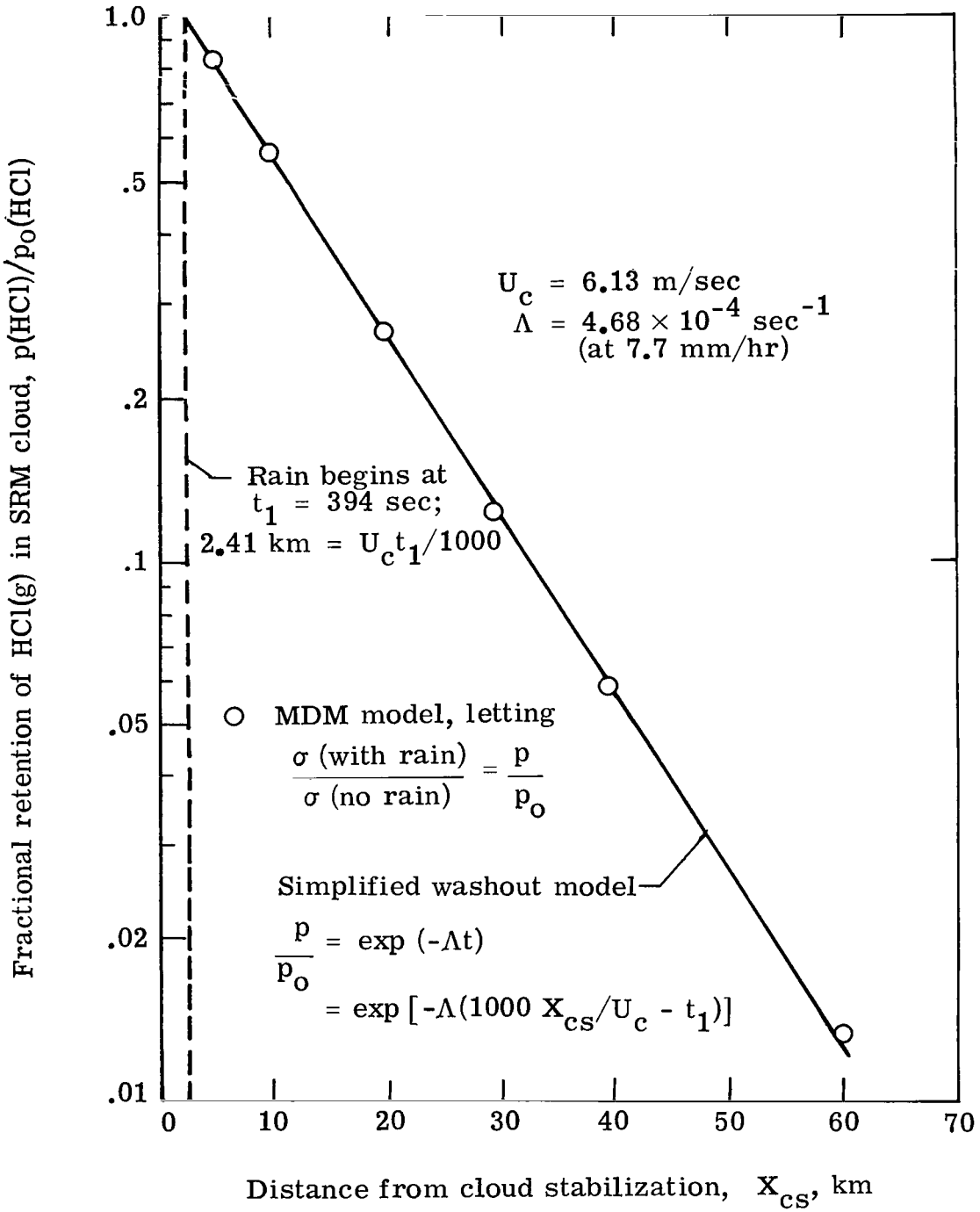

(a) FFW Titan III exhaust cloud.

Figure 14.- Results of check on MDM-5(II) calculations of HCl(g) washout from SRM exhaust clouds.

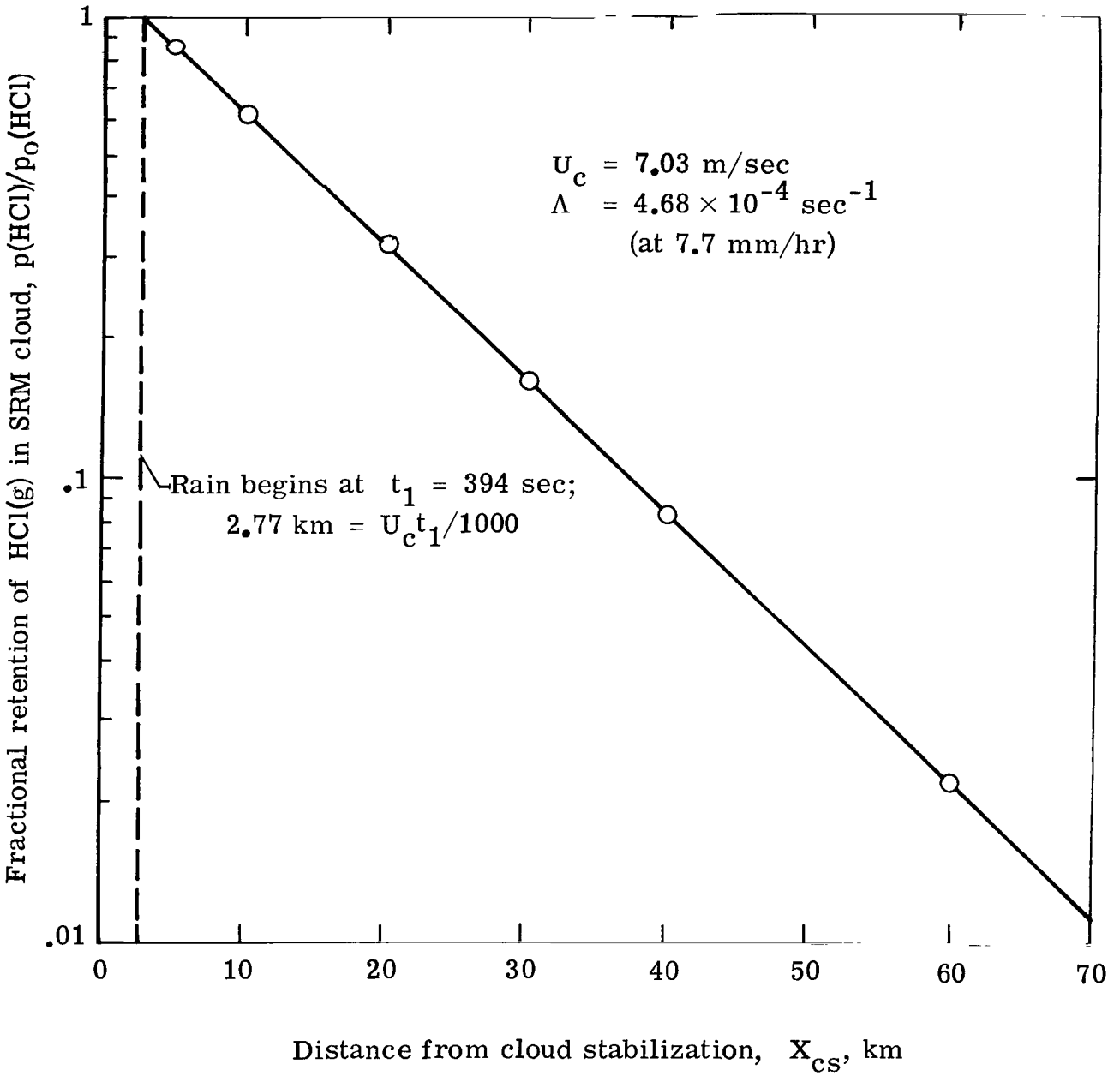

(b) SFW Titan III exhaust cloud.

Figure 14.- Concluded.

1. Report No.	2. Government Accession No.	3. Recipient's Catalog No.
NASA TP-1956		

4. Title and Subtitle	5. Report Date
APPLICATION OF A GAUSSIAN MULTILAYER DIFFUSION MODEL TO CHARACTERIZE DISPERSION OF VERTICAL HCl COLUMN DENSITY IN ROCKET EXHAUST CLOUDS	December 1981
	6. Performing Organization Code 989-15-20-02

7. Author(s)	8. Performing Organization Report No.
G. L. Pellett and W. L. Staton	L-14715
	10. Work Unit No.

9. Performing Organization Name and Address	11. Contract or Grant No.
NASA Langley Research Center Hampton, VA 23665	
	13. Type of Report and Period Covered Technical Paper

12. Sponsoring Agency Name and Address	14. Sponsoring Agency Code
National Aeronautics and Space Administration Washington, DC 20546	

15. Supplementary Notes

16. Abstract

Solid rocket exhaust cloud dispersion cases, based on seven meteorological regimes for overland advection in the Cape Canaveral, Florida, area, are examined for launch-vehicle environmental impacts. They include a Space Shuttle case (60 metric tons HCl exhausted below 2.5-km altitude) and all seven meteorological cases for the Titan III, which exhausts 60 percent less HCl. Vertical HCl column densities σ are well characterized by decay expressions $\sigma = \alpha X^{-\beta}$, where α and β are constants and X is downwind distance corrected for virtual-source location. Averaged HCl concentrations C(HCl) are also given. Decays of σ and C(HCl) differ greatly among the regimes. Significantly large σ and C(HCl) are shown possible out to 50 km and 5 hr, which suggests possible acid-rain impacts. C(HCl) decays are also compared with recent in-cloud peak-HCl data from eight Titan III launches. Power-law data fits are adequate; the total data span is >100 times for >1 hr; an envelope bounding C(HCl) also bounds HCl data for >0.2 hr; and data span at 1 hr (0.3 to 20 ppmv HCl) matches C(HCl). Finally, measured β varies principally from 1.25 to 0.54, whereas calculated β varies from 1.98 to 0.83. This difference is discussed. While good overall agreement provides some validation of the model, its limitations are considerable and a dynamics model is clearly needed to handle local convective situations.

17. Key Words (Suggested by Author(s))	18. Distribution Statement
Environmental pollution Atmospheric dispersion Solid rocket exhaust Hydrogen chloride	Unclassified - Unlimited Subject Category 45

19. Security Classif. (of this report)	20. Security Classif. (of this page)	21. No. of Pages	22. Price
Unclassified	Unclassified	73	A04

For sale by the National Technical Information Service, Springfield, Virginia 22161

NASA-Langley, 1981

7 1 1U,G, 121881 S00903DS
DEPT OF THE AIR FORCE
AF WEAPONS LABORATORY
ATTN: TECHNICAL LIBRARY (SUL)
KIRTLAND AFB NM 87117